A multi-species model for selective pruritus via the direct activation of TRPA1

Kali Paige Esancy

A dissertation

submitted in partial fulfillment of the

requirements for the degree of

Doctor of Philosophy

University of Washington

2020

Reading Committee:

Ajay Dhaka, Chair

David Raible

Jeff Riffell

Program Authorized to Offer Degree:

Neuroscience

University of Washington

Abstract

A multi-species model for selective pruritus via the direct activation of TRPA1

Kali Paige Esancy

Chair of the Supervisory Committee:

Ajay Dhaka

Department of Biological Structure

Pruritus, or itch, is an unpleasant cutaneous sensation that elicits a desire to scratch. In mammals, this sensation occurs when itch-inducing stimuli activate pruritic receptor proteins on somatosensory neurons, which functionally couple to transient receptor potential (TRP) ion channels to elicit neuronal activation. However, little is known about the capacity of lower vertebrates to experience itch, or the potential neuronal mechanisms that might underlie this sensation. To address this gap in knowledge, we used a variety of experimental methods to determine whether itch existed in a lower vertebrate, the zebrafish (*Danio rerio*). We confirmed that zebrafish are indeed capable of uniquely pruritic behavioral responses to itch stimuli that are distinct from nocifensive (pain) responses. Unlike previously-described itch transduction mechanisms in mammals, these pruritic responses resulted from the direct activation of the TRP ion channel TRPA1 on a selective subset of somatosensory neurons that were primed to respond to lower-intensity noxious stimuli like pruritogens. Higher-intensity stimuli that elicited nocifensive behaviors instead activated additional subpopulations of less-sensitive, higher-threshold TRPA1 neurons. This suggests that distinct populations of differentially-tuned TRPA1 neurons can be activated to relay either itch or pain. Intriguingly, this mechanism was also

present in the mouse, implying that this form of itch transduction is perhaps a rudimentary, evolutionarily early form of itch that persisted, and was later expanded upon, in terrestrial vertebrates. Additional experiments provided anatomical evidence that multiple subpopulations of TRPA1 neurons exist in both the mouse and the zebrafish, and found that PLC activity may play a role in setting the gain of the more sensitive neurons. Together, these results suggest a multi-species model for selective itch via the activation of a specialized subpopulation of somatosensory neurons with a heightened sensitivity to noxious stimuli.

Table of Contents

Acknowledgments

I would like to dedicate this dissertation to my family, in particular my parents, Michelle and James, who have always encouraged me to pursue my interests and have personally modeled the traits of perseverance and curiosity so integral to science—I'm not sure I've ever known people who worked harder, or asked more questions. Without their support and the introduction to science they provided me at a young age, I wouldn't be here today. My sister Camden has similarly been a wonderful source of encouragement and support.

I would also like to acknowledge my advisor, Ajay Dhaka, whose mentorship throughout this project was critical to its completion, and who always had a ready supply of energy, ideas, advice, and feedback. I greatly appreciate his commitment to fostering my growth as a scientist inside the lab as well as his flexibility in allowing me to develop my interests in teaching, science communication, and outreach. My committee members, the various labs and administrative staff within the Department of Biological Structure, and the Neuroscience Graduate Program deserve particular thanks as well.

Lastly, I want to thank all of the amazing friends, both near and far, at the University and Washington and outside of it, who have enriched my life during my years in graduate school. I am so privileged to be a part of several wonderful communities in Seattle, and the friends I have made here have supported me more than they know.

Chapter 1: Introduction

1.1 Definitions and function of itch and pain

The detection of noxious stimuli is inherently protective and of great evolutionary significance to an organism, and can often lead to the unpleasant sensations of itch and pain. Pain, as defined by the International Association for the Study of Pain, is an "unpleasant sensory and emotional experience associated with actual or potential tissue damage, described in terms of such damage"[1]. The affective (emotional) components of pain distinguish it from nociception, which is the process by which noxious thermal, mechanical, or chemical stimuli are detected by a subpopulation of peripheral nerve fibers called nociceptors[2–4]. Itch, or pruritus, is an unpleasant, cutaneous sensation that elicits a desire to scratch[5]. Pain is thought to be protective in anticipation of tissue damage, eliciting both reflexive and adaptive behaviors in many species[6–12]. Itch is likewise thought to have evolved in order to promote protective behaviors such as scratching, which can rid the skin of pathogens and stimulate immune responses[13]. The inability to respond to noxious, potentially damaging stimuli such as extreme temperatures, corrosive chemicals, and harmful mechanical forces, can have severe consequences. For example, patients with congenital insensitivity to pain (CIP), a rare disorder most frequently caused by mutations in the SCNA9 gene (which encodes a voltage-gated sodium channel found in nociceptors) or PRDM12 gene (which encodes a transcriptional regulator), often suffer from broken bones, serious burns, and other injuries resulting from their inability to sense, and thus avoid, environmental dangers, and many die prematurely[14–17].

While the detection of acute unpleasant stimuli is protective, aberrant activation of these systems (as occurs with neuropathic or chronic pain) can significantly affect quality of life. Chronic pain is widespread, and affects an estimated 20.4% of the U.S. population, with high-

impact chronic pain (that which prevents people from engaging in daily life or work activities) affecting ~8.0%[18]. It is the most common reason people seek medical treatment. Low efficacy of current pain treatments, coupled with inappropriate prescribing practices, has contributed in large part to the current opioid epidemic crisis—as of 2017, 67.8% of drug overdose deaths in the United States were caused by opioids, and within just one year (2016-2017), death rates increased for all categories of opioids[19]. Itch, another unpleasant sense, can also become disordered—though not as well-publicized as pain conditions, dermatological disorders causing itch, such as psoriasis, cholestatic itch, and atopic dermatitis, all negatively affect quality of life for millions of people[20–23]. One study found that skin disorders, which include many itch disorders, were the most prevalent diagnoses within a surveyed population[24]. Other studies have found chronic itch is particularly prevalent in the elderly, and that pruritus prevalence increases with age[21,25]. Understanding the function of the neurons responsible for mediating these sensations, in both normal and pathological contexts, is important from a basic science standpoint and may help inform clinical interventions.

1.2 A brief anatomical overview of the somatosensory system

The somatosensory, or "body-sensing", system is the collection of neural circuitry that mediates exteroception (the sense of direct interactions of the body and external environment, such as touch, pain, and thermal senses), interoception (the sense of the visceral organs and internal state), and proprioception (the sense of oneself)[26]. Somatosensory stimuli are first detected by peripheral neurons located in the trigeminal ganglia (TG) and dorsal root ganglia (DRG), which respectively innervate the face and the rest of the body (trunk, limbs)[26,27]. These first-order neurons are pseudounipolar in structure, with one afferent process extending into the

target tissue (skin, skeletal muscle, or visceral organ), and the other process extending into the central nervous system.

First-order neurons are specialized; i.e., they are functionally segregated, with different subtypes responding to certain stimuli and not others. They also vary extensively in size, myelination status, firing patterns, conduction velocity, activation threshold, and gene expression patterns[26–28]. Broadly, they can be categorized into fiber types based upon size, myelination status, and conduction velocity. Within these types (the Aα, Aβ, Aδ, and C-fibers), there are additional subcategories. Aα fibers, which have the widest diameters and are the most heavily myelinated (and thus have the fastest conduction velocities, ~120 m/s), are most frequently proprocieptors, neurons capable of detecting muscle stretch, contraction, and joint angle, alerting the body to changes in position and where it is in space[26,29]. Aβ fibers, slightly smaller in diameter than Aα fibers (>50 μm), have slightly slower conduction velocities (30-70 m/s), and are less heavily myelinated; they primarily constitute the low-threshold mechanoreceptors (LTMRs)[26,27]. Depending upon their firing patterns (rapidly versus slowly adapting) and association with other cells and structures within the skin (Merkel cells, Pacinian corpuscles, Meissner's corpuscles, Ruffini's endings, etc.), they are capable of discerning different tactile sensations, including vibration, light pressure, stretch, and fine/discriminative touch[26,30,31]. Aδ fibers, are smaller than Aβ fibers and lightly myelinated (with a maximum conduction velocity of 30 m/s), and are primarily high-threshold mechanoreceptors; the neurons responsible for signaling sharp, "fast", mechanical pain[2,4,27,32]. Unmyelinated C-fibers have the smallest diameters (10-30 μm) and slowest conduction velocities (<2 m/s), and include chemoreceptors, thermoreceptors, and certain LTMRs[26,27]. Depending upon their complement of cell membrane receptors, these neurons can respond to algogens (pain-inducing stimuli), pruritogens (itch-

inducing stimuli), and innocuous stimuli (neutral temperatures, pleasant/affective touch)[2,4,33]. These distinctions, however, are not always exceptionally clean; some somatosensory neurons are polymodal in nature. Frequently, a population of C-fibers may respond to both chemical and thermal stimuli[34,35]. Other neurons can respond to both mechanical and thermal stimuli[2,26,36]. Historically, different categories of peripheral somatosensory neurons have been distinguished not only by their size, conduction velocity, and responsiveness to certain stimuli, but also by the expression of protein markers—for example, certain neuropeptides such as CGRP and Substance P are only present in a subset of peptidergic C-fibers, and proteins such as parvalbumin and NF200 reliably label Aα and Aβ proprioceptors and mechanoreceptors[27]. More recently, transcriptomic profiling studies have further classified somatosensory neurons into subgroups based upon gene expression[37,38].

Input to the spinal cord and beyond is also segregated based upon modality, helping to preserve these "labeled lines". For example, C-fibers project into the most superficial layers (or laminae) of the dorsal horn, whereas fibers relaying innocuous touch project to deeper layers. Ascending neural circuits to higher-order brain structures such as the thalamus and somatosensory cortex are likewise separated based upon modality, with innocuous touch and proprioceptive information ascending through the dorsal column-medial lemniscus pathway, and thermal/chemical/pain information ascending through the spinothalamic tract[26]. The somatosensory cortex is responsible for attributing the discriminative and basic sensory components of a stimulus (localization, intensity, etc.) but not the emotional or affective components[26,39].

Other brain regions and neural circuits are also involved in the processing of somatosensory information, particularly in the context of pain. A significant amount of modulation occurs at the

level of the spinal cord, where segregated information streams from primary afferent fibers can interact via interneurons. In particular, these interneurons can allow for the "gating" of one sense by another—inhibitory interneurons can be activated by light touch afferents to dampen the output of pain projection neurons, and itch projection neurons can similarly be gated by mechanical/pain circuitry[40–44]. The dorsal horn of the spinal cord is also the target of descending modulatory information from higher cortical structures. The periaqueductal gray (PAG) and the rostroventromedial medulla (RVM) are important in relaying pain modulatory information to the spinal cord, which often involves signaling via endogenous opioids[45,46]. Other ascending pathways bring information from peripheral neurons to brain regions that can assign emotional/affective components and valence to sensations, or initiate autonomic responses. The basolateral amygdala, for example, contains a population of neurons that contribute the affective, or unpleasant, components of pain[47]. The parabrachial nucleus is another key processing center in pain, receiving inputs from pain projection neurons in the superficial dorsal horn, and relaying it to brain regions involved in emotional affect (like the amygdala) and autonomic homeostatic adaptation (hypothalamus, ventrolateral medulla)[48,49]. The insular cortex and dorsal raphe nucleus also have demonstrable roles in integrating sensory and emotional information regarding both itch and pain stimuli[50].

1.3 The cellular mechanisms of relaying itch and pain

1.3.1 TRP ion channels play a major role in relaying chemical and thermal stimuli

Transient receptor potential (TRP) ion channels in C-fiber nociceptors play a critical role in transducing chemical and thermal stimuli, many of which are associated with pain and tissue damage. These channels can be described generally as tetrameric calcium-permeable cation

channels with polymodal activation properties[51]. TRP channel subunits are composed of six transmembrane (TM) protein domains, with a well-conserved pore domain between TM segments 5 and 6[51]. Most TRP channel subunits also have a loosely-conserved intracellular TRP domain consisting of approximately 25 residues in the C-terminal region, which lends its name to the ion channel family and is thought to be important for binding PIP2, an important signaling molecule[52,53]. Apart from these generalities, the structure of the TRPs varies wildly between subgroups, perhaps reflecting their functional diversity. Depending upon the TRP channel in question, they can be homomeric or heteromeric[51,54,55], and can be activated by a wide variety of external and internal stimuli, including exogenous chemicals, endogenous compounds, intracellular signaling molecules, temperature, cell swelling, and fluid flow[53,55]. Different families of TRP channels also have structural modifications attuned to their particular function; for example, the TRPM often have enzymatically active protein regions fused to the channel[56,57].

A single TRP receptor itself can respond to multiple stimuli—one of the most well-studied of these is TRPV1, the mammalian ortholog of which activates following exposure to capsaicin (the chemical found in chili peppers that elicits a burning sensation), low pH (high H+), 2-APB, resiniferotoxin, PMA, endocannabinoids, and high temperatures[34,51,58]. Positive ion influx through TRP channels depolarizes the cell membrane, and the influx of calcium ions is an especially critical feature of TRP channel activation. Calcium ions are vital second messengers, and their entry through TRP receptors can vastly alter downstream calcium-dependent signaling cascades; TRP receptors themselves can be modulated by calcium as well as regulated by these cascades, potentially leading to further signal amplification[51,53]. TRPA1 is another noteworthy TRP channel that relays nociceptive signals. Initially described as a cold sensitive channel that activates to temperatures <17 ºC[59], it is now known to be activated as well by a variety of

reactive ligands (e.g., allyl isothiocyanate, cinnamaldehyde, gingerol, eugenol, methyl salicylate, acrolein) that covalently modify cysteine residues[60–64]. Although there was some initial controversy surrounding its potential role as a mechanotransducing channel, the general consensus is that it is not mechanoreceptive[65,66]. Because of its activation by pungent chemicals, it can be thought of as a detector of noxious chemical stimuli. TRPM3 is similar nociceptive TRP ion channel expressed in somatosensory neurons and is activated by neuroactive steroids (i.e., pregnenolone sulfate) as well as noxious heat[67].

Interestingly, TRP channels can be activated in different ways by their different agonists. This is perhaps most notable for TRPA1, which undergoes irreversible covalent modification of cysteine residues when activated by noxious pungent (often electrophilic) compounds; activation by other substances such as icilin, however, occurs via different, reversible mechanisms[61]. Distinct activation mechanisms also mediate the activation of TRPV1 by different stimuli—proton and peptide toxins bind to the extracellular pore domain, while capsaicin binding sites are localized to the transmembrane domain and volatile anesthetics activate TRPV1 through the pore loop domain[68,69]. The functional significance of these different sites of activation can be seen when comparing TRPV1 responses across species—while TRPV1 from fish and birds maintains heat sensitivity, the structure of these proteins is different enough from mammalian TRPV1 such that it is not activated by capsaicin[70,71].

Behavioral studies in rodent models have shown that these ion channels are functionally relevant for nociception. When either TRPV1 and TRPA1 are directly activated by their agonists, they can elicit sensations of pain. For example, TRPV1 agonists such as capsaicin will elicit pain behaviors such as licking/biting when injected into the hindpaw of mice[34]. Furthermore, TRPV1 knockout mice have reduced behavioral responses to noxious thermal

stimuli, and DRG neurons obtained from these animals are not responsive to any typical TRPV1 agonists in either calcium imaging or electrophysiology studies[34]. Similarly, TRPA1 agonists such as cinnamaldehyde can also elicit pain behaviors[72]. TRPM3 knockout mice also exhibit deficits in noxious heat sensation[67].

It should be noted, however, that not all TRP channels are involved in the transduction of pain. TRPM8 detects innocuous cool temperatures in addition to relaying unpleasant cold sensations, and is also activated by the chemical menthol, found in mint[73–76]. Other TRP channels, such as TRPV4, TRPV3, and TRPM4/5, detect innocuous warmth[77,78]. Additionally, not all TRP channels are somatosensory in nature; TRPM2, for instance, is widely expressed in the central nervous system, particularly the hypothalamus, where it is activated by both high temperatures and oxidative stress[79]. As such, it is thought to play role in the body's response to regulating temperature during fevers. Many other TRP channels are expressed in tissues aside from somatosensory neurons, functioning in a great diversity of roles—TRPM1 is important for retinal function, for instance, and TRPC5 in hippocampal neurons helps to regulate growth cone morphology in the hippocampus[78,80]. Furthermore, not all receptors relaying somatosensory information are TRP channels. Piezo2, for example, is a specific mechanotransducer in neurons that mediate light touch and proprioception; it is also required for Merkel cell mechanotransduction[81,82].

1.3.2 TRP ion channels couple with pruritic receptors to relay itch

While TRP channels can be directly activated by exogenous stimuli, they often do not function in isolation. Instead, they can functionally couple to other cellular sensors, such as G-protein coupled receptors (GPCRs) associated with inflammatory or pruritic (itch-inducing stimuli), and are integral in mediating both itch and inflammatory pain. While we will focus

primarily on the interaction between TRP channels and pruritic GPCRs, it should be noted that in some cases, the same GPCR may be implicated in both inflammation and pruritus; the "inflammatory soup" released following injury can include many endogenous pruritogens. Pruritic stimuli can take the form of exogenous chemicals, like the medicines chloroquine and imiquimod, or endogenous molecules, such as those released during immune responses or inflammation. Pruritic GPCRs abound in mammalian systems, and examples include H1R (a histamine receptor), 5HT2A (a serotonin receptor), TGR5 (a receptor for bile acids), MrgprA3 (a chloroquine receptor), PAR2 (a protease receptor), MrgprD (a β-alanine receptor); ETAR (the endothelin-1 receptor), MrgprC11 (another protease receptor), IL31Ra (the IL31 receptor), and S1PR3 (a receptor for an inflammatory phospholipid)[83–92]. When activated, these receptors initiate downstream signaling cascades that then activate the TRP ion channel they are associated with, eliciting an influx of positively-charged ions and thus neuronal activation[85,91,92].

TRPV1 and TRPA1 are the major TRP channels associated with the relay of itch, although some recent evidence suggests that TRPV4 may also play a role. Different subpopulations of somatosensory itch neurons in the TG and DRG express different combinations of pruritic receptors and TRP ion channels, and make use of different intracellular signaling cascades to functionally couple the two. One population, for example, is responsible for relaying histaminergic itch—these neurons express H1R, which when activated by histamine relies on phospholipase A2 and PLCβ3 pathways to activate TRPV1[13,88,93]. By contrast, chloroquine activates MrgprA3 on a subset of TRPA1-expressing neurons; MrpgrA3 activation results in the liberation of the G protein subunit Gβγ, which can then stimulate TRPA1[85,86]. Similarly, TGR5 can activate TRPA1 via Gβγ and PKC signaling within a subpopulation of TRPA1 neurons[83]. Serotonin-induced itch has been shown to result from a coupling of 5HT2A

and TRPV4 in a subset of DRG neurons[94], though the intracellular signaling mechanism linking the two is unknown.

1.3.3 Theories of itch coding

If the activation of TRP ion channels is associated with both itch and pain, how can these two distinct sensations be distinguished from each other? Various theories have emerged over time to describe the neural strategies through which this could be achieved. Most evidence supports the idea of population coding, in which different subpopulations of somatosensory neurons are specifically tuned to respond to different stimuli, as an explanation for these different sensations[13,92,95–97]. In such models, pruritic stimuli are detected by neurons expressing both pruritic receptors as well as nociceptive TRP ion channels, whereas algogenic stimuli are detected and relayed by other neurons in the TG and DRG which only express nociceptive TRP ion channels[13,92]. The existence of distinct subpopulations of neurons is one piece of evidence implying that itch and pain are conveyed via "labeled lines", and are functionally and structurally segregated. Furthermore, distinct populations of neurons within the spinal cord help to relay itch, and are characterized by receptors such as GRPR and Npr1, which bind to the pruritic transmitter peptides gastrin-releasing peptide (GRP) and natriuretic peptide b (Nppb), respectively[91].

Other research implies that such an explanation may not be so simple, and an alternate theory of intensity coding has been proposed to describe how the nervous system determines whether a stimulus is perceived as itchy or painful. In such a model, the same neurons could relay both itch and pain information, which would be distinguished by changes in action potential firing rates and patterning. Some psychophysical evidence supports this—increasing the concentration of certain stimuli, for instance, may shift perception from pruritus to pain[89,98,99]. Still other theories are based in population coding, but are more nuanced. For

example, the spatial-contrast theory posits that the differential localization of neurons in the skin determines which sensation is experienced[92]. This is bolstered by observations in human subjects, that intradermal injections of an algogen like capsaicin will elicit pain, whereas topical application will generally elicit itch[100–102]. Additionally, the regulation of itch and pain is not relegated solely to the periphery, as further refinement of signals occurs in the dorsal horn of the spinal cord, which receives primary afferent input from somatosensory neurons. The selectivity theory describes a coding strategy based upon such higher-order processing, and states that itch is experienced when selective subsets of "itch" neurons are activated but that pain predominates when both itch and pain neurons are activated together[92,99,103]. Inhibitory interactions abound in the spinal cord, providing a potential mechanism for this theory. In particular, pain signals are thought to inhibit itch signals via local inhibitory interneurons that release dynorphin, which binds to kappa opioid receptors on itch projection neurons and prevents their activation[41,42,91]. Through these means, normally noxious stimuli such as scratching may inhibit itch[104].

1.4 Are other species capable of experiencing itch and pain?

Some scientists suggest that only humans can definitively experience pain, and that researchers should remain "agnostic" as to the capacity of non-human animals to do the same, since their subjective experience can only be inferred[105]. Other scientists argue that certain animals (particularly "lower vertebrates") are incapable of experiencing pain in the way higher vertebrates such as mammals do as a result of multiple factors: they lack the cortical complexity (i.e., neocortex) associated with conscious awareness, most of their behavioral processing (aversive or otherwise) appears to be under the control of basal brainstem and hindbrain structures, and their reactions to "painful" stimuli cannot be distinguished from other escape responses[106]. At the opposite end of this spectrum, some argue that the distinction between the

sensory and emotional/cognitive aspects of pain is "artificial" and should be discontinued, asserting that scientists make no similar distinction between activation of sensory receptors and higher cortical processing for other sensory modalities, such as hearing or vision[107]. Still others have tried to bridge this gap by generalizing criteria used to assess pain in humans to other animals, based upon known comparable behaviors and mechanisms. Using this assessment, an animal must fulfill eight criteria in order to experience "pain": the possession of noxious stimuli receptors in functionally useful locations on the body, possession of brain structures analogous to the human cerebral cortex, possession of neural pathways connecting nociceptive receptors to higher brain structures, possession of opioid receptors in the central nervous system, the ability of analgesics to modify pain responses, behavioral response to noxious stimuli, relatively inelastic avoidance of noxious stimuli, and avoidance learning when confronted with noxious stimuli[108]. Nociception comprises the sensory components of these criteria[2]. In higher vertebrates such as humans, the percept of pain extends beyond nociception, and can exist without the activation of nociceptors, for example when higher brain structures involved in pain processing (somatosensory cortex, anterior cingulate cortex, insula) are activated, as has been demonstrated in people who report phantom limb pain[109] and in those who experience pain due to thalamic strokes[110]. Mammalian models fulfill all these criteria, and as such rodents (primarily mice and rats, with some exceptions) have been used to study both pain and nociception. Particular behavioral assays within these models can also be used to distinguish between reflexive-nociceptive and affective-motivational responses to noxious stimuli; withdrawal behavior to a stimulus, for example, is reflexive-nociceptive (and can be assayed via Von Frey, pin prick, and similar tests), while adaptive avoidance relies on affective-motivational responses (and can be assayed via conditioned place preference, two-choice tests, and similar tests)[9,111].

But what about lower vertebrates, such as fish, reptiles, amphibians, and birds? Most lower vertebrates are capable of nociception. Even invertebrates, such as the medicinal leech *Hirudo medicinalis*[112], the gastropod *Aplysia californica*[113], and fruit fly *Drosophila melanogaster*[114], possess nociceptive neurons whose activity can often be correlated with nocifensive behavior. It is believed that this sensory transduction is often accomplished through homologs of the same TRP channels observed in mammalian nociceptors[115]. In higher vertebrates, nociceptors are distinguished by their complement of TRP channels and receptor protein molecules, their morphology, their firing patterns, and distinctive action potential shapes[2,4,115,116]. Even the most primitive vertebrates, the agnathans (a subgroup of jawless fish that includes lampreys and hagfish) possess C-fiber nociceptors that respond to noxious temperatures and have the same action potential properties as those found in higher vertebrates[117]. Whether elasmobranchs, the cartilaginous fish, possess functional nociceptors is contentious—they lack C-fibers entirely, and most evidence suggests that their Aδ fibers do not function to relay nociceptive stimuli[117,118]. Teleost fish, by contrast, possess both Aδ and C-fibers, as evidenced by studies in rainbow trout, catfish, and goldfish[119–123]. Nocifensive behaviors in fish have been widely reported[124]. Ampibians and reptiles have also been shown to exhibit nocifensive responses to noxious stimuli. For example, nocifensive behavior following formalin injection has also been documented in a species of toad[125]. Results from formalin, capsaicin, and hot plate tests likewise demonstrate that crocodiles are capable of nociception[126].

Assessing "pain" in lower vertebrates beyond the level of nociception is more complicated. In her review, Sneddon uses Bateson's criteria to conclude that teleost fish, but not agnathans or elasmobranchs, are capable of experiencing pain[117]. All fish possess the proper brain regions required for nociception (such as the pons, medulla, and thalamus), but the percept

of pain is known to require cortical regions. Though not as well-developed as in higher vertebrates, both teleosts and elasmobranchs possess a rudimentary cortical area with extensive thalamic input; in agnathans, the forebrain is smaller and less complex, and likely not as suitable for higher processing[127]. Teleosts and elasmobranchs also have the same well-defined trigeminal nuclei as found in higher vertebrates, and the organization of their spinal cord, especially regarding the laminae of the dorsal horn and ascending projection pathways, is remarkably similar to that of mammals, fulfilling Bateson's third criterion[117,128]. Substance P immunoreactivity has also been observed in the dorsal horn of chickens, implying the existence of pain projection neurons and thus connectivity between peripheral neurons and higher brain regions[129]. Some work, including a PET study performed on parrots, suggests that birds are capable of experiencing pain and that the nido-pallium is the avian brain structure analogous to some mammalian pain centers[130,131].

Elasmobranch and teleost fish (as well as other lower vertebrates such as amphibians) likewise possess endogenous opioid receptors[117,132–134], although some evidence suggests that typical analgesics that target these receptors are not able to reduce the amount of anesthetic required to prevent nocifensive responses in the chain dogfish, an elasmobranch[135]. Amphibians possess all three kinds of endogenous opioid receptors (kappa, mu, and delta) that function to reduce "pain" responses[105]; birds likewise express enkephalins in patterns similar to that of mammals[136]. Analgesics have demonstrably similar effects in lower vertebrates as mammals[137]. Several studies in teleost fish indicate that opioid analgesics are very effective at reducing pain behavioral responses, and suggest that teleost fish are potentially good model organisms for studying pain[10,138–140]. Both opioid and adrenergic analgesics are effective in an amphibian (frog) model, and exert their effects through mechanisms analogous to those in mammals[141,142].

Morphine can increase the latency of responses to nociceptive stimuli in crocodile, indicating that endogenous opioids likely function in pain modulatory systems in this species[143]. Teleost fish are also capable of avoidance learning—goldfish, for example, can be conditioned to avoid electric shocks[12,144], and both cod and pike display learned hook avoidance[11,145]. Although some scientists argue that avoidance behavior does not constitute a conscious cortical response reflective of higher-order mammalian pain, there are studies showing that avoidance learning is markedly diminished following removal of forebrain/rudimentary cortical areas[106,146]. Suspension of normal behavior in response to noxious pain stimuli has also been demonstrated in teleosts: for instance, trout injected with acetic acid exhibit reduced feeding behavior and abnormal fear conditioning[123,147]. Similar results have been observed in reptiles such as the ball python, where two different pain models (capsaicin and surgical injury) can disrupt feeding behaviors[148].

It can reasonably be concluded, then, that the complex percept of pain likely first evolved in teleost fish, and that all groups higher than this are capable of experiencing pain, albeit with some exceptions (i.e., mammalian species who evolved insensitivity to specific forms of pain, such as the grasshopper mouse and certain mole rats)[149–151]. As such, certain lower vertebrate species have gained traction in both nociception and pain research[70,140,152].

Arguments about whether non-human animals are capable of experiencing itch are discussed less frequently in the literature, which overall makes less of a distinction between the sensory and affective components of itch. Even though “itch”, like pain, certainly includes both stimulus detection and the addition of negative affect (unpleasantness), there is not as great a distinction in the field between these two aspects, as there is between pain and nociception; “pruritus” is often used interchangeably with “itch”. There have not, therefore, been attempts to

establish criteria of whether a non-human was experiencing itch in the way that there have been for pain[108]. Mammals have largely been accepted as experiencing itch, and rodents have been extensively used in itch studies. Like humans, mice and rats demonstrate scratch behaviors following the acute application of pruritic stimuli, and the accompanying genetic tools in these models allows for detailed exploration of the underlying neural circuitry. Furthermore, certain behavioral assays have been established in rodent models that allow for the distinction of pain and itch behaviors[153,154]. While rodents models have received the bulk of attention in basic science and clinical studies of itch phenomena, pruritic response behaviors have been observed in a variety of other mammalian species, including elephants, cows, and bears[155–158].

While the existence of nociception and pain has been widely explored in lower vertebrates, the sensation of itch has largely been neglected. Though some publications have reported pruritic behaviors in on-mammals, these studies have been largely observational. Birds have often been reported to engage in pruritic behaviors[159]. For example, both captive parrots and wild puffins have been observed to scratch themselves with sticks, presumably to address a pruritic stimulus[160,161]. Fish have been observed to engage in "scratch-like" behaviors such as rubbing against rocks and inclusions in aquariums, but these reports are primarily anecdotal. To the best of our knowledge, systemic attempts to explore pruritus and its neural underpinnings in lower vertebrates have not been made.

1.5 Thesis Goal/Motivation:

It is the goal of this dissertation to ask the question of whether a lower vertebrate, the zebrafish (*Danio rerio*), is capable of experiencing itch. The Dhaka lab has already extensively employed this model organism in studies of nociception[70,152], and possesses available tools to probe this question from a variety of different perspectives. Using a combination of behavioral

and neural activity assays, I aim to determine if specific pruritic behaviors can be observed following exposure to pruritogens as well as establish whether pruritogens are capable of activating zebrafish somatosensory neurons. If initial findings are promising, I will then explore the cellular and molecular mechanisms through which pruritic stimuli are encoded, and determine whether these strategies are analogous to those that have been documented in mammalian systems. Having a thorough understanding of the neural circuitry underlying pain and itch in a variety of animal models is critical to gaining insight into how these important senses may have evolved, and could potentially inform novel treatment strategies for a variety of clinical disorders.

Chapter 2: A zebrafish and mouse model for selective pruritus via direct activation of TRPA1

2.1 Chapter Abstract

Little is known about the capacity of lower vertebrates to experience itch. A screen of itch-inducing compounds (pruritogens) in zebrafish larvae yielded a single pruritogen, the TLR7 agonist imiquimod, that elicited a somatosensory neuron response. Imiquimod induced itch-like behaviors in zebrafish distinct from those induced by the noxious TRPA1 agonist, allyl isothiocyanate. In the zebrafish, imiquimod-evoked somatosensory neuronal responses and behaviors were entirely dependent upon TRPA1, while in the mouse TRPA1 was required for the direct activation of somatosensory neurons and partially responsible for behaviors elicited by this pruritogen. Imiquimod was found to be a direct but weak TRPA1 agonist that activated a subset of TRPA1 expressing neurons. Imiquimod-responsive TRPA1 expressing neurons were significantly more sensitive to noxious stimuli than other TRPA1 expressing neurons. Together, these results suggest a model for selective itch via activation of a specialized subpopulation of somatosensory neurons with a heightened sensitivity to noxious stimuli.

2.2 Introduction

Itch is an unpleasant sensation that elicits a scratch behavior in terrestrial vertebrates. In mammals, chemically-induced itch is thought to be mediated by pruritic receptors on somatosensory neurons[91,92]. These receptors are typically G-protein coupled receptors (GPCRs) that, upon activation, prompt the opening of downstream transient receptor potential (TRP) channels, facilitating activation of the neuron[13,89]. This coupling of pruritic receptors to TRPA1 or TRPV1 is especially intriguing in that these TRP channels also serve as nociceptors,

mediating responses to algogenic (painful) stimuli[5,77].

Zebrafish (*Danio rerio*) have proven to be a valuable tool in the study of nociception[70]. The zebrafish ortholog of *Trpa1*, *trpa1b*, is required for nociceptive responses to aversive pungent chemicals[65]. Orthologs of genes involved in mammalian itch transduction are also present in the zebrafish[162–164]. Studying how these itch genes operate in the somatosensory system of zebrafish could reveal conserved itch transduction mechanisms, providing insight into the evolution of itch.

2.3 Results

2.3.1 Imiquimod evokes itch in zebrafish.

In an effort to determine if pruritic stimuli are capable of eliciting somatosensory activity in zebrafish, we screened five compounds known to both induce acute pruritus in mammals and act on receptors expressed by zebrafish[83,165–168], excluding pruritogens that act on receptors that do not have a zebrafish ortholog, such as MRGPR agonists. Allyl isothiocyanate (AITC), a known algogen and TRPA1 agonist[64,65], was used as the positive control. We evaluated somatosensory neuronal responses to pruritic compounds using transgenic larvae that pan-neuronally express the neuronal activity indicator CaMPARI (*elavl3*:CaMPARI), a fluorescent protein that permanently photoconverts from green to red in the presence of calcium and 405 nm light[169]. Using this approach, we were able to view trigeminal neuronal activity in 3 day post fertilization (dpf) larval zebrafish following the application of each pruritogen (**Figure 1A-H**). Of the pruritogens screened, only imiquimod (IMQ) significantly ($p < 0.05$) activated zebrafish trigeminal ganglia (TG) neurons (**Figure 1I**).

We have previously reported that noxious stimuli evoke locomotion in larval zebrafish[70].

When 5dpf larval zebrafish were exposed to individual pruritogens, only IMQ elevated baseline locomotion ($p < 0.001$), producing a dose dependent increase (**Figure 1-figure supplement 1A**). When coupled with our findings in CaMPARI transgenics, these results indicate that IMQ likely acts through somatosensory neurons to evoke behavioral responses. While 5-HT did produce a reduction in locomotion, it did not activate somatosensory neurons (**Figure 1I, J**). Given the limited sensitivity of the locomotor assay we were unable to differentiate nocifensive behavior elicited by AITC from potentially pruritic behavior elicited by IMQ. To address this issue, we employed an adult zebrafish behavioral assay[139,170]. Injection of IMQ into the lip elicited a lip-rubbing behavior that may constitute a form of itch-scratch response in zebrafish, a behavior that was absent in sham-injected control fish ($p < 0.001$) (**Figure 1K, L; Supplemental Videos**) and distinct from previously described zebrafish nocifensive, escape, or exploratory behaviors[171–173]. Consistent with studies of nocifensive behaviors, injection of AITC produced freezing behavior ($p < 0.01$) (**Figure 1-figure supplement 1C**) as well as a significant decrease ($p < 0.05$) in velocity not observed in control or IMQ injected fish (**Figure 1-figure supplement 1B**). Such distinct behavioral responses imply that zebrafish are capable of experiencing, and responding differentially to, discrete stimuli analogous to itch and pain in mammals.

2.3.2 *Trpa1b*, but not *tlr7*, is required for both neuronal and behavioral responses to imiquimod.

The mechanism by which IMQ elicits itch in mammals is unclear. IMQ, a treatment for various skin disorders, acts through TLR7 to stimulate an immune response, with intense itching and painful burning commonly reported as side effects[174,175]. In mice, however, IMQ is reported to be itch selective, and only elicits scratching, but not nociceptive, behaviors[176,177]. Furthermore, there is dispute surrounding TLR7's role in IMQ-induced itch. One study found that *Tlr7*$^{-/-}$ mice

showed deficits in IMQ evoked itch and proposed that *Tlr7* expressed in dorsal root ganglion (DRG) neurons was mediating IMQ transduction[176]. TLR7 has also been reported to couple with TRPA1 in DRG neurons to evoke nociception in response to other TLR7 agonists[178]. However, conflicting studies found that *Tlr7*$^{-/-}$ mice exhibited no deficits in IMQ-evoked itch, and RNAseq analysis of DRG neurons found no evidence for *Tlr7*expression[37,177,179]. We therefore investigated whether TLR7 and/or TRPA1 were involved in transducing the neural and behavioral responses to IMQ in zebrafish.

In situ hybridization studies in zebrafish larvae revealed that *tlr7* mRNA expression is restricted to known hematopoietic regions in larval zebrafish[180,181], and was notably absent in both TG and Rohon-Beard (RB) neurons (**Figure 2A; Figure 2-figure supplement 1I**). As expected, *trpa1b* expression was observed in both TG and RB neurons (**Figure 2B; Figure 2-figure supplement 1C**). Therefore, any role TLR7 could play in IMQ-evoked behavior would be via indirect mechanisms.

To determine if *trpa1b* and/or *tlr7* are required for IMQ induced behaviors, we introduced early nonsense mutations in the coding sequences of both genes[182]. *Tlr7*$^{-/-}$ zebrafish larvae exhibited a significant ($p < 0.001$) increase in total locomotion when exposed to IMQ (100 μM) that was indistinguishable from controls (**Figure 2C**). However, *trpa1b*$^{-/-}$ larvae demonstrated no response to IMQ (100 μM), while their WT siblings displayed normal IMQ induced behaviors ($p < 0.01$, **Figure 2D**). These data support a mechanism where *trpa1b*, but not *tlr7*, is necessary for mediating behavioral responses to IMQ in larval zebrafish. As expected based on previous reports, behavioral responses to AITC were absent in *trpa1b*$^{-/-}$ fish (**Figure 2-figure supplement 1F**)[65]. Notably, *trpa1b*$^{-/-}$ fish demonstrated an equivalent increase in locomotor behavior as their WT siblings when exposed to increased temperatures (**Figure 2-**

figure supplement 1E). This indicates that the *trpa1b* mutation specifically affects Trpa1b-mediated sensations, rather than causing generalized sensory impairment.

To test whether the presence of Trpa1b was necessary to mediate neuronal responses in larval zebrafish TG, we conducted *in-vivo* calcium imaging using *elavl3*:GCaMP5g larvae[183] (**Figure 2G**). In WT larvae, IMQ activation was seen exclusively in a subset of AITC responsive neurons (4/36, $n = 5$ larvae). *Trpa1b*$^{-/-}$ fish, however, exhibited no response to either IMQ or AITC (0/89 total neurons, $n = 5$ larvae) (**Figure 2H**).

Notably, the highly specific TLR7 agonist loxoribine did not evoke TG neuron activation, larval locomotion, or adult lip-rubbing behavior, further strengthening the finding that Tlr7 does not play a role in IMQ evoked behaviors in zebrafish (**Figure 1I, J; Figure 1-figure supplement 1D**). This finding is similar to reports in the mouse demonstrating that loxoribine does not elicit pruritic behavioral responses[177].

2.3.3 Imiquimod directly activates TRPA1.

To determine if TRPA1 directly interacts with IMQ to produce itch, we utilized the TLR7-deficient cell line HEK293T[184]. HEK cells transfected with zebrafish, mouse, and human *Trpa1* showed a dose-dependent increase in intracellular calcium following application of IMQ and AITC that was not observed in HEK cells alone (**Figure 3A-F; Figure 3-figure supplement 1A, C**). Importantly, we found that loxoribine did not activate HEK cells transfected with zebrafish or mouse *Trpa1* (**Figure 3-figure supplement 2A-D**), indicating that TRPA1 is responsive to IMQ, and not to TLR7 agonists in general.

While we observed no expression of *tlr7* in the zebrafish TG (**Figure 2A**), given the lack of consensus over its functional role we sought to determine whether TLR7 might serve as a pruritic co-receptor that potentiates the TRPA1 response. We co-transfected HEK cells with

Trpa1 and *Tlr7* and examined the calcium responses following treatment with IMQ and observed no discernible differences in the average peak responses to IMQ between *Trpa1* and *Trpa1+Tlr7* conditions (**Figure 3A-C, Figure 3-figure supplement 1C**). Whole cell electrophysiological experiments corroborated these findings. When stimulated with IMQ, voltage-clamped HEK cells transfected with mouse or zebrafish *Trpa1* demonstrated a significant increase in current (**Figure 3G; Figure 3-figure supplement 1G**). Co-transfecting mouse *Tlr7* with mouse *Trpa1* in HEK cells had no demonstrable effect on current influx (**Figure 3-figure supplement 1H**). Additionally, no difference was found in the IMQ current density dose-response curves for cells transfected with zebrafish *trpa1b*, mouse *Trpa1*, or mouse *Trpa1* + mouse *Tlr7* (**Figure 3H**). In contrast to previous reports, we found no evidence that TLR7 coupled with TRPA1 in the presence of loxoribine as measured by ratiometric calcium imaging and whole cell electrophysiology in mouse and zebrafish (**Figure 3-figure supplement 2A-D**)[176]. Together, our data suggest that TLR7 plays no role in the direct activation of somatosensory neurons, and does not appear to potentiate the response of TRPA1 to IMQ.

Following these results, we confirmed that mouse and human TLR7 were present and functional in our assays (**Figure 3-figure supplement 1I-K**)[185]. Intriguingly, zebrafish Tlr7 did not respond to either IMQ or loxoribine in a dual-luciferase assay, suggesting that zebrafish Tlr7 is not activated by mammalian TLR7 agonists (**Figure 3-figure supplement 2E**). However, due to a lack of a Tlr7 positive control, we were unable to confirm that Tlr7 was functional in our heterologous expression system. With this caveat in mind, the lack of zebrafish Tlr7 response to these TLR7 agonists lends further credence to the conclusion that Tlr7 is not involved in somatosensory neuronal activation or behavior in this species.

If TRPA1 does not couple with TLR7, but is instead directly activated by both IMQ and

AITC, how could IMQ be itch-selective in the mouse? To address this question we assessed the EC_{50} and peak responses to IMQ and AITC in HEK cells transfected with *Trpa1* from different species. The EC_{50} of IMQ for zebrafish, mouse and human TRPA1 was consistently higher than the AITC EC_{50} , demonstrating that IMQ is a weaker agonist than AITC (**Figure 3-figure supplement 3F**). Notably, while the IMQ EC_{50} of zebrafish Trpa1 and human TRPA1 were only 2-3 fold greater than that of the EC_{50} of AITC, mouse TRPA1 demonstrated a ~40 fold difference between the EC_{50} of AITC and IMQ. Furthermore, only mouse TRPA1 elicited significantly lower maximum responses to IMQ than AITC (**Figure 3D-F**). In similar electrophysiology experiments, HEK cells transfected with zebrafish *trpa1b* exhibited identical current density responses upon stimulation with the maximum dose of either AITC or IMQ, but cells transfected with mouse *Trpa1* exhibited significantly higher current density responses following stimulation with AITC, relative to IMQ (**Figure 3I**). Such physiological differences in TRPA1 function between species could provide a potential mechanism for the itch selectivity of IMQ in mice, implying that IMQ is not a strong enough mouse TRPA1 agonist to elicit nociception in this species. Conversely, the ability of both zebrafish and human TRPA1 to respond equally to AITC and IMQ at maximal doses potentially explains how IMQ can elicit both itch and pain sensations in humans, and suggests that the same may be observable in fish.

2.3.4 Imiquimod responsive neurons are a primed subpopulation of TRPA1-expressing neurons.

In the preceding *in vivo* calcium imaging experiments, we observed that only a small proportion of zebrafish Trpa1+ neurons, identified by their responsiveness to AITC, were also responsive to the IMQ stimulus. To further explore this result, we used *elval3*:H2BGCaMP6[186] transgenic zebrafish to record the response properties of larval TG neurons to IMQ and AITC.

No IMQ+/AITC- neurons were found across 13 larvae. Among AITC+ neurons, 28% (31/111) were responsive to IMQ (**Figure 4A-C**).

The above data affirms that IMQ+ neurons are a subset within a larger population of Trpa1+ TG neurons, implying that a population coding strategy for pruritus might be at play. This does not itself answer the question of how such an itch-selective Trpa1+ subpopulation might be activated by a TRPA1 agonist without recruiting other Trpa1+ neurons that may code for nociceptive behaviors. Based on our finding that IMQ is a weaker TRPA1 agonist than AITC, one potential explanation is that such an itch-selective Trpa1+ population is more sensitive to TRPA1 agonists, and can be activated by weaker (pruritic) stimuli. In IMQ+/AITC+ neurons, we determined that the average maximum fluorescence intensity response to the IMQ stimulus was significantly lower than that of the AITC stimulus ($p < 0.001$), implying that at the concentrations used, IMQ is indeed a weaker TRPA1 stimulus than AITC *in vivo* (**Figure 3-figure supplement 2A**). Furthermore, we found that the maximum AITC response of IMQ+/AITC+ neurons was significantly greater than that of AITC+ only neurons (**Figure 4D**). Likewise, IMQ+/AITC+ neurons displayed a significantly greater average AITC response than AITC+ only neurons ($p < 0.05$, **Figure 4-figure supplement 1B**).

These data suggest that IMQ+ TG neurons are primed to respond to TRPA1 agonists and support a model where relatively weak TRPA1 stimuli, such as IMQ at the concentration used, could selectively recruit a potential itch-coding subpopulation of Trpa1+ neurons. Higher intensity stimuli like AITC at the concentrations used, however, would activate the majority of Trpa1+ neurons to evoke nocifensive behaviors, positively correlating with findings that nociception takes precedence over itch sensation[41,96,187].

To verify that IMQ activates a selective subset of Trpa1+ neurons as opposed to

activating Trpa1+ neurons stochastically, we performed calcium imaging experiments in which 3dpf *elavl3*:H2BGCaMP6 were exposed to successive pulses of 100 μM IMQ. Of the IMQ+ neurons we identified across five fish, 92.3% (12/13) responded to both pulses of IMQ, whereas only 7.7% (1/13) responded only to the second pulse of IMQ (**Figure 4-figure supplement 2A-C**). Additionally, it is possible the single neuron that responded only to the second pulse of IMQ may also be a dual-responder. While the GCaMP fluorescence change only crossed our response threshold during the second pulse, it is possible that the sloping baseline may have obscured a minimal response to the first pulse, especially considering the low amplitude of the second response. However, for purposes of completion we decided to include this trace in our final counts. Given the finding that only ~30% of AITC responsive neurons responded to one pulse of IMQ (100 μM), if one assumes that this is the probability that any given AITC responsive neuron would respond to IMQ (100 μM), and that responses to IMQ are stochastic in nature, one would expect only a small fraction of neurons to be double responders (~9%) (**Figure 4D**). The finding that nearly all IMQ-responsive neurons were dual responders, argues that these neurons comprise a distinct population of Trpa1 expressing neurons, primed to respond to low intensity TRPA1 dependent stimuli.

2.3.5 Stimulus intensity affects behavioral and neuronal responses.

Although the IMQ dose-response curve in zebrafish *trpa1b*-transfected HEK cells was rightward shifted, it was eventually able to elicit the same amount of intracellular calcium flux that AITC evoked. This implies that at a sufficiently high concentration, IMQ might be able to recruit neurons outside of the IMQ+ subpopulation observed in the above larval calcium imaging experiments, thus eliciting neuronal and behavioral responses characteristic of AITC at nociceptive concentrations. Likewise, it is also possible that at low enough concentrations, AITC

is capable of eliciting the pruritic neuronal and behavioral responses we observed following application of IMQ.

In CaMPARI fish we observed that decreasing the concentration of applied AITC correlated with a reduction in the number of photoconverted neurons (**Figure 4E**). Additionally, administering higher IMQ concentrations converts an equivalent number of neurons as high concentrations of AITC (**Figure 4E**), suggesting that for TRPA1 agonists, eliciting pruritus or nociception is dependent more on stimulus intensity than identity.

In vivo GCaMP imaging bolstered our CaMPARI findings that stimulus intensity affects which subpopulations of Trpa1+ neurons are activated. In these experiments, we observed that increasing the stimulus intensity activated more neurons. Only a subset of neurons that responded to a high concentration (50 μM) of AITC responded to a lower concentration (10 μM) of AITC (11/42), and of those even fewer neurons responded to 100 μM IMQ (4/11) (**Figure 4-figure supplement 1C**). Furthermore, increasing the IMQ concentration to 200 μM in adult behavioral experiments evoked nocifensive behaviors such as elevated freezing and significantly reduced velocity, and the itch-like lip rubbing behavior seen at 100 μM was notably absent[124,170] (**Figure 4F; Figure 1-figure supplement 1C, Figure 4-figure supplement 1D**). Conversely, low concentrations of AITC (5 μM) elicited both itch-like lip rubbing behavior and increased velocity (**Figure 4F; Figure 4-figure supplement 1C**). These data indicate that the subpopulation of Trpa1+ neurons that drive itch behavior in the zebrafish are distinct in their sensitivity to TRPA1 agonists, but can be activated by either AITC or IMQ at the appropriate concentration to produce equivalent behaviors.

2.3.6 TRPA1 mediates itch behavior and neuronal responses in in the mouse.

We found that IMQ elicited responses in 9.6% (83/864) of cultured AITC+ DRG neurons (**Figure 5A**) from WT animals. To determine if TRPA1 mediates IMQ responses in mice, we examined IMQ-evoked responses in DRG neurons from both WT and *Trpa1*$^{-/-}$ animals using ratiometric calcium imaging. We found that both IMQ and AITC responses were completely abolished in DRG neurons obtained from *Trpa1*$^{-/-}$ animals, while neurons from WT siblings exhibited normal responsivity to both stimuli (**Figure 5B, C**). Furthermore, application of loxoribine did not elicit calcium responses in mouse DRG neurons, providing evidence that TLR7 stimulation does not result in activation of somatosensory neurons (**Figure 5-figure supplement 1H**). We next explored whether IMQ-evoked scratching behavior was also dependent on TRPA1. High-dose IMQ (125 μg) paw injections did not evoke nocifensive behaviors in WT mice (n= 0/10 IMQ-injected), consistent with previous reports[177]. However, scratching bouts at a low concentration of IMQ (10 μg, nape injected) were significantly attenuated in *Trpa1*$^{-/-}$ mice, demonstrating that TRPA1 is required for normal IMQ-induced scratching behavior (**Figure 5D**). Interestingly, a higher dose of IMQ (50 μg) evoked equivalent scratching behavior in both WT and *Trpa1*$^{-/-}$ mice (**Figure 5-figure supplement 1G**). This result taken together with our finding that isolated mouse DRG neuron responses to IMQ are TRPA1-dependent suggests that IMQ can also evokes itch via indirect activation of somatosensory neurons, perhaps downstream of an immune response[91,92].

Given the itch selectivity of IMQ in the mouse, we sought to determine whether IMQ+ neurons were part of a population of DRG neurons that encode TRPA1-dependent pruritus. We therefore measured the overlap of IMQ+ neurons with DRG neurons that responded to a mixture of the TRPA1-dependent pruritogens deoxycholic acid (DC) and chloroquine (CQ) (**Figure 5E-**

F)[85,86,168]. We found that the vast majority of IMQ+ neurons (73%, 23/30) also responded to these pruritic stimuli (**Figure 5G**), indicating that in the mouse, IMQ+ neurons belong to a subpopulation of itch-encoding neurons.

Due to the parallels noted between zebrafish and mouse IMQ responses, we proceeded to investigate whether the correlation between stimulus intensity and neuronal activation that we observed in the zebrafish was conserved in the mouse. In the mouse, increasing the concentration of AITC activated more DRG neurons in a dose-dependent manner (**Figure 5-figure supplement 1I**). Furthermore, within the population of neurons that responded to lower concentrations of AITC, the IMQ+ subpopulation was enriched (**Figure 5-figure supplement 1J**). We also found that IMQ+ neurons in the mouse had a smaller peak responses to IMQ than AITC (**Figure 5-figure supplement 1A-C**). Additionally, AITC peak responses within the IMQ+ population were significantly greater than in the AITC+ only population ($p<0.01$), demonstrating that the heightened sensitivity of IMQ+ neurons to TRPA1 agonists is conserved in the mouse (**Figure 5H**). Subsequent experiments revealed that IMQ+ DRG neurons exhibited a significantly higher maximum response to the TRPV1 agonist capsaicin (CAPS) than CAPS+ only neurons (**Figure 5-figure supplement 1D-F**), implying that the IMQ+ neurons may be intrinsically more sensitive to noxious stimuli, not exclusively TRPA1 agonists. Finally, in accordance with our zebrafish data, we observed that AITC stimulus intensity dictates whether mice exhibit pruritic or nocifensive behaviors. In order to discriminate between nocifensive and pruritic behaviors, we employed a "cheek model of itch" assay in which compounds injected into the cheek may elicit scratching (a pruritic response) or wiping (a nocifensive response)[153,154]. We observed that AITC (50 mM) produces significant scratching behavior with no appreciable wiping behavior ($p < 0.001$ and N.S. respectively), while a higher dose of AITC (100 mM)

results in a significant attenuation of the observed scratching behavior, as well as a significant wiping behavior ($p < 0.05$ and $p < 0.001$ respectively) (**Figure 5I**).

2.4 Discussion

The sense of itch in mammals has been thoroughly explored, but there is a dearth of knowledge on the presence of itch, and the neural mechanisms which transduce it, in lower vertebrates such as fish. Here, we use a popular model organism, the zebrafish, to demonstrate that fish are potentially capable of experiencing a form of rudimentary itch in response to the pruritogen IMQ, and suggest that this sensation is conveyed by the direct activation of TRPA1 on a specialized subset of somatosensory neurons highly sensitive to TRPA1 agonists.

Through a combination of experimental procedures, we show that the pruritogen IMQ can elicit behavior and neuronal responses in zebrafish. In larvae, IMQ elicits an increase in locomotion and activation of somatosensory TG neurons, suggesting that the observed locomotor effects likely originate in the periphery, and are not due to the direct action of IMQ upon more central structures. Furthermore, in adult zebrafish, peripherally applied IMQ produces a scratching-analogous lip-rubbing behavioral response that is distinct from the nocifensive behaviors evoked by the algogen AITC as well as previously described escape behaviors[139,170,172,173,188]. The fact that IMQ-evoked behavioral responses manifest as lip-rubbing, as opposed to nocifensive or escape behaviors, further suggests that these fish are indeed experiencing an itch-like sensation. For animals whose anatomy prohibits scratching behavior with claws, the use of another body part or an external object is perhaps the only recourse to address a pruritic stimulus. Such scratching behaviors have previously been documented in animals from a variety of taxa[155–159].

There is currently a lack of consensus in the literature as to how IMQ induces itch in mammals, although all studies show that TRPV1-expressing neurons are required[176,177]. A major point of contention surrounds the involvement of the immune receptor TLR7, the therapeutic target of IMQ. Our work provides additional evidence that TLR7 is not involved in the direct activation of somatosensory neurons by IMQ[37,177,179]. Instead, the TRPA1 ion channel appears to play a key role in transducing IMQ-evoked neuronal effects and the behaviors that result from such neuronal activity. Unlike *trpa1b*, *tlr7* is not expressed in zebrafish somatosensory tissue, as demonstrated by *in situ* hybridization. Moreover, zebrafish that lacked functional TLR7 behaved equivalently to wildtype animals in response to IMQ application. By contrast, behavioral and neuronal responses to IMQ in both fish and mice were largely dependent upon TRPA1. Utilizing both electrophysiology and calcium-imaging, we showed that IMQ was able to directly activate TRPA1, and that co-transfection of *Tlr7* did not potentiate IMQ-evoked responses. However, greater concentrations of IMQ were required to elicit the same levels of calcium flux that were evoked by lower concentrations of AITC, implying that IMQ is a weaker agonist than AITC in all species we examined. With zebrafish and human TRPA1, IMQ eventually reached the same maximal calcium response levels as AITC, while IMQ responses with mouse TRPA1 plateaued at lower maximal levels than AITC. This suggests that in the mouse, IMQ is incapable of evoking the same intensity of neuronal responses as AITC can, even at high concentrations. Our findings may provide a molecular explanation for previously-documented observations that in the mouse, IMQ appears to be itch-selective, while in humans, IMQ has been reported to elicit sensations of both itch and pain[174–177]. Findings from these *in vitro* experiments may also underlie our own observations in both mice and adult zebrafish behavioral experiments. In the context of TRPA1 activation, stronger stimuli elicited nocifensive behaviors, whereas weaker

stimuli evoked pruritic behaviors. Furthermore, the effects of stimulus intensity upon neuronal activation and behavior were largely but not entirely independent of stimulus identity. In adult zebrafish low concentrations of IMQ evoked pruritic behaviors while higher concentrations of IMQ were capable of eliciting nocifensive freezing behaviors. In line with previous reports, we were unable to elicit murine nocifensive behaviors with high concentrations of IMQ, which we hypothesize was due to the inability of IMQ to maximally activate mouse TRPA1[176,177]. In contrast AITC evoked behaviors were not species dependent as predicted by the dose response curves of zebrafish Trpa1 and mouse TRPA1 to this agonist. Low concentrations of AITC produced scratching behaviors, while higher concentrations of AITC evoked nocifensive behaviors in both species. While the direct activation of a TRP channel to evoke itch by a pruritogen or algogen is somewhat surprising, as it deviates from canonical pathways requiring both pruritic GPCRs and TRP ion channels, such a mechanism supports observations of itch in both human and mouse studies following application of typically noxious TRP channel agonists[100,153,189].

Intriguingly, our observation that behaviors transitioned from a pruritic to a nocifensive phenotype as stimulus intensity increased was mirrored by our observations in calcium imaging studies. Experiments with two different calcium indicators of neuronal activity, GCaMP and CaMPARI, revealed a correlation between TRPA1 agonist stimulus intensity and neuronal recruitment. Specifically, stronger stimuli (high concentrations of TRPA1 agonists) activated more neurons than weaker stimuli (lower concentrations of TRPA1 agonists).

Based on these findings we hypothesized that a population coding strategy was being employed. In our model, low intensity stimuli would selectively activate a subset of TRPA1-expressing neurons that encode pruriception, whereas higher intensity stimuli would activate a

another population of TRPA1-expressing neurons that encode nociception. This hypothesis would be in line with recent findings that pruriception is encoded by different populations of somatosensory neurons than those that encode nociception[91,96,190]. Calcium imaging of zebrafish and mouse somatosensory neurons revealed the existence of at least two functionally distinct neuronal subpopulations. In both species, we observed a population of neurons that responded to both low and high intensity TRPA1 agonists and another that only responded to high intensity TRPA1 agonists. Our observation that sequential pulses of IMQ (100 μM) activate the low intensity TRPA1 agonist responsive population in zebrafish demonstrates that this population is likely genetically defined, and not determined stochastically. Furthermore, in the mouse, we observed that the vast majority of IMQ (100 μM) responsive neurons also responded to the TRPA1-dependent pruritogens chloroquine and deoxycholic acid, supporting the conclusion that these neurons constitute a pruritic subpopulation. Unfortunately, equivalent experiments could not be performed in the zebrafish, as we were unable to identify other pruritogens for this species.

In alignment with these results, in both species, neurons that responded to low intensity TRPA1 agonists also exhibited a greater response to high intensity AITC stimulation than neurons that only responded to high intensity AITC stimulation. This implies that putative itch-encoding neurons comprise a more sensitive subset of somatosensory neurons than nociceptive neurons. Additionally, in both species, IMQ (100 μM) responsive neurons were enriched within populations of neurons that responded to low concentrations of AITC; in other words, we observed a high degree of overlap in the populations of neurons that responded to low intensity TRPA1 agonists irrespective of stimulus identity. Together, this provides further evidence of the greater sensitivity of a population of itch-encoding neurons to TRPA1 agonists.

Itch is a complex physiological phenomenon, and several models have been proposed to explain its transduction in the periphery and beyond[13,91,92,99,191]. Here, we describe a mechanism through which acute IMQ-evoked itch is mediated by the peripheral somatosensory neurons of two species. Weak stimuli such as lower concentrations of the TRPA1 agonists IMQ and AITC activate only a subset of highly sensitive pruriceptive TRPA1-expressing neurons (pruriceptive), while the remaining TRPA1-expressing neurons (nociceptive) are only recruited by higher intensity TRPA1 stimuli. Our proposed model clearly is not the sole mechanism by which itch is coded as a distinct sensation from pain[13,91,92]. However, in the context of pruritogens and algogens that are direct TPRA1 agonists, our findings overwhelmingly support a population-coding model for the discrimination of itch and pain.

Our data implicates a mechanism for the direct activation of TRPA1 by IMQ to elicit sensations of itch in both zebrafish and mice. Our findings that IMQ-induced itch was attenuated, but not abolished, in *Trpa1*$^{-/-}$ mice supports additional mechanisms for IMQ-evoked itch in this species. One may speculate that the activation of an immune response by IMQ in other cell types could result in a cascade of downstream signaling that could ultimately lead to a release of endogenous pruritic stimuli (e.g. histamine and serotonin from mast cells). In the zebrafish, TLR7 is unlikely to contribute even indirectly to IMQ-induced itch sensation, as we observed no behavioral phenotype in *tlr7*$^{-/-}$ animals. However, this does not rule out the possibility that pathogen exposure could stimulate the immune system via TLR activation or other pathways, leading to an indirect activation of pruritic somatosensory neurons and triggering both itch sensations and scratching behaviors. Several studies have implicated that Tlrs in several species of fish play a role in immunity[192–197]. However, no study has explicitly queried potential connections between such immune responses and downstream neuronal activation or behavior in

any fish species. While our results demonstrate that TLR7 is not involved in transducing IMQ-evoked itch in the zebrafish, investigating the role of immune responses in mediating somatosensations (both in zebrafish and other species) would be an interesting route for future exploration.

It is plausible that an unknown receptor is activated by IMQ and couples with TRPA1 *in vivo* to evoke a somatosensory neuron response. Our TRPA1 mutant experiments would be unable to detect the existence of such a receptor, which would presumably not function to elicit neuronal activity in the absence of TRPA1. However, our *in vitro* experiments suggest that the existence of such an unknown receptor is unlikely, as it would also have to be endogenously expressed in HEK cells. Furthermore, the dose-dependent overlap we observed in the number of neurons that were responsive to IMQ and AITC, as well as similarities in the dose dependent itch and nociceptive behaviors elicited by these compounds in both zebrafish and mice, implies that these compounds are acting via the direct activation of TRPA1.

We observed that out of the several mammalian pruritogens, only IMQ elicited behavioral and neuronal responses in zebrafish. While we tested pruritogens that targeted mammalian pruritic receptors with a known zebrafish ortholog, it is possible that other stimuli we did not test may also evoke sensations of itch in these animals. It is likewise possible that histamine, serotonin, TGR5, and PAR-2 receptors do not function in the itch pathway as pruritic receptors on primary sensory neurons in zebrafish, as they do in mammals. For example, zebrafish have an extensive histaminergic system with multiple histamine receptors, but histamine receptor expression appears to be restricted to the central nervous system[198]. Furthermore, while zebrafish do possess mast cells (which in mammals release histamine and serotonin that act upon peripheral sensory neurons to elicit itch), studies indicate that these mast

cells do not contain histamine or serotonin[199,200]. It is therefore plausible that in the zebrafish, histamine and serotonin do not play a functional role in pruritic sensation or immune responses, but are restricted to more central processes such as mediating sleep-wakefulness cycles, mood, and anxiety[163,201].

The direct activation of a TRP channel to elicit itch or pain through the recruitment of distinct populations of somatosensory neurons via stimulus sensitivity is mechanistically simple. That such a mechanism is present in both zebrafish and mouse may imply that this particular form of itch transduction appeared before the emergence of terrestrial vertebrates, and may have been conserved throughout evolutionary history to persist in mammals. One could therefore postulate that this rudimentary form of itch potentially evolved from existing pain-transducing molecular and neural machinery as a means to differentiate high- and low-intensity noxious stimuli for which an alternative behavioral response was more appropriate. While data from only two species is not sufficient to declare that our proposed mechanism is evolutionarily conserved, we hope that our findings provide a springboard for future research into pruritus across multiple taxa, which would help elucidate the evolutionary development of this important sense.

2.5 Conclusion

Our work demonstrates that IMQ can directly activate TRPA1 to elicit pruritic behavioral responses in both the zebrafish and mouse. Furthermore, we have shown that the immune receptor TLR7 does not mediate somatosensory neuronal responses to IMQ. Our results imply that in both species a subset of highly sensitive TRPA1-expressing itch-encoding neurons can respond to weaker TRPA1 agonists to encode sensations of itch and elicit discrete itch behaviors. More intense stimuli, such as those that evoke nocifensive behaviors, appear to recruit this highly-sensitive subset as well as less-sensitive TRPA1-expressing neurons. Our finding that

IMQ responsive neurons in the mouse are part of a TRPA1-expressing subpopulation that is activated by other TRPA1 dependent pruritogens provides further evidence that these more sensitive neurons indeed signal itch. Parallel observations between the zebrafish and mouse suggest that this relatively simple mechanism for conveying, and distinguishing between, pruritic and algogenic stimuli originated early in vertebrate evolution and appears to be preserved in mammals. In sum, our results support the existence of a population-coding based strategy through which differential activation of TRPA1-expressing somatosensory neurons with high or low sensitivities to TRPA1 agonists can relay the discrete sensations of itch and pain respectively.

2.6 Chapter Methods

Zebrafish husbandry: Adult Zebrafish (*Danio rerio)* were raised with constant filtration, temperature control (28.5 ± 2°C), illumination (14 h:10 h light-dark cycle, lights on at 9:00 AM), and feeding. All animals were maintained in these standard conditions and the Institutional Animal Care and Use Committee approved all experiments. Adult zebrafish not used in behavioral experiments were bred in spawning traps (Thoren Caging Systems) from which embryos were collected. Embryonic and larval zebrafish were raised in petri dishes (Fisher Scientific) of E2 medium with no more than 50 embryos per dish at 28.5 ± 1°C in an incubator (Sanyo). Embryos were staged essentially as described[202] and kept until 5dpf.

Mouse husbandry: *Trpa1*$^{+/+}$ and congenic *Trpa1*$^{-/-}$ mice on the *C57BL/6J* background were described previously[203]. All mice were housed under a 12 h light/dark cycle with food and water provided ad libitum. All behavioral tests were videotaped from a side angle, and behavioral assessments were done by observers blind to the treatments or genotypes of animals. All mice

used for behavior tests were age, gender and body weight matched. All experiments were performed in accordance with the guidelines of the National Institutes of Health and the International Association for the Study of Pain, and were approved by the Animal Studies Committee at Washington University School of Medicine.

Cell lines: HEK 293T cell stocks were initially purchased from ATCC, which authenticated their identity via STR profiling. Cells tested negative for mycoplasma contamination. Cells were cultured in DMEM (Life Technologies) supplemented with fetal bovine serum and antibiotics (penicillin/streptomycin), and passaged every 2-3 days.

Genomic DNA extraction: Individual larvae were processed as previously described[204]. Larvae were anesthetized with tricaine, and placed in individual PCR tubes with a small quantity of E2 media. An equivalent amount of a 2X base solution made from a 50x stock (1.25 M NaOH, 10mM EDTA pH 12) was then added to each tube, and all tubes were incubated at 95°C for 30 min. Following this, 1x neutralization solution (again made from from a 50x solution, 2M Tris-HCl pH 5) was added, and the resulting DNA solutions were stored at -20°C. Adult genomic DNA was extracted using similar methods, but with a few minor modifications. Individual fish were anesthetized with tricaine, and a small portion of the tail fin was removed with a scalpel and placed into an individual PCR tube. 1X base solution was then applied to the piece of tissue, which was incubated for 30 minutes at 95°C until an equivalent amount of 1X neutralization solution was added.

Nonsense mutant generation: Nonsense mutants for both TRPA1 and TLR7 were generated essentially as previously described[205]. To synthesize the template DNA required for the *in vitro* transcription we employed a two oligo PCR method, one oligo contained the RNA loop structure required for recognition by the Cas9 enzyme and had the sequence 5'[gatccgcaccgactcggtgccacttttcaagttgataacggactagccttattttaacttgctatttctagctctaaaac]3'. The second, gene specific, oligo had the sequence 5'[aattaatacgactcactata(N20)gttttagagctagaaatagc]3', where (N20) refers to the 20 nucleotide oligo that binds the genome. In the case of the TRPA1 nonsense mutants the N20 oligo was 5'[GGCGTATAAATACATGCCAC]3'. In the case of the TLR7 nonsense mutant the N20 oligo was 5'[GGGGATGTAGGACAAGTTGT]3'. A mixture of 400 μL of Cas9-encoding mRNA and 200ng/μL of the proper sgRNA was injected into zebrafish embryos of the AB background at the one cell stage.

Fish were then screened for mutations using the following primers, TLR7 5' GGATGCGTTTATGCTGCTTGACAA, TLR7 3' AATGTTGTTGTTGTACAGGTAGAGCTC, TRPA1 5'-CTCATACATTCATAAACCTGCCTGATAT, and TRPA1 3' – TGGAGGGGCGTCAGACCCTTT, and Sanger Sequencing.

We identified two nonsense mutants for TRPA1, one that possessed a 4bp insertion and one that possessed a 7bp deletion. We then outcrossed these founders (F0) to WT fish of the same genetic background (AB line) and screened for germline transmission in the F1 generation. Members of the F1 generation were additionally backcrossed to WT fish to establish an F2 generation. Heterozygous F2 zebrafish were then crossed to each other to produce an F3 generation that was

used for experiments; additionally F2 zebrafish were crossed to transgenics expressing calcium indicator proteins (CaMPARI, GCaMP) under neuronal promoters in order to perform functional imaging studies. In some instances, F3 zebrafish were backcrossed a fourth time to establish younger generations of fish. Animals that were homozygous for either the 4bp insertion or 7bp deletion possessed identical phenotypes (i.e., lack of behavioral response to AITC). Likewise, zebrafish with a 4bp/7bp phenotype possessed an identical phenotype as 4bp/4bp and 7bp/7bp homozygotes.

We identified one nonsense mutant for TLR7 that possessed a 1bp deletion. As with the generation of the TRPA1 mutant line, this founder was outcrossed to a WT fish and the offspring were screened for germline transmission. Subsequent generations were backcrossed in the manner described above.

In the TRPA1 experiments, WT siblings of $TRPA1^{-/-}$ fish were used as the controls. In the TLR7 experiments, a pure $TLR7^{-/-}$ line was established and compared to age-matched WT fish, since we were unable to genotype the 1bp mutation via conventional methods (gel electrophoresis, HRMA) and could only be identified via sequencing.

Larval zebrafish behavior: At 5dpf, larval zebrafish (AB background) were placed into individual wells on a 96-well mesh bottom plate (Millipore) resting in a bath of E2 medium. The 96-well plate was then transferred to a hot plate that was maintained at a constant temperature of 28.5°C. Then the 96-well plate was moved from the E2 medium bath to the experimental bath for four minutes, during which the behavioral response of the larval zebrafish was recorded with

a HD camcorder (Canon). Experiments were performed blindly and each larva's total locomotive behavioral response was tracked using Ethovision (Noldus). Statistical analysis was done using an analysis of variance (Graphpad Prism 6) or Student's T-test. All experimental compounds were purchased from Sigma Aldrich unless otherwise noted and were made up in 1% dimethyl sulfoxide (DMSO, Sigma Aldrich) and E2 medium.

In experiments involving nonsense mutants and their WT siblings, all larvae were genotyped following video capture of the behavioral response. Briefly, each larva was removed from its well and placed into a PCR tube in 25 µL of E2 media. gDNA was extracted using the base extraction technique described above. For experiments involving TPRA1b$^{-/-}$ fish, all larvae were genotyped by HRMA (CFX Connect, BioRad) using the primers 5'-CTCATACATTCATAAACCTGCCTGATAT and 3'-TGGAGGGGCGTCAGACCCTTT. As mentioned previously, due to difficulties in genotyping the 1bp deletion in TLR7 nonsense mutants, animals were identified by genomic sequencing, and a pure TLR7$^{-/-}$ was created for use in behavioral experiments and were compared to AB fish.

Examining neuronal activation with CaMPARI transgenic zebrafish: *elavl3*:CaMPARI zebrafish in the Casper background were simultaneously exposed to chemical stimuli and a 405 nm light in order to permanently photoconvert active neurons[169]. Briefly, 3dpf larval zebrafish were paralysed by injecting α-bungarotoxin protein (Sigma) into the chest cavity using microinjection needles pulled on a Flaming-Brown Micropipette Puller (model P-87, Sutter Instrument Co.) and a Picrosprizter II microinjection apparatus (General Valve Corporation). Paralysed fish were then placed in small glass-bottomed dishes (Wilco Wells) filled with an individual chemical from the

pruritic screen and allowed to incubate for 2 minutes. Following this incubation period, glass-bottomed dishes were placed on the stage of an inverted fluorescent microscope (Olympus, model Ix81S1F-3) and the larvae were exposed to a 405 nm light for 40 seconds using MetaMorph software (Molecular Devices). Post-exposure fish were removed from the chemical and placed in a petri dish filled with embryo media and tricaine to prevent any future activation of sensory neurons. Immediately prior to imaging, larvae were mounted on coverslips in 1.5% agarose + tricaine in EM. TG and surrounding neural tissue were imaged using a 20x lens on an LSM 880 confocal microscope (Zeiss). Zen Black software was used to scan through the entire TG, acquiring a 1024 x 1024 pixel image slice at every ~5 µm that could then be stacked in the Z plane until the entire ganglion was imaged. Images were examined for photoconverted (red-labeled) neurons, and totals were established for each TG in each condition. When used, ANOVA statistical tests were done against control.

Adult zebrafish behavior: Adult zebrafish were placed in traps (Thoren Caging Systems) and were transported to the experimental area, which was maintained at 28.5 ± 2°C, where they were left to acclimate for one hour. After completing acclimation fish were transported one at a time to the injection area. Each fish was anaesthetized by exposure to 12.0 ± 0.3°C system water. They were then immobilized and injected in the upper lip using a 33 gauge Hamilton needle and 20 µL Hamilton syringe. Fish were injected with 10 µL of experimental or control solution, all of which were made up in 1% DMSO, 1x PBS, and distilled water. After injection, fish were placed into a trap and transferred to the recording area. The behavioral response was recorded for five minutes using an HD camcorder (Cannon). The velocity of the fish was then analyzed using Ethovision (Noldus) and all facial interactions were manually scored to prevent any bias in the

data. All analysis was blinded. All statistical analysis were done with an analysis of variance (Graphpad Prism 6) or Student's T-test.

In the case of nonsense mutant experiments, after the behavioral responses were captured, each fish was euthanized by tricaine overdose and fin clipped, and the fin section was placed in a PCR tube. Then, gDNA was extracted from the excised tissue using the previously described base extraction technique. TRPA1 genotype was determined using the same HRMA strategy as employed in the larval behavioral experiments. Since a homozygous TLR7-/- line was employed for adult behavioral experiments, genotyping post-experiment was unnecessary. When used, ANOVA statistical tests were done against control.

Larval *in situ* hybridization experiments (zebrafish): Whole-mount colorimetric *in situ* hybridization to determine TRPA1b and TLR7 expression was performed on 3dpf larvae as described previously[70]. Pigment formation was inhibited by exposing larvae to 1-phenyl 2-thiourea (PTU) at 24hpf. Larvae were hybridized with DIG-labeled riboprobes for TRPA1 or TLR7 overnight at 65°C. They then underwent a series of stringent washes, followed by incubation in α-DIG conjugated Fab fragments (Roche, 1:10,000) and staining in NBT/BCIP solution. Larvae were washed with PBTw and stored in glycerol until imaging, whereupon they were mounted in 100% glycerol and photographed using an upright Axioplan2 microscope (Zeiss).

Calcium imaging with *elavl3*:GCaMP transgenic zebrafish: 3dpf zebrafish larvae from or *elavl3*:GCaMP5[183] or *elavl3*:H2BGCaMP6[186] transgenic line were paralysed as described above.

After paralysis, larvae were mounted in 2% agarose in EM on coverslips, which were then placed into a perfusion chamber (Warner Instruments). Once solidified, the agarose immediately surrounding the head was cut away with a scalpel to ensure maximal exposure to chemical stimuli. The perfusion chamber was placed onto the stage of an Olympus Fluoview FV-1000 multiphoton microscope equipped with an infrared laser controlled by Mai Tai software (Spectra-Physics, Thermo Electron Corporation). Larvae were imaged under the following parameters: laser wavelength of 880 nm, resolution of 4.0 μs/pixel, frame rate of 1-3 seconds per frame, frame size of 512 x 512 pixels. Laser intensity, HV, and zoom were optimized for individual larva. For experiments comparing multiple stimuli, each stimulus was separated by an equivalent period of E2 media washout. All solutions were made in E2 media containing 2% DMSO.

For calcium imaging experiments involving TRPA1b$^{-/-}$ animals and their WT/TRPA1b$^{+/-}$ siblings, *elavl3*:GCaMP5:TRPA1b$^{-/-}$ larvae were employed. One day prior to imaging, larvae were anesthetized with tricaine, tail-clipped, genotyped via HRMA, and housed in individual wells within a 24-well plate until ready for use in experiments. 2-APB was used a positive control.

Ratiometric Calcium Imaging: DRGs were isolated from 6- to 12-week-old C57Bl/6J mice. All experiments were performed in compliance with institutional animal care and use committee standards and experiments were performed essentially as described[69]. Dissociation and culturing of mouse DRG neurons were performed as described with the following modifications[59]. Dissected DRGs were dissociated by incubation for 1 hour at 37°C in a solution of culture medium [Ham's F12/Dulbecco's modified Eagle's medium (DMEM) with 10% horse serum, 1%

penicillin-streptomycin (Life Technologies, Carlsbad, CA)] containing 0.125% collagenase (Worthington Biochemicals, Lakewood, NJ), followed by a 30-minute incubation in 10 ml of culture media plus 1.25 units of papain. Calcium imaging was performed essentially as described previously (Story et al, 2003). Growth media were supplemented with 100 ng/ml nerve growth factor. For experiments involving heterologous expression, human embryonic kidney (HEK) 293T cells were transiently transfected with one or two of the following plasmid constructs: zebrafish *trpa1b*, zebrafish *tlr7*, mouse *Trpa1*, mouse *Tlr7*, human *TRPA1*, and/or human *TLR7*. All constructs except for the one encoding zebrafish *tlr7* were also co-transfected with pIRES-eGFP plasmid in order to estimate transfection efficiency. (For zebrafish *tlr7*, this step was unnecessary because the construct was already in the pIRES-eGFP vector.) The buffer solution for all experiments was 10 mM HEPES in 1X Hanks' balanced salt solution (HBSS) (Invitrogen, Carlsbad, CA).

The threshold for activation was defined as 30% above baseline for both DRG and heterologous expression experiments. Student's t test was used for all statistical calculations. All averaged traces represent mean ± S.E.M. All reported fluorescence values of each cell were normalized to the fluorescence of that cell during the initial baseline wash period. Maximum response values of each cell were calculated as the difference between the maximum and minimum fluorescence values of the cell during a stimulus application period.

Dual Luciferase Assay: To verify the functionality of our transfected *Tlr7* constructs, we determined levels of NF-kB induction following stimulation with the TLR7 agonist loxoribine using a Dual-Luciferase Reporter Assay System (Promega). Briefly, HEK 293T cells were

seeded at ~80% confluency in individual wells of a 24-well plate (N ≈ 4 x 10^5 cells per well) and transiently transfected with the same zebrafish, mouse, or human *Tlr7* constructs as employed in calcium imaging following a standard lipofectamine protocol. All cells were also co-transfected with a nF-kB Firefly luciferase reporter plasmid (p1242 3x-KB-L, Addgene[185]), a Renilla luciferase control plasmid (p207-CMV-Renilla, gift from Tom Reh), and pIRES-eGFP (if necessary) for estimating transfection efficiency. As a negative control, another set of HEK 293T cells were transfected only with pIRES-eGFP. Twenty-four hours following transfection, the culture media was removed from all cells and replaced with normal serum-free media or with serum-free media containing 200 μM loxoribine. Following a 24-hour treatment period, culture media was removed, plated cells were rinsed briefly with DPBS, then lysed with passive lysis buffer (Promega) and gentle agitation on a multi-purpose rotator (Barnstead). Lysates were analyzed on a Viktor3 1420 Multilabel Counter (PerkinElmer), which generated luminescence values in CPS (counts per second) for both Firefly and Renilla luciferase activity. Assays were also performed on 1X PLB samples to estimate background luminescence. Background luminescence was subtracted from each measurement, and the Firefly/Renilla CPS ratio was calculated for each condition.

Immunohistochemistry on HEK 293T cells: To verify that TLR7 was being expressed by HEK 293T cells used in our experiments, we transfected cells on coverslips with either mouse or human *Tlr7* constructs and pIRES-eGFP; some cells were only transfected with pIRES-eGFP to serve as a negative control. 48 hours following transfection, cell culture media was removed, and coverslips were washed briefly with 1X DPBS and fixed for 10 minutes at room temperature in 4% paraformaldehyde in 1X PBS (Electron Microscopy Sciences). Coverslips were again rinsed

briefly in DBPS and then blocked in 10% goat serum in 1X PBST (PBS with 0.1% Tween-20) for 1 hour at room temperature. Primary antibodies against TLR7 (rabbit anti-TLR7, Boster, 1:250) and GFP (chick anti-GFP, 1:1000, Invitrogen) were made in PBST with 10% goat serum and applied to the coverslips, which were incubated overnight at 4 °C. Coverslips were then rinsed 3X in PBST to remove primary antibodies, treated with secondary antibodies (AlexaFluor goat anti-chicken 488 and AlexaFluor goat anti-rabbit 568, both at 1:1000, Life Technologies and Invitrogen, respectively) for approximately 2 hours at room temperature, washed in PBST, and mounted on slides with DAPI-containing Vectashield medium (Vector Laboratories, Inc.). Confocal imaging of mounted cells was performed using a Zeiss microscope and Zen Black acquisition software.

Electrophysiology: Whole-cell patch-clamp recordings were performed at room temperature (22-24°C) using an Axon 700B amplifier (Molecular Devices, Sunnyvale, CA, USA) on the stage of an inverted phase-contrast microscope equipped with a filter set for GFP visualization (Nikon Instruments Inc., Melville, NY, USA)[206]. Pipettes pulled from borosilicate glass (BF 150-86-10; Sutter Instrument, Novato, CA, USA) with a Sutter P-1000 pipette puller had resistances of 2-4 for whole-cell patch-clamp recordings when filled with pipette solution containing 140 mM CsCl, 2 mM EGTA, and 10 mM HEPES with pH 7.3 and 315 mOsm/l osmolarity. Cells were perfused with extracellular solution containing 140 mM NaCl, 5 mM KCl, 0.5 mM EGTA, 1 mM $MgCl_2$, 2 mM $CaCl_2$, 10 mM glucose, and 10 mM HEPES (pH was adjusted to 7.4 with NaOH, and the osmolarity was adjusted to ≈ 340 mOsm/l with sucrose). The whole-cell membrane currents were recorded using voltage ramps from -100 to +100 mV for 500 ms at holding potential of 0 mV. Data were acquired using Clampex 10.4 software (Molecular

Devices, Novato, CA, USA). Currents were filtered at 2 kHz and digitized at 10 kHz. Data were analyzed and plotted using Clampfit 10 (Molecular Devices, Novato, CA, USA). The concentration-response curve was fitted with the logistic equation: Y = Ymin + (Ymax − Ymin)/(1 + 10^[(logEC_{50} − X) × Hill slope]), where Y is the response at a given concentration, Ymax and Ymin are the maximum and minimum responses, X is the logarithmic value of the concentration and Hill slope is the slope factor of the curve. EC_{50} is the concentration that gives a response halfway between Ymax and Ymin. All data are presented as mean ± SEM.

Mouse Behavior: Mice were shaved on the nape of the neck or in the face two days before assay. On the day of experiment, mice were acclimated for 1 hr by placing each of them individually in the recording chamber followed by intradermal injection of 10 μg of IMQ to the nape of the neck. Immediately after the injection, mice were videotaped for 30 min without any person in the recording room. After the recording, the videotapes were played back and the number of scratching bouts towards the injection site was counted by an investigator blinded to the treatment.

Cheek injection of AITC was performed as described[154]. Briefly, during anesthesia with isoflurane (2% in 100% oxygen), the right cheek (approx. 5 × 8 mm area) was shaved. Mice were acclimated in the recording chambers at least two days before experiments began. AITC was dissolved in DMSO to make a 5 M stock solution and diluted in saline to make the working solution. Every mouse received an injection of 10 ul volume at the shaved area. Immediately after the injection, mice were videotaped for 30 min without any person in the recording room.

After the recording, the videotapes were played back and the number of scratching and wiping bouts towards the injection site was counted by an investigator blinded to the treatment.

Footpad injections were performed as described previously (Liu et al, 2016). Briefly, either a saline control or IMQ (125 μg) was injected into the footpad of the hindpaw. Animals were filmed, and nocifensive behaviors (licking, biting) in the recorded videos were scored by an investigator blind to the treatment.

2.7 Chapter Notes

This chapter was published in the journal *eLife* as a research article with the following citation: Kali Esancy, Logan Condon, Jing Feng, Corinna Kimball, Andrew Curtright, and Ajay Dhaka. "A zebrafish and mouse model for selective pruritus via direct activation of TRPA1". Elife Vol. 7, 1-24 (2018). Detailed author information follows:

Kali Esancy[*,1,2], Logan Condon[*,1], Jing Feng[*,3], Corinna Kimball[1], Andrew Curtright[1], Ajay Dhaka[1,2,†].

*Contributed equally to the manuscript. [†]Corresponding author. 1. Department of Biological Structure, University of Washington, Seattle, Washington 98195, USA. 2. Graduate Program in Neuroscience, University of Washington, Seattle, WA, 981095, USA. 3. Center for the Study of Itch, Washington University, St. Louis, Missouri 63130, USA.

Competing Financial Information: The authors declare no competing financial interests.

Corresponding Authors: Correspondence and requests for materials should be addressed to dhaka@uw.edu.

Acknowledgments: This work was primarily supported by NIH R01DE23730 (AD). Other support includes the Levinson Emerging Scholars award (LC) and a Mary Gates Undergraduate Research Award (LC). We thank David Raible and Hongzhen Hu for extensive feedback on experimental design and the manuscript, Paul Nakamura and Quynh Nguyen for technical support with the dual luciferase assay, Tom Reh for the p207-CMV-Renilla luciferase plasmid, Rachel Wong for use of the FluoView 1000 multiphoton microscope, and David White for zebrafish husbandry support.

2.8 Chapter Figures

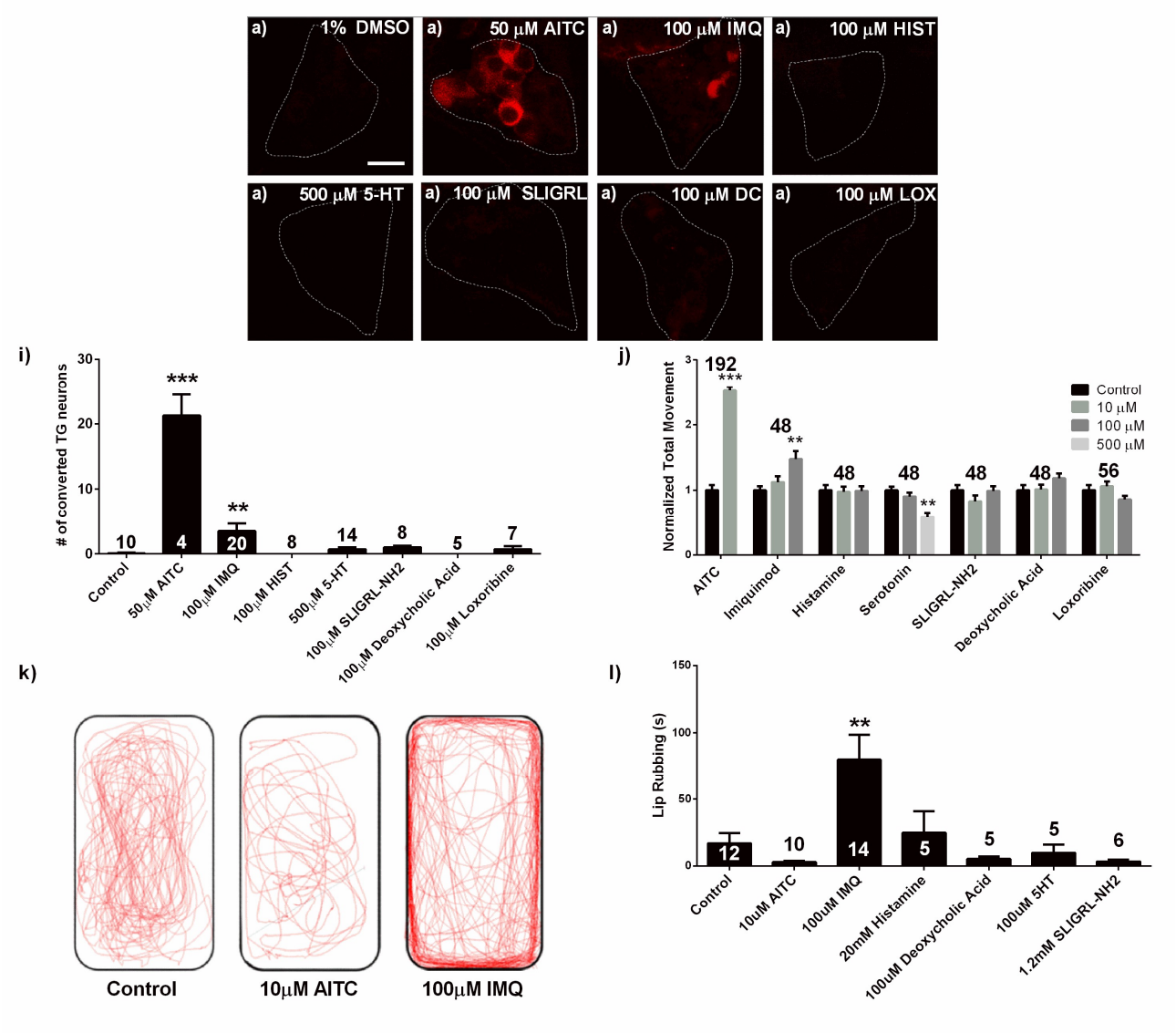

Figure 1: Imiquimod produces behavioral and neuronal responses in the zebrafish. (**A-H)** 3dpf live *elavl3*:CaMPARI TG imaging of larvae exposed to 405 nm light and control (**A**), 50 μM allyl isothiocyanate (AITC) (**B**), 100 μM imiquimod (IMQ) (**C**), 100 μM histamine (HIST) (**D**), 500 μM serotonin (5-HT) (**E**), 100 μM SLIGRL-NH2 (**F**), 100 μM deoxycholic acid (DCA) (**G**), and 100 μM loxoribine (LOX) solutions (**H**). (**I**), Counts of photoconverted cells from experiments **a-h**. (**J**), 5dpf WT larval locomotor behavior screen. **(K)** Representative traces of adult behavior. **(L)** Adult lip-rubbing behavioral assay. **I, J, L**, ***P < 0.001, **P < 0.01, one-way ANOVA. Bars represent mean ± s.e.m.

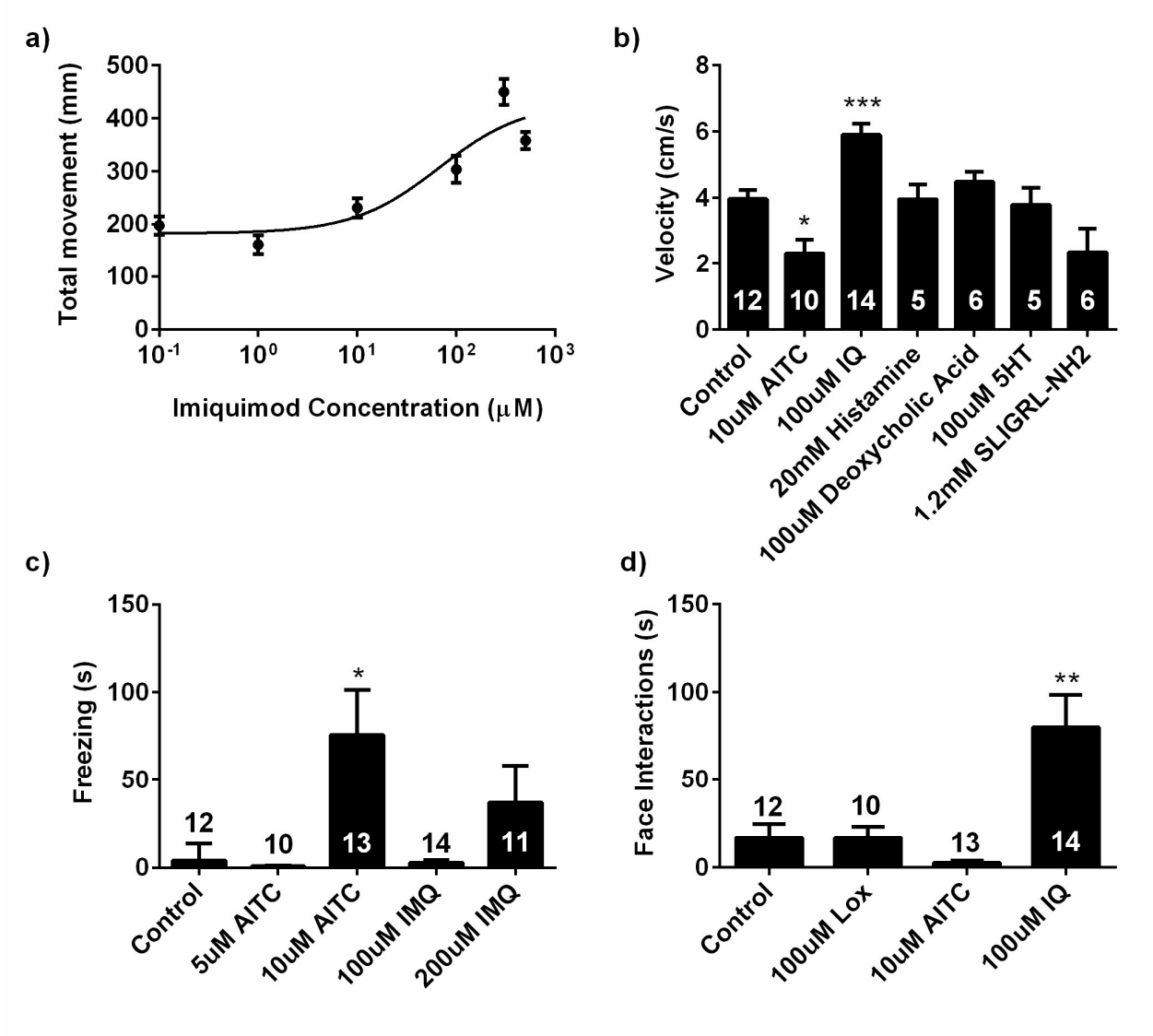

Figure 1-figure supplement 1: Behavioral effects of noxious pruritic and algogenic stimuli in the zebrafish. (A) Dose-response curve for IMQ in larval locomotion assay, $n = 48$ for all conditions. **(B)** Average velocity of adult zebrafish injected with AITC or known pruritogens. 10 μM AITC induced a significant decrease in swimming velocity, whereas 100 μM IMQ elicited increased velocity. **(C)** Quantification of freezing behavior in the adult behavioral assay. Of the stimuli tested, only 10 μM AITC elicited significant freezing behaviors in adult zebrafish, although fish injected with 200 μM IMQ displayed a trend towards elevated freezing behaviors. **(D)** A comparison of lip-rubbing behavior in adult zebrafish injected with 10 μM AITC, 100 μM IMQ, and 100 μM loxoribine. Only IMQ evoked significant lip-rubbing behavior. ***$P < 0.001$, **$P < 0.01$, one-way ANOVA.

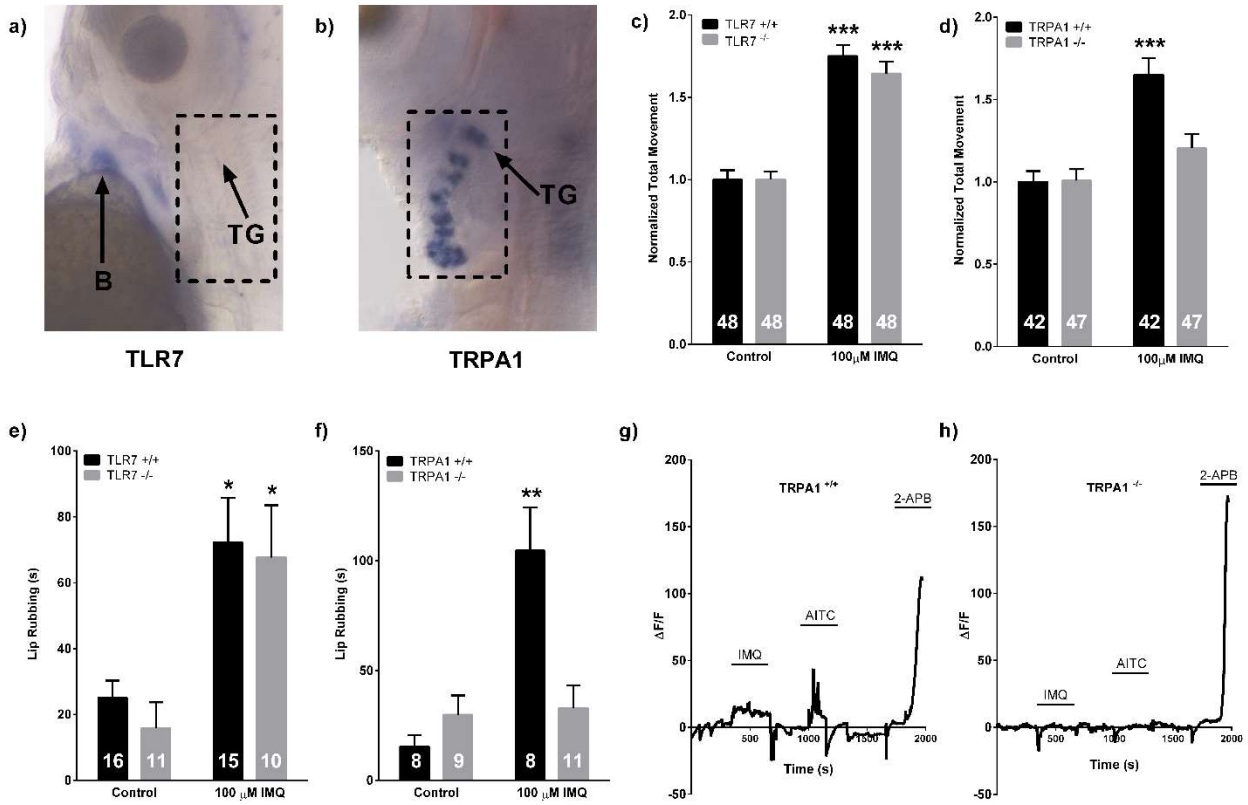

Figure 2: Trpa1b, but not Tlr7, is required for both neuronal and behavioral responses to IMQ. (A, B) *In situ* hybridization in 3dpf WT larvae probing for *tlr7* and *trpa1b* mRNA respectively. **(C, D)** Larval locomotor assay of 5dpf $tlr7^{+/+}$ and $tlr7^{-/-}$ (**C**) or $trpa1b^{+/+}$and $trpa1b^{-/-}$ (**D**) larvae. **(E, F)** Adult lip-rubbing behavioral assay of $tlr7^{+/+}/tlr7^{-/-}$ (**E**) and $TRPA1^{+/+}/TRPA1^{-/-}$ (**F**) fish. **C**, **D**, **E**, **F**, 100 μM IMQ used. ***P < 0.001, **P < 0.01, Student's *t*-test. Bars represent mean ± s.e.m. **(G, H)** Representative calcium imaging traces of 3dpf $trpa1b^{+/+}$ (**G**) and $trpa1b^{-/-}$ (**H**) larvae in a transgenic *elavl3*HuC:GCaMP5 background exposed to 100 μM IMQ, 50 μM AITC, and 1 mM 2-APB. B = blood, TG = trigeminal ganglion.

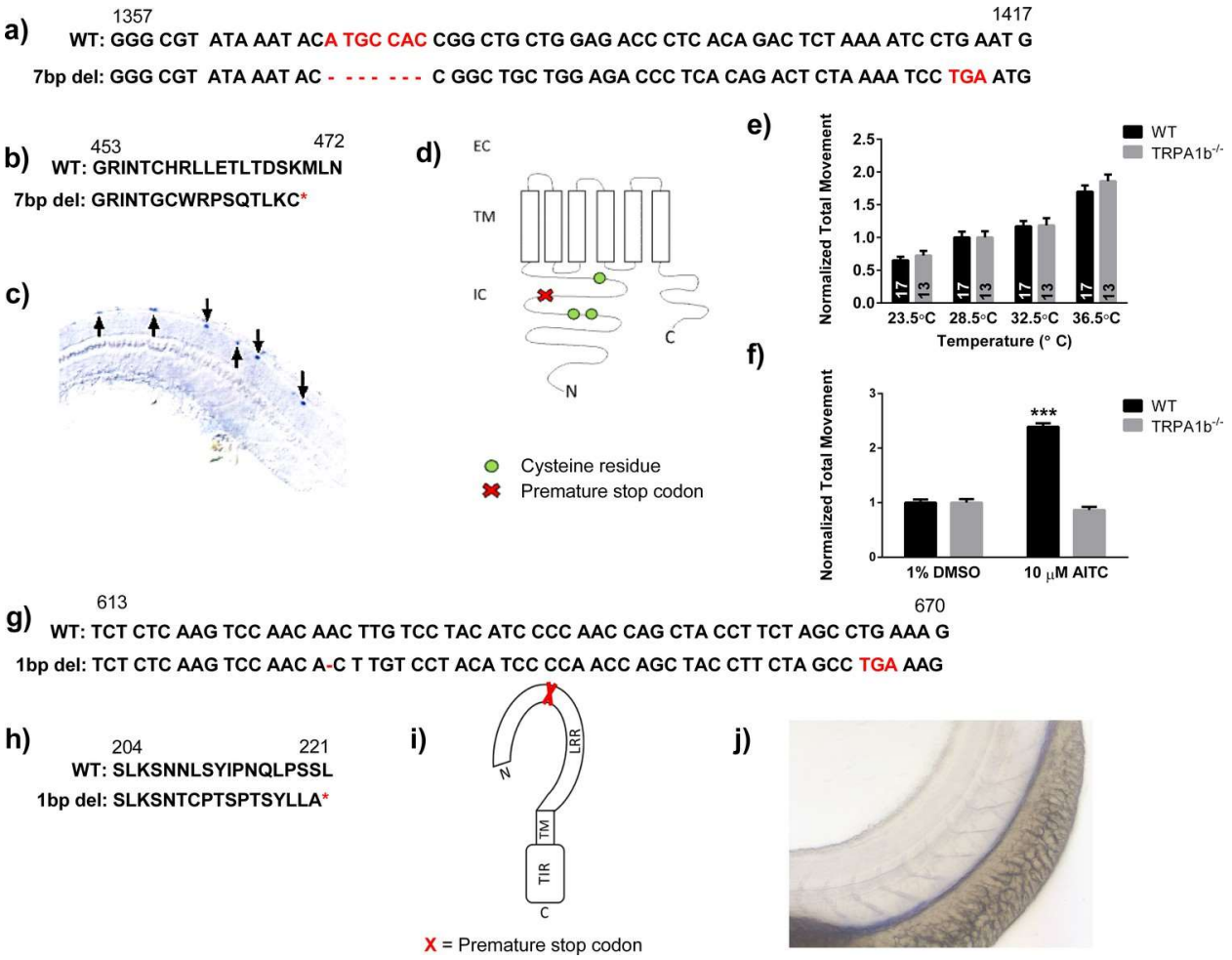

Figure 2-figure supplement 1: TRPA1b and TLR7 nonsense mutations in the zebrafish. (A) The 7bp deletion in the *trpa1b* coding sequence generated a premature stop codon at 1412 bp. **(B)** Amino acid sequences of the WT and mutant Trpa1b proteins. **(C)** *In situ* hybridization probing for *trpa1b* mRNA in WT 3dpf larval zebrafish, demonstrating expression in RB neurons. **(D)** Schematic of the Trpa1b protein structure, demonstrating that a truncated protein (in the unlikely event that it was translated) would lack a critical cysteine residue required for agonist binding (Macpherson, L. J. *et al.*, 2007). **(E)** *Trpa1b*$^{-/-}$ nonsense mutants locomoted more in response to increasing temperatures at levels equivalent to their WT/heterozygous siblings. **(F)** Normal AITC behavioral responses (increased locomotion) are abolished in *trpa1b*$^{-/-}$ nonsense mutants. **(G)** The 1bp deletion in the *tlr7* coding sequence generated a premature stop codon at bp 665. **(H)** Amino acid sequences of WT and mutant Tlr7 proteins. **(I)** Schematic of the Tlr7 protein, demonstrating that a truncated protein (in the unlikely event of translation) would lack critical functional domains. **(J)** *in situ* hybridization probing for *tlr7* mRNA in WT 3dpf larval zebrafish. No *tlr7* expression was observed in RB somatosensory neurons. Premature stops are denoted with red highlighting. EC = extracellular, IC = intracellular, TM= transmembrane domain, LRR = leucine rich repeat, TIR = Toll Interleukin-1 Resistance domain. C and N denote c- and n-termini. **E,** Student's t test.

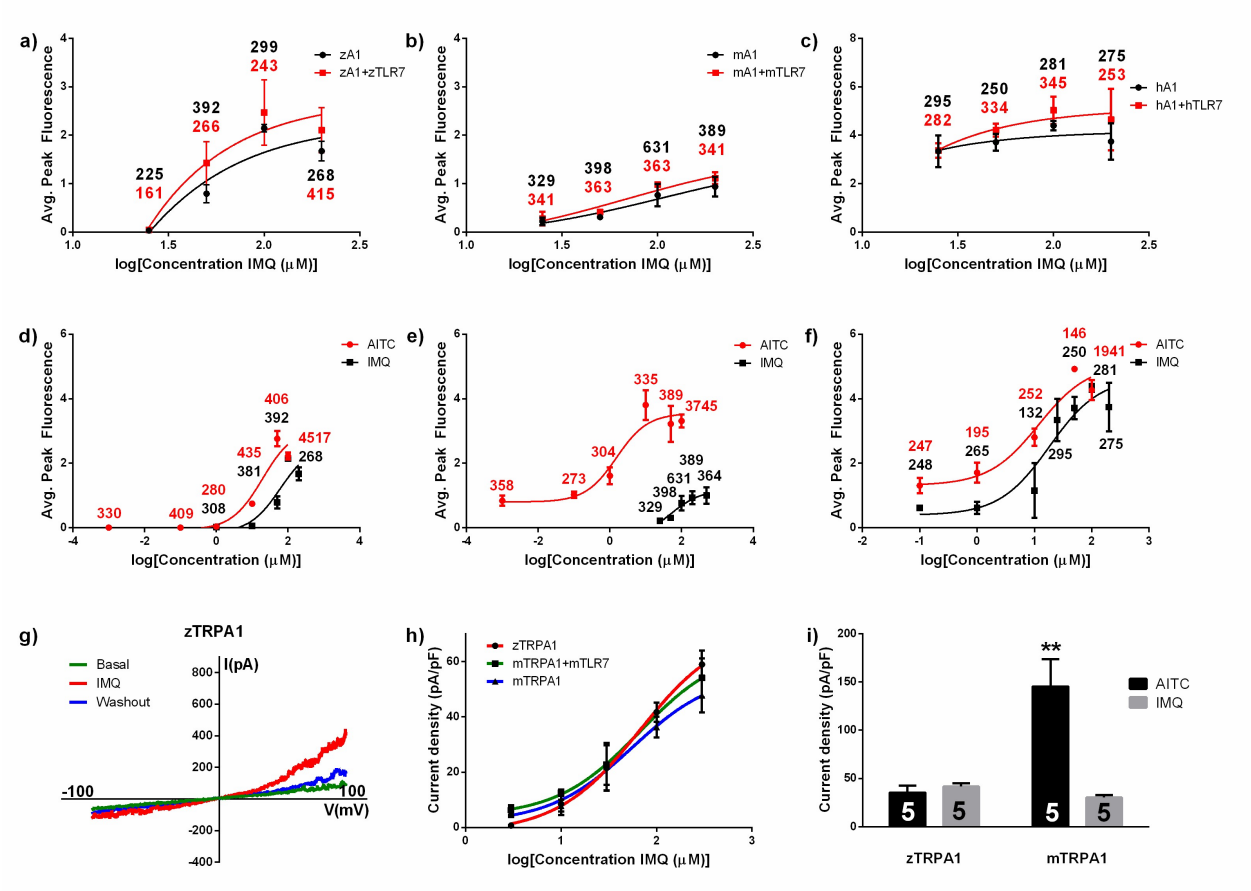

Figure 3: Imiquimod directly activates TRPA1. (A-C) Calcium imaging of HEK cells transfected with zebrafish (**A**), mouse (**B**), and human (**C**) *Trpa1* or *Trpa1+Tlr7*. (**D**, **E**, **F**) Calcium imaging dose response curves of HEK cells transfected with zebrafish (**D**), mouse (**E**), and human (**F**) *Trpa1*, exposed to IMQ or AITC. **A-F** Numbers represent total cell counts per condition. **(G)** Patch clamp of HEK cell transfected with zebrafish *trpa1b* exposed to 100 μM IMQ. **(H)** Patch clamp dose response curve for HEK cells transfected with zebrafish *trpa1b*, mouse *Trpa1*, or mouse *Trpa1*+mouse *Tlr7*. **(I)** Current density values of HEK cells exposed transfected with zebrafish *trpa1b* or mouse *Trpa1* and exposed to 100 μM AITC or 100 μM IMQ. **G-I,** $n = 5$ cells per condition. **P < 0.01, Student's *t*-test. Bars represent mean ± s.e.m.

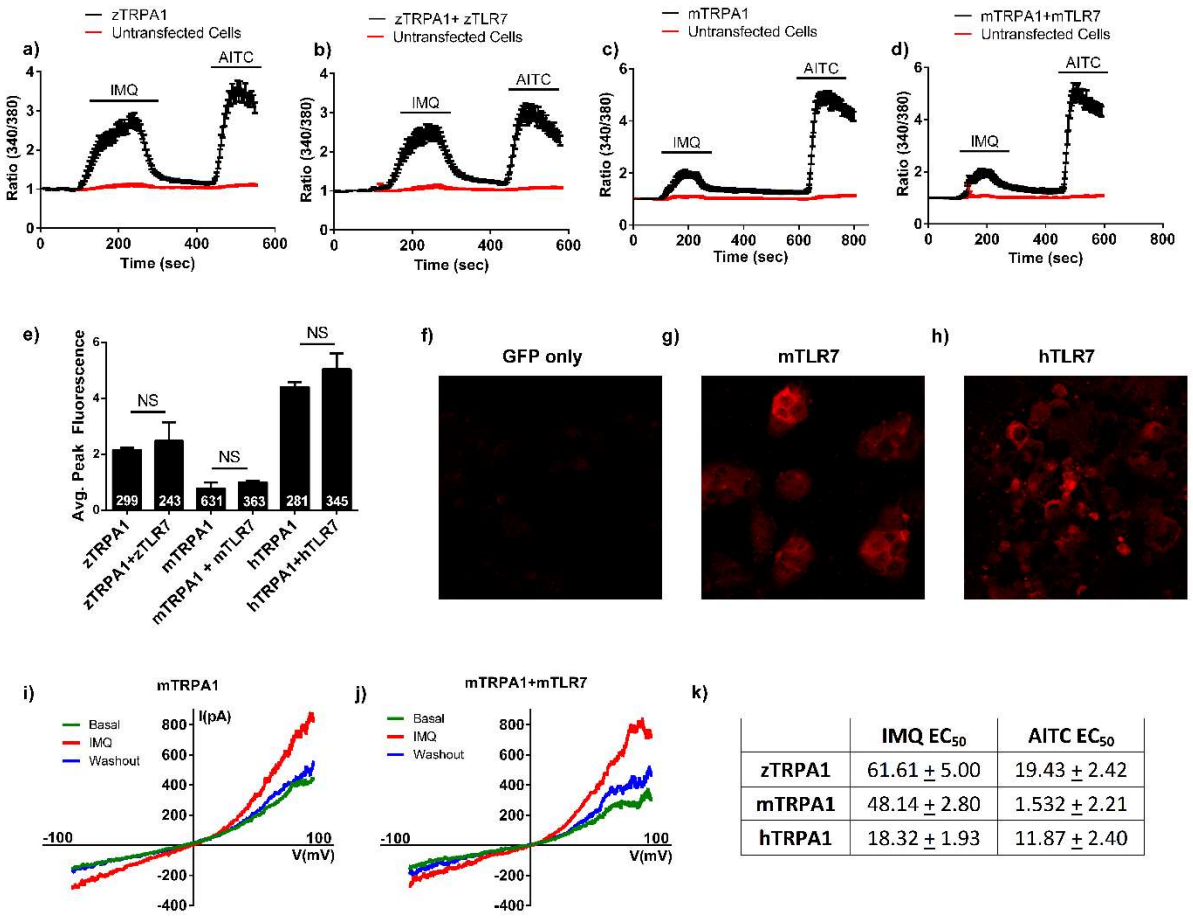

	IMQ EC_{50}	AITC EC_{50}
zTRPA1	61.61 ± 5.00	19.43 ± 2.42
mTRPA1	48.14 ± 2.80	1.532 ± 2.21
hTRPA1	18.32 ± 1.93	11.87 ± 2.40

Figure 3-figure supplement 1: Transfected HEK cell gene expression and functionality. (A-D) Average traces from calcium imaging experiments with HEK cells transiently transfected with zebrafish *trpa1b* (*n* = 85) (**A**), zebrafish *trpa1b*+zebrafish *tlr7* (*n* = 80) (**B**), mouse *Trpa1* (*n* = 134) (**C**), or mouse *Trpa1*+mouse *Tlr7* (*n* = 89) (**D**). *n* = 22, 23, 10, and 19 untransfected control HEK cells per experiment, respectively. No gross differences were observed between the two conditions for each species. **€** Quantification of peak fluorescence intensity achieved during stimulation with 100 µM IMQ across all HEK cell transfection conditions. In all species examined, no significant difference was observed between cells transfected with only *Trpa1* and cells transfected with *Trpa1* plus the corresponding *Tlr7*. **(F-H)**, Immunohistochemistry performed on HEK cells transfected with pIRES-eGFP only (**F**), mouse *Tlr7* (**G**), or human *TLR7* (**H**). As shown, TLR7 labeling (red) was only observed HEK cells transfected with *Tlr7* constructs. **(I-J),** I/V curves from voltage clamp experiments using cells transfected with mTRPA1 (**I**) and mouse *Trpa1*+mouse *Tlr7* (**J**). As shown in **(I)**, 100 µM IMQ elicited greater current influx in transfected cells than under basal conditions, an effect that disappeared during washout. Cells transfected with both mouse *Trpa1* and mouse *Tlr7* also showed significant current flux during IMQ stimulus, but this was not different from cells transfected only with mTRPA1. *n* = 5 cells per condition. **(K)** a table of EC50 values for both IMQ and AITC stimuli in cells transfected with zebrafish *trpa1b*, mouse *Trpa1*, and human *TRPA1* in **Figure 3D-F**. As shown, the EC50 values for IMQ are much greater than those of AITC for all species of

TRPA1. ΔF/F (fluorescence intensity change) is expressed as a normalized 340nm/380nm intensity ratio. (*P < 0.05, **P < 0.01, ***P < 0.001, Student's t-test. Bars are expressed as means $\pm$ s.e.m.

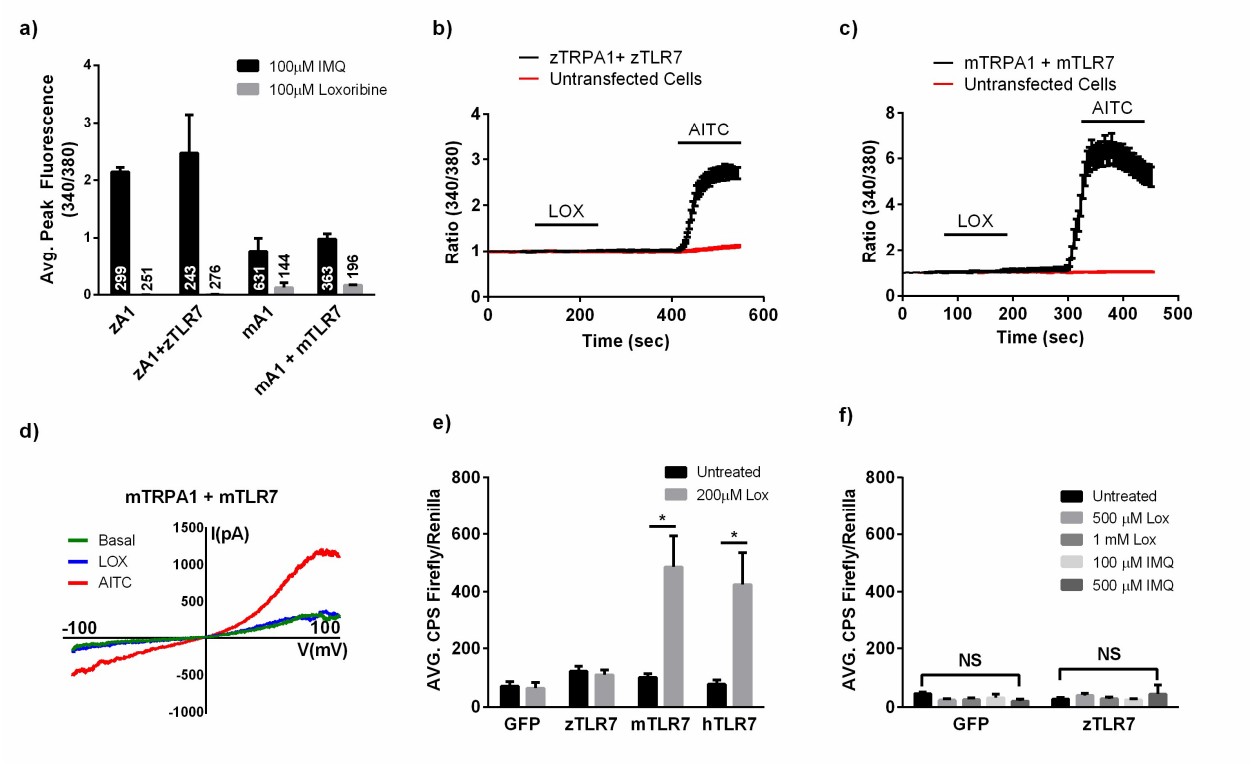

Figure 3-figure supplement 2: Loxoribine effectively stimulates TLR7-transfected HEK cells but does not evoke intracellular calcium flux. (A) A comparison of average peak fluorescence values obtained from *Trpa1* or *Trpa1*+*Tlr7* transfected HEK cells in calcium imaging experiments following stimulation by 100 μM IMQ or 100 μM loxoribine. **(B, C)** Average traces from calcium experiments in which HEK cells were transfected with zebrafish *Trpa1b*+zebrafish *tlr7* (n = 102) (**B**) or mouse *Trpa1*+mouse *Tlr7* (n = 45) (**C**) and treated with 100 μM loxoribine and 100 μM AITC. 15 and 21 untransfected control cells were present in each respective experiment. As shown, loxoribine did not elicit any calcium flux. **(D)** I/V curve from voltage clamp experiments in which HEK cells were transfected with mouse *Trpa1*+mouse *Tlr7* and stimulated with both loxoribine (100 μM) and AITC (100 μM). While AITC elicited remarkable current influx, current change associated with application of loxoribine did not change current flow above baseline levels. **(E)** A dual luciferase assay to verify the functionality of transfected TLR7 and loxoribine. Cells transfected with only the two luciferase constructs and pIRES-eGFP did not demonstrate any NF-kB induction following stimulation with 200 μM loxoribine, as expected. Notable NF-kB induction was observed in cells transfected with the two luciferase constructs and either mouse *Tlr7* or human *TLR7* following stimulation with loxoribine. Intriguingly, cells transfected with the zebrafish *tlr7* did not exhibit any significant NF-kB induction following application of loxoribine. **(F)** A dual luciferase assay in which both pIRES-eGFP-transfected control HEK cells and zebrafish *tlr7*-transfected cells were treated with TLR7 agonists loxoribine (500 μM and 1 mM) and IMQ (100 μM and 500 μM). There was no difference in NF-kB induction between pIRES-eGFP-only and zebrafish *tlr7* transfected cells, potentially indicating that zebrafish Tlr7 is unresponsive to typical mammalian TLR7 agonists. ΔF/F (fluorescence intensity change) is expressed as a normalized 340nm/380nm intensity ratio. Luminosity values are expressed as the firefly/renilla ratio of relative light units in counts per

second (CPS) following background subtraction. *P < 0.05, **P < 0.01, ***P < 0.001, Student's t-test (**A, E**) or one-way ANOVA (**F**). Bars are expressed as means $\pm$ s.e.m.

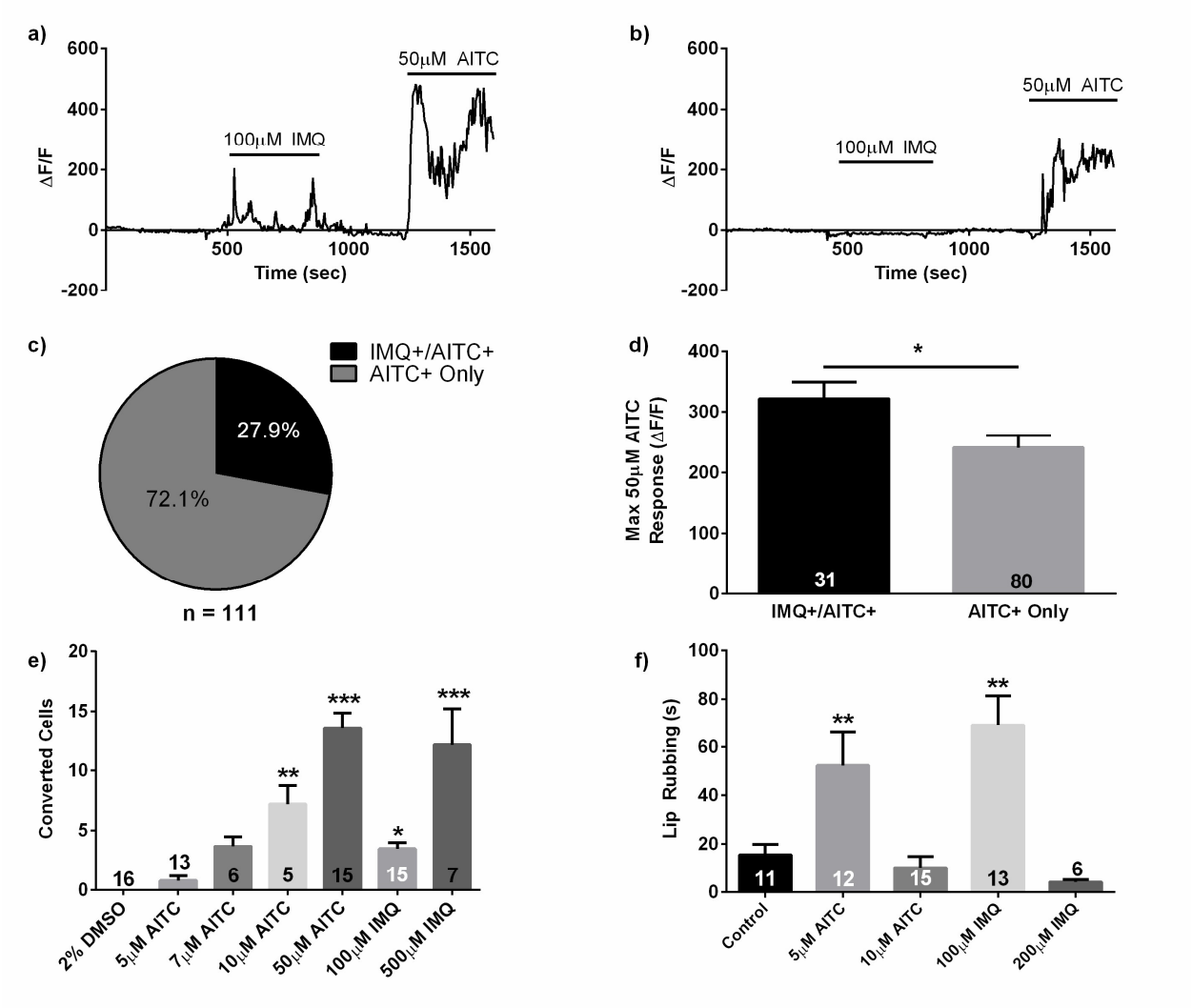

Figure 4: Imiquimod responsive cells are a primed subpopulation of TRPA1 positive cells and stimulus intensity affects behavioral and neuronal responses. (**A, B)** Representative traces from calcium imaging experiments in 3dpf *elavl3*:H2BGCaMP6 zebrafish exposed to 100 μM IMQ and 50 μM AITC. An IMQ+/AITC+ TG neuron is shown in (**A**), while an AITC+ only neuron is shown in (**B**). **(C)** Quantification of neuronal subtypes within AITC+ neurons. *n* = 31 IMQ+/AITC+ neurons, *n* = 80 AITC+ only neurons. **(D)** Comparison of the maximum ΔF/F during the 50 μM AITC stimulus between neuronal subtypes. **(E)** Number of photoconverted neurons in 3dpf *elavl3*:CaMPARI zebrafish TG following stimulation with TRPA1 agonists. **(F)** Quantification of lip-rubbing behavior in adult zebrafish following exposure to TRPA1 agonists. Bars represent means ± s.e.m. *P < 0.05, **P < 0.01, ***P < 0.001, Student's t-test (**D),** one-way ANOVA (**E, F**).

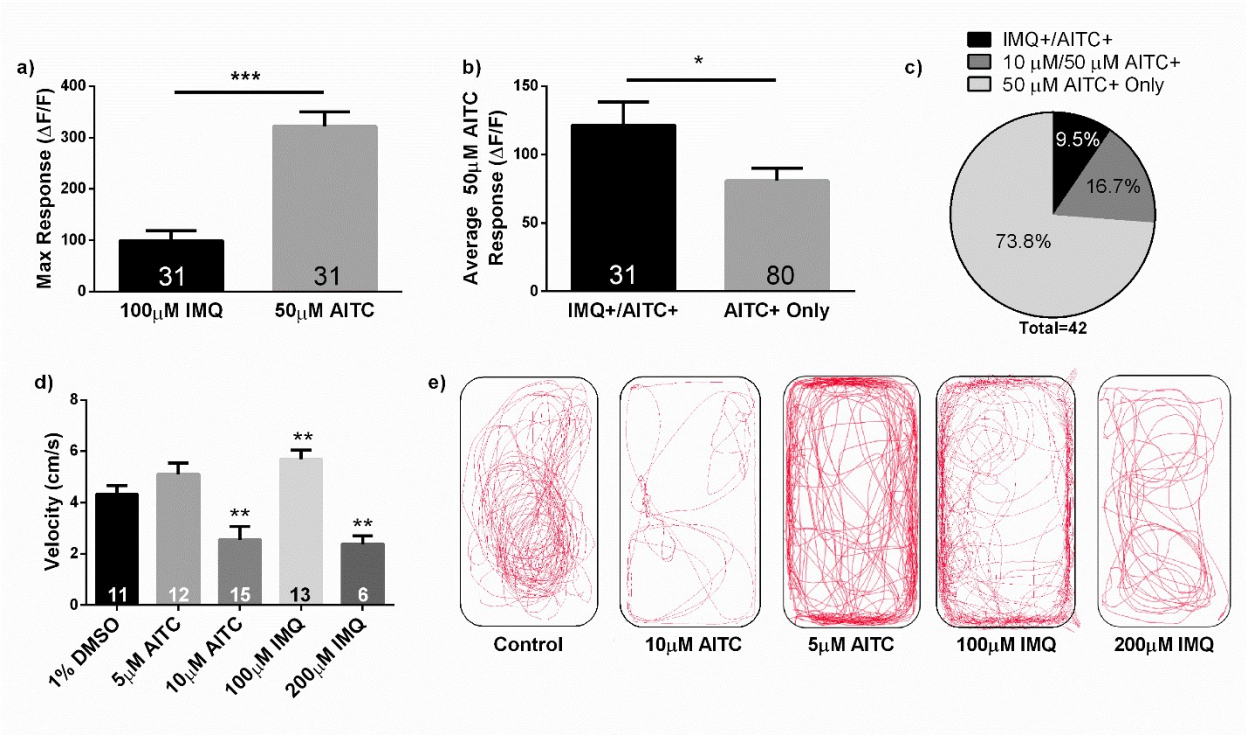

Figure 4-figure supplement 1: Further effects of stimulus intensity on zebrafish neuronal activity and behavior. (A) IMQ is a lower intensity stimulus than AITC. Application of 100 μM IMQ elicited a lower maximal ΔF/F response than application of 50 μM AITC in IMQ+/AITC+ TG neurons in 3dpf larval zebrafish. **(B)** In an effort to ensure that our analyses in **Figure 4D** were accurate reflections of neuronal activity, we also examined the average ΔF/F across the stimulus period. We found that IMQ+/AITC+ cells exhibited a significantly higher average fluorescence change across the entire 50 μM AITC stimulus period than AITC+ only responding neurons. **(C)** Sequential application of 100 μM IMQ, 10 μM AITC, and 50 μM AITC revealed that IMQ+ neurons (n = 4) were only found in a subset of neurons that responded to 10 μM AITC (n = 11), which themselves were included in a larger population of 50 μM AITC+ neurons (n = 42). 50 μM AITC results were consistent with previous experiments. **(D)** Swimming velocity in adult zebrafish also varied as a function of stimulus intensity. Fish that were injected with 100 μM IMQ (n = 13) exhibited a significant increase in swimming velocity as compared to fish injected with 1% DMSO vehicle (n = 11). Fish injected with 10 μM AITC (n = 15) and 200 μM IMQ (n = 6) exhibited significant reductions in swimming velocity as compared to vehicle-injected controls, suggesting that these stimuli at these particular concentrations are effectually algogenic. 5 μM AITC evoked no significant change in swimming velocity (n = 12). ΔF/F (fluorescence intensity change) is calculated as the percent change over baseline fluorescence. Bars are expressed as means $\pm$ s.e.m. *P < 0.05, **P < 0.01, ***P < 0.001, Student's t-test (**A, B**), one-way ANOVA (**D**). (**E**) Representative traces of adult behavior.

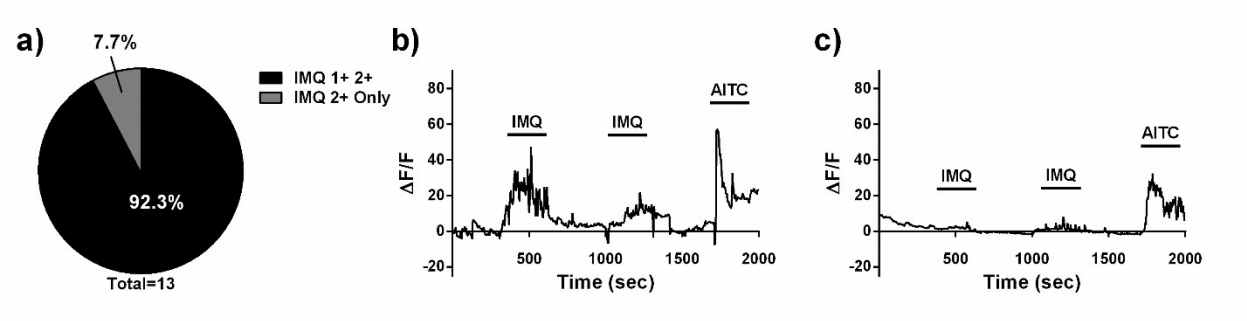

Figure 4-figure supplement 2: Imiquimod activates a specific subset of neurons in a non-stochastic manner in the zebrafish. (A) Proportions of neurons responding to two sequential pulses of 100 μM IMQ, only the first pulse, or only the second pulse in 3dpf larval zebrafish. **(B)** Representative trace of a TG neuron that responded to both pulses of 100 μM IMQ. **(C)** Representative trace of a TG neuron that responded to only the second pulse of 100 μM IMQ.

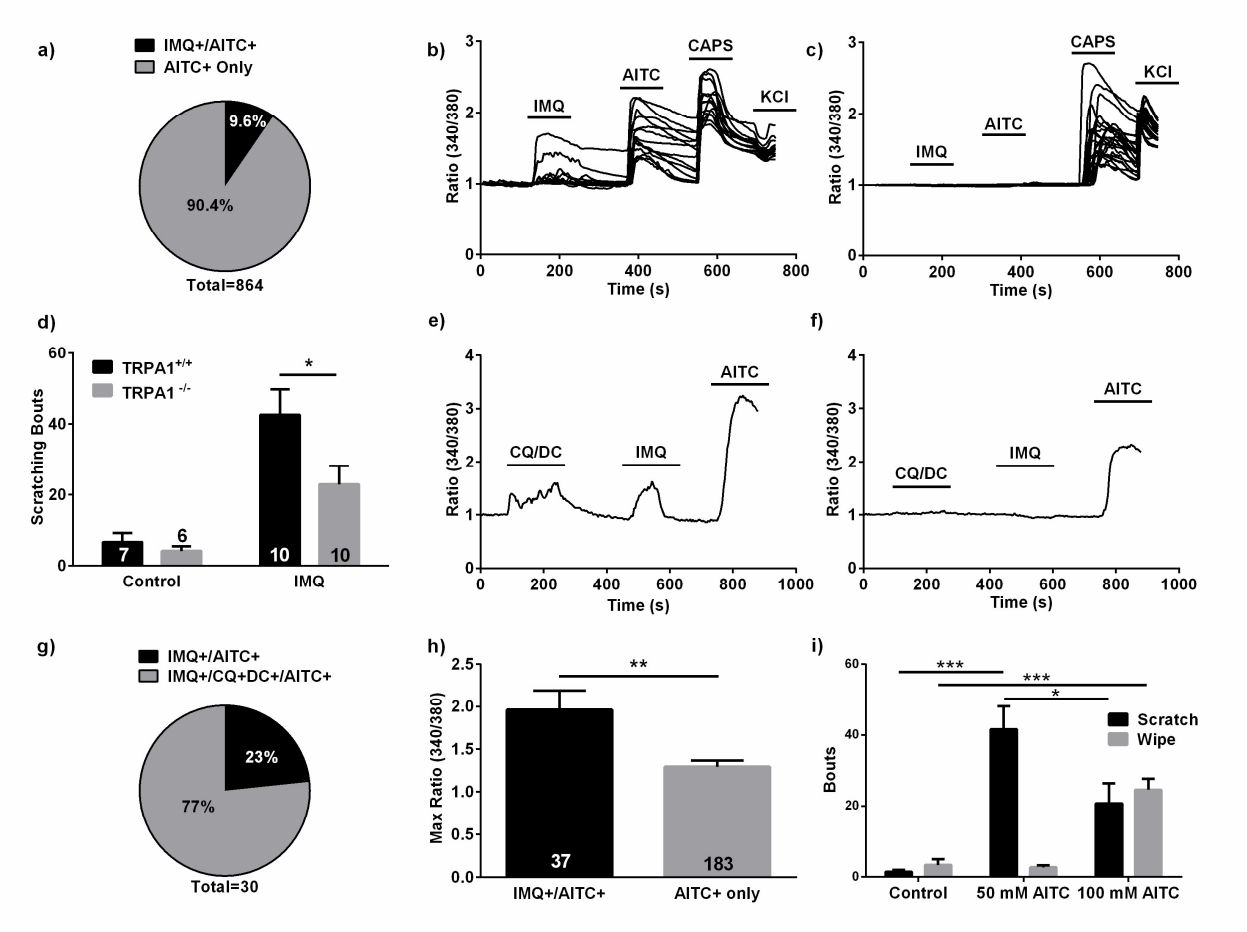

Figure 5: Imiquimod's effects in the mouse. (A) Proportions of IMQ+/AITC+ and AITC+ only DRG neurons observed in calcium imaging experiments (n = 83 IMQ+/AITC+ neurons, n = 781 AITC+ only DRG neurons). **(B, C)** Representative traces from calcium imaging experiments on dissociated mouse DRG neurons from WT (**B**) (n = 15 neurons) and *Trpa1*$^{-/-}$ (**C**) (n = 23 neurons) mice. **A-C**, 100 μM IMQ and 100 μM AITC used. **(D)** Quantification of scratching bouts in WT and *Trpa1*$^{-/-}$ mice following IMQ (10 μg) injections. **(E, F)** Representative traces from calcium imaging experiments in which 100 μM IMQ, 100 μM CQ, 100 μM DC, and 100 μM AITC were applied. IMQ+/CQ+DCA+/AITC+ (**e**) and AITC+ only (**f**) neurons are shown. **(G)** Quantification of the IMQ+ neuronal populations from the experiments shown in **(E, F)** (n = 27 IMQ+/CQ+DCA+/AITC+ neurons, 7 IMQ+/AITC+ neurons). **(H)** Comparison of maximum ΔF/F between IMQ+/AITC+ and AITC+ only. 100 μM IMQ, 10 μM AITC used. All calcium imaging experiments performed on dissociated mouse DRG neurons. **(I)** Quantification of scratching bouts in WT mice following injections of varying AITC concentrations. *P < 0.05, **P < 0.01, ***P < 0.001, Student's t-test. Bars are expressed as mean + s.e.m.

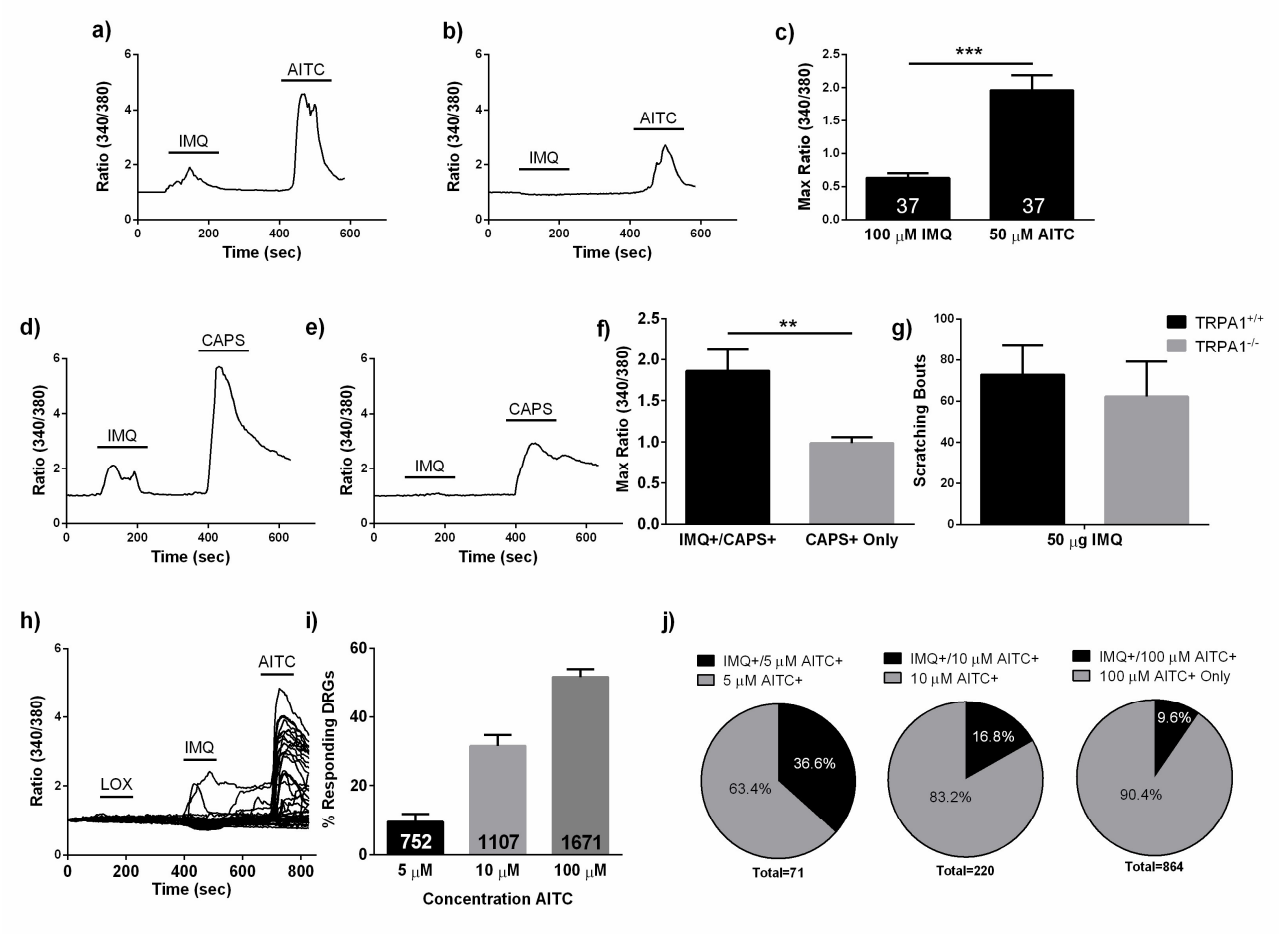

Figure 5-figure supplement 1: Calcium imaging of discrete neuronal subpopulations in the mouse. (A, B) Representative traces from calcium imaging experiments featuring dissociated mouse DRG neurons sequentially bathed in 100 μM IMQ and 10 μM AITC. IMQ+/AITC+ (**A**) and AITC+ only (**B**) neurons were both identified. As shown in (**B**), many of the AITC+ only neurons peaked at lower ΔF/F values than the IMQ+/AITC+ neurons. **(C)** Within the IMQ+/AITC+ population (*n* = 37 neurons), 100 μM IMQ was demonstrated to be a weaker stimulus than 10 μM AITC. **(D, E)** Representative traces of calcium imaging experiments where DRG neurons were stimulated with 100 μM IMQ and 100 nM CAPS. Two main functional subpopulations were identified--one that responded to both IMQ and CAPS (**D**), and another that responded only to 100 nM CAPS (**E**). Interestingly, many of the CAPS+ only cells peaked at lower ΔF/F values during the CAPS stimulus than the neurons that responded to both IMQ and CAPS. **(F)** Comparison of maximum ΔF/F between IMQ+/CAPS+ and CAPS+ only neurons. **(G)** Quantification of scratching bouts in WT and *Trpa1*$^{-/-}$ mice following IMQ injections. **(H)** Representative traces from from one calcium imaging experiment in which 100 μM loxoribine was applied to dissociated DRG neurons. As shown, loxoribine did not elicit any fluorescence changes in DRG neurons (*n* = 51), whereas 100 μM IMQ and 100 μM AITC elicited robust intracellular calcium flux. **(I)** Increasing the concentration of AITC activates greater proportions of DRG neurons (71/752, 379/1107, and 864/1671 neurons for the 5 μM, 10 μM, and μM AITC experiments). **(J)** IMQ+ neuron populations are enriched within populations that respond to

lower concentrations of AITC (26/71 5 μM AITC+ neurons, 37/220 10 μM AITC+ neurons, 83/864 100 μM AITC+ neurons). Fluorescence intensity is expressed as ΔF/F using the 340/380 ratio values. Bars represented as means + s.e.m., Student's t-test. *P < 0.05, **P < 0.01, ***P < 0.001.

2.9 Chapter Videos

Video 1: Normal adult zebrafish swimming behavior. This video is an example of typical swimming behavior following a cutaneous injection of 1% DMSO into the upper lip of an adult zebrafish. Note that the zebrafish exhibits minimal interaction with the walls of the tank, and its swimming capacity is not compromised. https://doi.org/10.7554/eLife.32036.005

Video 2: Adult zebrafish injected with AITC demonstrate nocifensive behaviors. This video is an example of typical swimming behavior following a cutaneous injection of 10 μM AITC into the upper lip of an adult zebrafish. The zebrafish exhibits previously described nocifensive behaviors, such as dramatically reduced locomotion, bouts of freezing, and heightened respiration. https://doi.org/10.7554/eLife.32036.006

Video 3: Adult zebrafish injected with IMQ demonstrate pruritic behaviors. This video provides a typical example of swimming behavior observed in adult zebrafish following a cutaneous upper lip injection of 100 μM IMQ. The fish not only exhibits increased swimming velocity in response to this stimulus, but also frequently rubs its lips against the walls of its tank, engaging in a behavior that is potentially analogous to mammalian scratching. https://doi.org/10.7554/eLife.32036.007

Chapter 3: Exploring the differences between distinct subpopulations of differentially-tuned TRPA1 neurons

3.1 Chapter Abstract

While we previously established that differential activation of subpopulations of TRPA1 neurons with differing sensitivities to agonists might underlie the differences in behavioral responses to low- and high-intensity stimuli, the factors that distinguished these neurons remained unclear. Through a combination of neuronal calcium imaging experiments in both zebrafish and mice, and behavioral studies in the zebrafish, we sought to elucidate whether certain morphological features may differ between subgroups of TRPA1 neurons, and whether certain intracellular signaling cascades may be involved in setting the gain within these populations. We found that, in the mouse, innervation destination did not determine the sensitivity of a neuron, as TRPA1 neurons of varying sensitivities could be found projecting to the same area. We established that neurons with heightened sensitivity to TRPA1 agonists were significantly smaller than less-sensitive neurons. Furthermore, we found that PLC activation increased neuronal recruitment to low-intensity stimuli in both zebrafish and mice, whereas PLC inhibition decreased neuronal recruitment to medium-intensity stimuli which had previously elicited responses from neurons in mice. PLC activation likewise sensitized behavioral responses to TRPA1 agonists in larval zebrafish. Together, these results indicate that highly-sensitive TRPA1 neurons are indeed part of a discrete subpopulation, and suggest that differences in basal PLC signaling between subpopulations of TRPA1 neurons may contribute to differences in their response thresholds to TRPA1 agonists, providing additional insight into the neural coding strategies underlying itch and pain sensation in different species.

3.2 Chapter Introduction

Findings from our previous studies implicate the existence of multiple subpopulations of TRPA1-expressing somatosensory neurons with varying sensitivities to noxious stimuli, and that differential activation of these neurons correlates with different behaviors (e.g., pruritic vs. nocifensive). This begs the following questions: what factors underlie the differences between these populations? Seeking the answer to this question motivated the following experiments. In particular, we opted to explore metrics such as morphological differences (e.g. cell size, innervation destination) and intracellular signaling cascades previously shown to modulate TRP ion channel function.

Somatosensory neurons of different modalities exhibit clear morphological differences. For example, neurons that relay proprioceptive information (the Aα fibers) and innocuous touch information (the Aβ fibers) have large soma and axon diameters (>50 μm and 6-20 μm, respectively), and are more heavily myelinated[26,27]. Aδ fibers, the high-threshold mechanoreceptors that relay painful touch, have smaller soma and axon diameters (~20-40 μm and 1-5 μm)[26,27,207]. Unmyelinated C-fibers, comprising the chemical/thermal nociceptors (including TRPA1 neurons) as well as neurons associated with pleasant or affective touch, have the smallest cell bodies (10-30 μm) and axon diameters (0.2-1.5 μm)[26,27]. Morphological differences beyond cell size and axon diameter have also been reported, even within neurons of the same subtype. Low-threshold mechanoreceptors (LTMRs), for example, can display both lanceolate and circumferential arborization patterns in the periphery[208–210]. CGRP-expressing peptidergic C-fiber nociceptors can likewise differ in peripheral morphology, exhibiting free nerve endings as well as circumferential endings in the skin[209–211]. Subtypes of somatosensory neurons in the mouse have been shown to project to distinct regions of the epidermis[212].

Diversity similarly exists in the central projections of somatosensory neurons of different subtypes. MrgprD-expressing C-fibers (a type of non-peptidergic nociceptor) exhibit different central arbor morphologies correlating to the sensory acuity of the body region they innervate[213]. Analogous observations have been made in the zebrafish, where some somatosensory subtypes in the trigeminal ganglia exhibit differences in branching morphology of central terminals and presynaptic site distribution[214]. Given the morphological distinctions both between and within groups of somatosensory neurons, we hypothesized that such differences may exist within our population of TRPA1 neurons, and may indeed be an indication that these neurons are distinct subpopulations.

On a molecular level, different populations of TRPA1 neurons associated with itch vary in the complement of additional pruritic and inflammatory GPCRs they co-express, and which intracellular signaling cascades functionally couple the two[13,62,72,83,85,89,92]. However, the participation of such signaling pathways in the transduction of itch resulting from the direct activation of a TRP channel is unknown. Interestingly, activation of these pathways has been shown to sensitize TRPA1, making them logical molecular candidates in establishing the responsivity of subpopulations. In other words, higher baseline activity levels of one of these pathways in a particular subpopulation may lend a heightened sensitivity to the neurons within this subpopulation. Of particular interest to us where the phospholipase C (PLC), protein kinase A (PKA), and protein kinase C (PKC) signaling cascades, as well as Gβγ signaling and NALCN activity.

The PLC and PKA pathways link activation of the bradykinin receptor (B2) to TRPA1[72,215]. Certain PLC isoforms (e.g. PLCβ3) function to cleave phospholipids, such as the phosphoinositides, to further generate signaling molecules. In this case, PLC activated by the

bradykinin receptor can cleave PIP2 to produce diacylglycerol (DAG), which can then in turn activate TRPA1[72]. IP3, another product of PIP2 cleavage, elicits the release of calcium from intracellular stores, and some evidence suggests that this calcium, along with other products of the PLC pathway (such as arachidonic acid, or AA) can also influence TRPA1 activity[72,85]. Both PKA and PLC activation can potentiate AITC-evoked currents in dissociated DRGs, and their blockade can reverse bradykinin-induced potentiation of AITC currents; additionally, occlusion experiments demonstrate that these pathways operate in parallel, rather than one being downstream of the other[215]. Only PKA activation has been shown to significantly potentiate behavioral responses to injections of AITC—PLC activation has instead been observed to elicit noticeable, but yet non-significant, increases in pain behaviors, although this might have been due to technical constraints in the study that demonstrated these phenomenon (i.e., the inability to increase the concentration of PLC activator drug without causing off-target effects from the vehicle solvent)[216]. Inhibiting PLC, however, has demonstrable behavioral effects. Systemic treatment with the PLC inhibitor drug U-73122 can reverse the decrease in pain thresholds elicited by spared nerve injury[217]. This method of inhibition has also been shown to block morphine-induced hyperalgesia[218] as well as carrageenan-induced inflammatory hyperalgesia[219]. PKA and PLC signaling are also critical in TRPA1 translocation to the membrane following stimulation with TRPA1 agonists[216]. As mentioned in Chapter 1, PLC signaling is not only restricted to the functional coupling between TRPA1 and the bradykinin receptor; MrgprC11, which is activated by endogenous pruritogens like BAM8-22, requires PLC signaling to activate TRPA1[85], and the pruritic and inflammation receptor PAR2, which is activated by endogenous proteases, similarly relies on PLC to potentiate TRPA1 activity[220].

In addition to generating signaling molecules like DAG and IP3, cleavage of PIP2 by PLC can deplete PIP2 from cell membranes, which itself can serve an important regulatory function. The sensitization of TRPA1 by PAR2 activation (via PLC activation) has been proposed to be a direct result of PIP2 depletion in the membrane—inclusion of PIP2 in the recording pipette diminishes the PAR2-induced potentiation of AITC currents from cultured DRG neurons, and applying a PIP2 antibody to sequester this phospholipid mimics the effects of PLC activation[220]. PIP2 has also been suggested to serve as a negative regulator of another TRP ion channel, TRPV1, though its exact role is controversial due to several conflicting reports[221]. Antibody sequestration of PIP2 recapitulates the potentiating effects of bradykinin and NGF on TRPV1 neurons[222]; electrophysiological experiments with TRPV1 reconstituted in artificial lysosomes likewise suggest that PIP2 negatively regulates this TRP channel[223]. However, similar excised patch experiments demonstrate that PIP2 may have opposing effects depending upon the membrane leaflet in which it is localized—this phospholipid can potentiate capsaicin currents when present in the intracellular leaflet, but can also inhibit the channel when present in both leaflets[221]. Whether this is analogous for TRPA1 is unknown.

Protein kinase C (PKC), another important intracellular signaling molecule, has also been implicated in TRP ion channel regulation and activation, but its role in sensitizing TRPA1 is unclear. The PKC pathway can be activated downstream of PLC (via DAG and intracellular calcium release)[219,224]. TRPV1 sensitization by PAR2 appears to involve PKC, as pharmacological inhibition of this enzyme prevented PAR2 agonist-induced potentiation of responses to capsaicin[225]. However, evidence linking PKC signaling to TRPA1 activation and regulation is mixed. Some studies have identified several putative PKC binding sites on TRPA1; although their functional roles have yet to be studied, this could imply a role for PKC signaling

in modulating TRPA1 activity and thus potentially neuronal sensitivity[226]. PKC signaling may be involved in the coupling of bile acid receptor TGR5 to TRPA1, as inhibition of this enzyme prevented responses to deoxycholic acid in both a heterologous expression system and somatosensory neurons[83]. Conversely, PKC did not appear to be involved in the sensitization of TRPA1 by PAR2 receptor agonists[220]. However, this study also found that OAG, a DAG analog, did not potentiate AITC or cinnamaldehyde-induced currents, in contrast to that observed by Bandell et al[72]. PKC also does not appear to underlie the sensitization of TPRA1 by bradykinin, as pharmacological inhibition with GF109203X did not significantly alter the effects of bradykinin on AITC currents in HEK cells transfected with TRPA1 and B2; similarly PMA, a PKC activator, did not potentiate AITC currents[215].

Most of the aforementioned signaling pathways function downstream of activated G proteins. PKA, for example, can be activated by Gs coupled to the B2 receptor[227], and Gq/11 proteins coupled to PAR2 can activate PLC pathways[220]. However, G proteins themselves can directly activate ion channels[228], and evidence suggests that the Gβγ subunit in particular can directly activate TRPA1. For example, the coupling of the chloroquine-sensitive itch receptor MrgprA3 to TRPA1 appears to rely on Gβγ proteins[85]. Similarly, S1PR3 is thought to signal through Gβγ to activate TRPA1 in a subpopulation of neurons, leading to the sensation of itch[84].

Other ion channels activated downstream of GPCRs may also play a role in mediating the excitability of somatosensory neurons. One such channel is NALCN, a sodium “leak” channel present in a variety of tissues, including the central nervous system, heart, adrenal glands, thyroid, lymphatic tissues, and pancreas[229]. It can be activated downstream of acetylcholine receptors[230]. In the central nervous system, NALCN is thought to contribute to neuronal excitability, leading to depolarization of the resting membrane potential; pharmacological

blockade of this channel significantly reduces the frequency of spontaneous firing in hippocampal neurons, and neurons obtained from NALCN mutant mice are hyperpolarized compared to those from wildtype mice[231]. The role of NALCN in pain is somewhat more complex. In spinal projection neurons of the superficial dorsal horn, which are critical for the transmission of nociceptive signals, NALCN is critical for maintaining excitability—neurons from NALCN knockout animals display hyperpolarized resting membrane potentials and a reduction in spontaneous firing[232]. Additionally, NALCN can be activated by substance P, a nociceptive neurotransmitter released by primary sensory afferents, via Src kinase pathways[232]. However, NALCN has been observed to play an opposite role in peripheral somatosensory neurons. In highveld mole rats, for example, high expression of NALCN in TRPA1 neurons may confer an insensitivity to TRPA1 agonist algogens—the increased depolarization due to NALCN currents is thought to prevent action potential firing by inactivating voltage-dependent sodium channels[150]. Given this latter observation, we sought to explore the possibility that differential expression of NALCN in murine TRPA1 neurons may lead to differences in excitability, and thus differences in the sensitivity to TRPA1 agonists, in different subpopulations.

While there is a wealth of research implicating these signaling pathways and other membrane channels in the activation and/or regulation of TRPA1, the role of these pathways in setting a baseline "tone", or responsivity, to TRPA1 agonists has yet to be examined, especially within the context of multiple subpopulations of TRPA1-expressing pruritic neurons. It is possible, for instance, that high levels of baseline signaling in the most sensitive neuron populations may prime these neurons to respond to low-intensity stimuli. For example, if PIP2 indeed functioned as a negative regulator of TRPA1, one could imagine that increased PLC signaling would reduce the effect of this gate, rendering TRPA1 more responsive to stimuli.

Therefore, we hypothesized that pharmacological activation or inhibition of these pathways could effectually serve to toggle the gain on these distinct subsets of TRPA1 neurons. In particular, if a pathway was involved in establishing this response threshold, inhibiting it could transform a highly-sensitive, low-threshold neuron into a less sensitive, high-threshold neuron capable of responding only to the most intense stimuli, a change that should be reflected in neuronal activity as well as behavior. We reasoned that the reverse would also be true—by pharmacologically activating these pathways, we would increase the gain on the system and be able to transform a high-threshold TRPA1 neuron into a low-threshold neuron, which would likewise be reflected in increased neuronal activity as well as behavior.

3.3 Results

3.3.1 Dose-dependent neuronal recruitment occurs independently of innervation target.

It is possible that the differences in AITC sensitivity we observed in our dissociated DRG experiments (**Figure 1A**) were due to differences in innervation target—for example, neurons that innervated regions with higher sensory acuity, such as distal limbs, might have lower thresholds than those innervating less sensitive areas, such as the trunk, visceral organs, and proximal limbs. We would not be able to distinguish these neurons in typical calcium imaging experiments, since DRGs across an entire animal are pooled before dissociation and culture. To address this, we used a lipophilic retrograde tracer, DiI, to label neurons that innervated a highly sensitive region of the skin, the plantar surface of the hindpaw, one week before animals were euthanized and prepared for imaging.

These intradermal DiI injections successfully labeled numerous peripheral somatosensory neurons, and this labeling persisted through dissociation and culturing (**Figure 1B**). Furthermore,

labeled neurons demonstrated the same stratification into subpopulations with differential responsiveness to AITC (**Figure 1C, D**). Labeled neurons did not demonstrate any significant differences from unlabeled lumbar neurons (**Figure 1C, D**). This indicates that the observed differences in sensitivity to AITC is likely a physiologically relevant phenomenon, and not due to differences in innervation target. It likewise indicates that neurons of different sensitivities are not topographically restricted to certain regions of the body.

3.3.2 Cell size correlates with response threshold.

We next sought to determine if neuronal size correlated with responsiveness to AITC. Specifically, we sought to determine if the more sensitive TRPA1 neurons, or those primed to respond to low-intensity stimuli, were smaller than those that were only activated by medium- or high-intensity stimuli. To test this idea, we once more turned towards calcium imaging of dissociated mouse DRG neurons. In these experiments, AITC of increasing concentrations (1 μM, 10 μM, and 100 μM) was applied sequentially to these neurons, and the cross-sectional area of each analyzed neuron was measured (**Figure 2A, B**). Diameter was then extrapolated from these measurements. Response threshold (i.e., whether a neuron was activated by 1 μM, 10 μM, or 100 μM AITC) was then compared to size.

We found that neurons responding to lower concentrations of AITC (the more sensitive neurons) tended to be smaller than neurons that only responded to higher concentrations of AITC or were entirely unresponsive to this stimulus (**Figure 2A, B**). As expected, all groups of AITC responsive neurons were significantly smaller ($p < 0.001$) than non-responsive neurons (cross sectional area: 383.3 ± 8.31 μm^2; diameter: 21.13 ± 0.23 μm, N=764 neurons), a difference that bore out despite the fact that this group of unresponsive neurons likely included other C-fibers (C-LTMRs, TRPM8-expressing neurons, etc.)[26,27]. The most sensitive group of TRPA1 neurons,

those that responded to 1 μM AITC, trended towards a smaller size (cross-sectional area: 211.5 ± 16.60 μm^2; diameter: 15.79 ± 0.61 μm, N=55 neurons) than neurons that responded to 10 μM (cross-sectional area: 282.2 ± 8.67 μm^2; diameter: 18.49 ± 0.283 μm, N=220 neurons) or 100 μM AITC (cross-sectional area: 274.0 ± 10.19 μm^2; diameter: 18.15 ± 0.326 μm, N=184 neurons), but this difference was only significant ($p < 0.05$) when diameter was used as a metric. In either case, neurons that first responded at either 10 μm or 100 μm were not significantly different in size. This morphological distinction further supports the conclusion that these highly-sensitive, pruritic TRPA1 neurons comprise an independent population.

3.3.3 DRG calcium imaging identifies PLC signaling as a potential mediator of response threshold in TRPA1 neurons.

Following completion of these experiments, we turned our attention to the many possible intracellular pathways that could play a role in establishing the baseline gain of the system. Given the wealth of previous research implicating PLC in the activation of TRPA1, we first targeted this pathway in DRG calcium imaging experiments. Initial experiments involved perfusing vehicle, a PLC activator (100 μM m-3M3FBS), or a mixture of PLC activator and inhibitor (100 μM m-3M3FBS + 20 μM U-73122) across dissociated mouse DRGs, followed by a pulse of a low-intensity (1 μM) AITC stimulus. After a brief washout, 100 μM AITC was perfused across cells as a "positive control" stimulus to identify all TRPA1 neurons (**Figure 3A**). As hypothesized, treatment with the PLC activator elicited a significant increase in the proportion of TRPA1 neurons that responded to this low-intensity stimulus (6.52 ± 1.00% vs. 55.16 ± 2.43%, $p < 0.001$, **Figure 3B**). Co-administration of the PLC inhibitor dramatically and significantly attenuated this effect ($p < 0.001$), with only 29.47 ± 2.42% of TRPA1 neurons responding to the 1 μM AITC stimulus (**Figure 3B**). Interestingly, while the PLC activator did

not increase the response intensity to 1 μM AITC of m-3M3FBS-treated cells relative to control-treated cells (0.68 ± 0.07, N=39 neurons vs. 0.86 ± 0.04, N=174 neurons), those co-treated with m-3M3FBS and U-73122 responded significantly less ($p < 0.001$) than those only treated with the activator (0.56 ± 0.04, 60 cells, **Figure 3C**). Interestingly, this effect was even more dramatic for responses to the 100 μM control AITC dose; within the population that responded to both the 1 μM AITC challenge and 100 μM positive control dose, neurons from the m-3M3FBS + U-73122 treated coverslips had significantly lower responses ($p < 0.001$) than neurons from control and m-3M3FBS-treated coverslips (control: 1.77 ± 0.26, N=35 neurons; m-3M3FBS: 1.58 ± 0.06 N=167 neurons; m-M3MFBS+U-73122: 0.83 ± 0.09, N=47 neurons, **Figure 3D**). When only the high-threshold neurons (those that only responded to the 100 μM AITC stimulus) were examined, both experimental groups had significantly lower responses ($p < 0.001$) than neurons from control coverslips, and neurons co-treated with activator and inhibitor had significantly lower responses ($p < 0.01$) than those treated only with the activator (control: 1.42 ± 0.04, N=580 neurons; m-3M3FBS: 0.97 ± 0.05, N=141 neurons; m-3M3FBS+U-73122: 0.65 ± 0.02, N= 152 neurons, **Figure 3E**). While we expected U-73122 treated coverslips to exhibit a decrease in response intensity to both the 1 μM and 100 μM AITC stimuli, we were intrigued that the high-threshold neurons from m-3M3FBS treated coverslips also had significantly lower responses to 100 μM AITC, opposite to our predictions. One could speculate that perhaps PLC activation sensitized the bulk of TRPA1 neurons with intermediate sensitivities, recruiting them to the low-intensity stimulus, such that the only neurons remaining to respond to the positive control stimulus were extremely high-threshold neurons of low sensitivity. However, more experimentation is necessary to confirm or reject this possibility.

Given these promising results, we turned to two-pulse experiments to more closely examine the effect of activating and inhibiting the PLC pathway upon neuronal recruitment to low- and medium-intensity stimuli. While one-pulse experiments gave us an overall sense of the bulk changes in neuronal recruitment, the two-pulse experiments allowed us to more closely examine how individual neurons were affected by pathway manipulation. More specifically, we could determine whether neurons that initially responded to an AITC dose were then silenced by pathway inhibition, or whether neurons that didn't initially respond to an AITC dose became responsive to that dose following pathway activation.

Application of PLC activator significantly increased the proportion of TRPA1 neurons that were "new responders" to a low-intensity AITC stimulus, i.e., neurons that did not initially respond to this concentration prior to PLC activation. This increase was significant ($p<0.001$) regardless of whether 1 μM or 5 μM AITC was used as the low-intensity stimulus. (1 μM: control—4.34 $\pm$ 1.96%, m-3M3FBS—42.09 $\pm$ 3.82%; 5 μM: control—6.40 $\pm$ 1.25%, m-3M3FBS—52.69 $\pm$ 10.67%, **Figure 4B**). The total percentage of AITC-responsive (TRPA1+) neurons did not vary significantly between control or treated coverslips (1 μM experiments: control: 51.62 $\pm$ 7.77%; m-3M3FBS: 51.06 $\pm$ 3.91; 5 μM experiments: control: 49.59 $\pm$ 5.86% ; m-3M3FBS: 45.03 $\pm$ 7.70%, **Figure 4H**), indicating that PLC activation most likely did not cause ectopic activation to AITC independent of TRPA1. While the response intensity to the second pulse of low-intensity AITC was not significantly different between control and PLC-activated conditions when 1 μM AITC was used as the stimulus, neurons that responded to the second pulse of 5 μM had significantly higher responses ($p < 0.05$) when they were treated with the PLC activator (1 μM experiments: control: 0.63 $\pm$ 0.11, N=16 neurons; m-3M3FBS: 0.70 $\pm$ 0.05, N=84 neurons; 5 μM experiments: control: 0.62 $\pm$ 0.07, N=24 cells; m-3M3FBS: 0.97 $\pm$

0.08, N=91 cells, **Figure 4C**). This increase appeared to be a contribution of both neurons that responded to the pre-m-3M3FBS AITC pulse (5 μM experiments: control: 0.72 + 0.1, N=16 cells; m-3M3FBS: 1.30 + 0.22, N=19 cells, **Figure 4D**) as well as neurons that were "new responders" (5 μM experiments: control: 0.41 ± 0.05, N=8 neurons; m-3M3FBS: 0.89 ± 0.08, N=71 neurons, **Figure 4E**). Interestingly, the response intensity to the 100 μM AITC dose was significantly lower within the population of neurons that only responded to this high-intensity stimulus in the m-3M3FBS treated condition (1 μM experiments: control: 1.27 ± 0.07, N= 191 neurons; m-3M3FBS: 0.97 ± 0.06, N= 105 neurons, $p < 0.01$; 5 μM experiments: control: 1.33 ± 0.09, N=98 cells; m-3M3FBS: 0.68 ± 0.06, N=38 cells, $p < 0.001$, **Figure 4F**), though the proportion of neurons in this population was not significantly affected. Like the one-pulse experiments, this might be due to the fact that the remaining neurons not recruited to respond to low concentrations of AITC might be of such low sensitivity that even PLC activation might not be sufficient to increase the robustness of their responses.

Two-pulse experiments in which PLC pathways were inhibited (**Figure 5A**) yielded a slightly more complex scenario. Unexpectedly, there was no significant decrease in the total proportion of TRPA1 neurons that responded to the second test pulse of 10 μM AITC (control: 56.32 ± 5.21%; U-73122: 44.62 ± 3.66%; **Figure 5B**). However, when we more closely examined this at the level of individual functional subpopulations, we did find evidence that PLC inhibition could reduce a neuron's responsiveness to a medium-intensity AITC stimulus. The proportion of TRPA1 neurons that responded to both AITC pulses was significantly and dramatically reduced ($p < 0.001$) for coverslips that received U-73122 treatment between AITC pulses (control: 39.76 ± 5.37%; U-73122: 4.43 ± 1.22, **Figure 5C**). Furthermore, the proportion of TRPA1 neurons that responded to the first AITC pulse, but not the second, was significantly

higher ($p = 0.0019$) in coverslips that received U-73122 treatment (Control: 5.14 ± 1.29%; U-73122: 25.85 ± 5.86, **Figure 5D**) Together, these two pieces of evidence indicate a shift in sensitivity following PLC inhibition; i.e., neurons that ordinarily would respond to two pulses of the 10 μM stimulus were no longer able to respond to the second pulse if it was preceded by U-73122 treatment. Instead, it appears that this reduction in neuronal recruitment was offset by increases in the proportion of TRPA1 neurons that were "new responders" to the 10 μM AITC stimulus (Control: 15.95 ± 2.80%; U-73122: 35.11 ± 4.33%, $p= 0.001$, **Figure 5F**). "New responders" also comprised a significantly greater proportion of neurons responding to this second pulse in PLC inhibited conditions (control: 30.05 ± 5.240%; U-73122: 75.53 ± 7.320, $p < 0.0001$). Additionally, the total proportion of TRPA1 neurons was higher in PLC inhibited coverslips (control: 39.13 ± 01.68; U-73122: 55.20 ± 2.88, $p < 0.0001$, **Figure 5H**). This could indicate that while PLC inhibition is capable of decreasing the sensitivity of neurons that typically responded to medium-intensity AITC stimuli, it is potentially recruiting additional neurons that ordinarily would not respond to such stimuli. Given the increase in the total percentage of TRPA1 neurons we observed in U-73122 treated coverslips, it is possible that these "new responders" may not be TRPA1 neurons. One potential explanation is that TRPV1+/TRPA1- neurons are being recruited following U-73122 application. TRPV1 has previously been demonstrated to be activated by AITC[233–235]. Other research has suggested that PIP2 is an activator of TRPV1[221,236,237]. Perhaps by inhibiting a pathway that inhibits an activator of TRPV1, U-73122 treatment may elicit activity from neurons that wouldn't ordinarily respond to TRPA1 agonists at those concentrations. An alternate possibility is that PIP2 plays a different role in activating/inhibiting TRPA1 in different neuronal subpopulations. Regardless, when all of the neurons responding to the second pulse of AITC were pooled, the response intensity to this

second pulse was significantly lower for U-73122 treated cells compared to control-treated cells (Control: 1.00 ± 0.05; U-73122: 0.73 ± 0.04, p< 0.0001, **Figure 5E**), indicating a decrease in overall response to medium-intensity AITC.

3.3.4 DRG calcium imaging experiments do not implicate PKA in setting the gain on TRPA1 neurons.

Once we had established the effects of PLC activation and inhibition upon neuronal recruitment to low or medium intensity AITC stimuli, we then decided to focus on the other most likely intracellular signaling target that might help to set the gain on different populations of TRPA1 neurons: protein kinase A (PKA). PKA activation experiments were structured similarly to the two-pulse PLC activation experiments and with 100 μM forskolin (FSK) used in place of 100 μM m-3M3FBS (**Figure 6A**). Intriguingly, PKA activation did not appear to affect neuronal recruitment or response intensity when either 1 μM or 5 μM AITC was used as the challenge concentration. We observed no significant increase in the proportion of TRPA1 neurons that were "new responders" to the low-intensity 1 μM AITC (control: 5.02 ± 01.11%; FSK: 5.40 ± 1.63%, **Figure 6D**) or 5 μM AITC (control: 15.00 ± 2.38; FSK: 19.22 ± 4.05%, **Figure 6E**). Additionally, there was no significant increase in the response intensity to the second pulse of AITC when either 1 μM AITC (control: 0.90 ± 0.10, N=45 neurons; FSK: 0.80 ± 0.09, N=43 neurons, **Figure 6F**) or 5 μM AITC (control: 0.84 ± 0.07, N=74 neurons; FSK: 0.85 ± 0.06, N=63 neurons, **Figure 6G**) was used. This measurement, however, reflects the AITC response for the pooled collection of all neurons that responded to the second pulse of AITC. Interestingly, in the 1 μM AITC experiments, FSK-treated "new responders" had significantly lower responses to the second pulse of AITC than the control neurons (control: 0.96 ± 0.21, n=14 neurons; FSK: 0.53 ± 0.05, n=16 neurons, p= 0.046). However, this was not observed in the 5

μM AITC experiments, and no other significant differences in response intensity were observed between control and FSK-treated coverslips in any of the other individual functional subpopulations of TRPA1 neurons in either of the experiments.

Inhibition experiments were performed in two discrete ways. In one-pulse experiments, coverslips were incubated in either vehicle or the PKA inhibitor 10 μM H-89 for 30 minutes prior to imaging, and maintained in the bath up until the perfusion was switched to the challenge pulse of 10 μM AITC (**Figure 6B**). Following the AITC application, there was a brief washout period, and a 100 μM positive control AITC stimulus was applied. We did not observe any decrement in neuronal recruitment to the 10μM stimulus following H-89 treatment (control: 50.17 ± 6.69%; H-89: 41.94 ± 2.65%, **Figure 6H**). Likewise, we did not observe any decrease in response intensity to 10 μM AITC (control: 1.10 ± 0.10, N=102 neurons; H-89: 1.20 ± 0.09, N=86, **Figure 6I**). Two-pulse experiments were performed in a manner analogous to that of two-pulse PLC inhibition experiments (**Figure 6C**). These experiments similarly did not yield any notable decrease in the proportion of TRPA1 neurons responsive to second pulse of AITC when treated with H-89 as compared to controls (control: 46.87 ± 7.56%; H-89: 52.67 ± 7.65, **Figure 6J**). Response intensity to the second pulse of 10 μM AITC was likewise unaffected (control: 0.89 ± 0.06, N=102 neurons; H-89: 0.83 ± 0.06, N=69 neurons, **Figure 6K**). Strangely, the total proportion of TRPA1 neurons was slightly lower in these two-pulse experiments; such a difference, however, was not observed in the one-pulse experiments (control: 39.45 ± 2.12%; H-89: 31.29 ± 1.2%, p=0.0082). No other significant differences in neuronal recruitment or response intensity were noted in any of the other subgroups of TRPA1 neurons.

Given reports made by others that PKA activation can potentiate TRPA1 currents to AITC[215], the lack of response to forskolin was perplexing. Comparing other metrics yielded

similarly insignificant differences between the two conditions. For example, when the ratios of response intensity of the second pulse to the first pulse (indicative of changes in response intensity within an individual neuron between the first and second pulse) were compared between control and forskolin-treated coverslips, we observed no differences in either 1 μM AITC (control: 1.15 ± 0.19, n=31 neurons; FSK: 1.04 ± 0.30, n=27 neurons) or 5 μM (control: 1.24 ± 0.12, n=38 neurons; FSK: 1.62 ± 0.28, n=21) conditions. One potential explanation of this discrepancy between our results and previously published findings is that we used different assays; e.g., the electrophysiology of transfected HEK cells employed in these studies is inherently different that the calcium imaging we did using cultured DRG neurons. Heterologously expressed ion channels may, for instance, be present in far greater numbers than what is typically found on a neuron in its natural state. It is possible that while forskolin may sensitize TRPA1 in heterologous expression systems, this sensitization may not be the most physiologically relevant factor for neurons.

3.3.5 DRG calcium imaging experiments do not implicate a role for PKC in setting the gain in TRPA1 neurons.

Experiments addressing the role of PKC in establishing the response threshold/setting the gain on TRPA1 neurons were performed identically to those investigating the role of PKA, although only 5 μM AITC was used as a test pulse in activation experiments (**Figure 7A-C**). Treatment with the PKC activator PMA (20 μM) did not increase neuronal recruitment to the second pulse of 5 μM AITC (control: 15.80 ± 2.78% of TRPA1 neurons; PMA: 17.39 ± 3.23%), indicating that response threshold was likely unshifted by PKC manipulation (**Figure 7D**). Similarly, within the population of neurons that responded to the second 5 μM AITC pulse, there was no change in the response intensity following PMA treatment (control: 0.73 ± 0.05, N=100

neurons; PMA: 0.68 ± 0.04, N=101 neurons, **Figure 7E**). No other significant differences were observed in neuronal recruitment or response intensity within other functional subgroups of TRPA1 neurons.

Inhibition of PKC similarly did not elicit any changes in neuronal recruitment to a medium-intensity AITC stimulus (10 μM) relative to control treatments. In one-pulse experiments, treatment with the PKC inhibitor BIM-I (1 μM) did not decrease the proportion of TRPA1 neurons that responded to 10 μM AITC (control: 48.69 ± 4.20%; BIM-I: 45.94 ± 5.83%, **Figure 7F**). PKC inhibition likewise did not decrease the response intensity to 10 μM AITC of neurons that responded to this stimulus (control: 1.04 ± 0.09, N=112 neurons; BIM-I: 1.121 ± 0.09159, n=77, **Figure 7G**). In two-pulse experiments, BIM-I did not reduce the proportion of TRPA1 neurons responding to the second 10 μM AITC pulse (control: 55.74 ± 4.44%; BIM-I: 58.91 ± 3.37%, **Figure 7H**), nor did it have any effect upon the response intensity of neurons that did respond to this second pulse (control: 0.82 ± 0.05, N=119 neurons ; BIM-I: 0.94 ± 0.06, N=124 neurons, **Figure 7I**). In fact, the only significant differences in response intensity we observed were relevant to the 100 μM AITC stimulus—BIM-I treatment elicited a significant increase in response intensity to this stimulus in both neurons that responded to dual AITC pulses and the control dose (control: 1.37 ± 0.09, N=84 neurons; BIM-I: 1.75 ± 0.11, N=79 neurons, p= 0.0073, **Figure 7K**) as well as neurons that responded only to the positive control dose (control: 0.66 ± 0.05, N=67 neurons; BIM-I: 0.81 ± 0.06, N=81 neurons, p=0.0498, **Figure 7J**). A possible interpretation of this data is that PKC is a weak negative regulator of TRPA1, such that relieving it with the BIM-I inhibitor increases TRPA1 responsiveness. Phosphorylation can have a variety of effects upon the functioning of an ion channel; PKC is one such kinase that can differentially modulate several ion channels, and can both augment and reduce currents

depending upon the identity of channel it phosphorylates[238,239]. The fact that we only observe differences in responses to high-intensity stimuli could imply that the role it plays in regulating TRPA1 function is not particularly significant. However, given that we did not observe a comparable degradation in TRPA1 responses to AITC following PKC activation, this conclusion is perhaps unlikely. Neuronal recruitment and response intensity were unaffected by BIM-I treatment within any other functional subgroup of TRPA1 neurons.

3.3.6 DRG calcium imaging experiments do not implicate Gβγ signaling in setting the gain of TRPA1 neurons.

Only inhibition experiments were performed to probe the role of Gβγ in setting the gain of TRPA1 neurons, and were structured similarly to those performed above (**Figure 8A, B**). 100 μM gallein was used to pharmacologically inhibit this pathway in both one-pulse and two-pulse inhibition experiments. In one-pulse experiments, application of this inhibitor did not significantly affect neuronal recruitment to 10 μM AITC (control: 43.40 ± 9.21%; GAL: 58.98 ± 5.42, **Figure 8C**), nor did it significantly alter response intensity to 10 μM within neurons that did respond to this stimulus (control: 1.00 ± 0.10, N=61 neurons; GAL: 1.11 ± 0.1, N=88 neurons, **Figure 8D**) or any other metrics examined. In two-pulse experiments, however, a few intriguing observations were made. Like the one-pulse experiments, we did not observe any decrement in the total proportion of TRPA1 neurons responding to the second pulse of 10 μM AITC (control: 48.28 ± 6.18; GAL: 63.75 ± 4.82%, **Figure 8E**) or the response intensity to 10 μM AITC of neurons that did respond to this stimulus (control: 0.93 ± 0.05760, N=144 neurons; GAL: 0.9020 ± 0.04675, N=175 neurons, **Figure 8F**). Interestingly, we did observe a significant increase in the proportion of TRPA1 neurons that were "new responders" to the 10 μM AITC stimulus (control: 18.04 ± 2.66%; GAL: 32.74 ± 3.42%, p= 0.0037, **Figure 8G**). Unlike the two-

pulse PLC inhibition experiments, however, we did not observe a corresponding change in the proportion of neurons that responded to the first AITC pulse but not the second (control: 8.78 ± 5.36%; GAL: 4.00 ± 1% , **Figure 8H**), which would have indicated that Gβγ inhibition negatively regulated the response threshold of neurons that were ordinarily responsive to this medium-intensity stimulus. Instead, this increase in new responders when Gβγ is inhibited implies that this G protein could potentially be a negative regulator of TRPA1. This is not unprecedented, as Gβγ has previously been shown to negatively regulate voltage-gated calcium ion channels and GIRKs downstream of μ opioid receptor activation[240,241]; additionally, Gβγ has been shown to inhibit some TRP channels, such as TRPM1 in the retina[242] and TRPM3 in peripheral nociceptors, where it plays a role in mediating μ opioid receptor dependent antinociception[243]. No other changes in neuronal recruitment were observed, and the total proportion of TRPA1 neurons was equivalent between control and treated conditions. Surprisingly, inhibiting the Gβγ pathway did appear to negatively affect the response intensity to the 100 μM AITC stimulus for neurons that responded to the second pulse of AITC (control: 1.61 ± 0.12, N=131 neurons; GAL: 1.33 ± 0.06, N=164 neurons, p=0.0281, **Figure 8I**) as well as neurons that only responded to the 100 μM pulse (control: 0.857 ± 0.05, N=119 neurons; GAL: 0.67 ± 0.04, n=91 neurons, p= 0.0058, **Figure 8J**) If we are indeed sensitizing TRPA1 by inhibiting Gβγ, it is possible that we are recruiting a large proportion of neurons away to respond to lower-intensity stimuli, leaving only the least sensitive neurons to respond to the positive control dose of AITC.

It would however be premature to conclude that Gβγ is a negative regulator of TRPA1 from this inconsistent data. Although we did observe a significant increase in the proportion of "new responders" to a medium-intensity AITC stimulus following inhibition with gallein in two-

pulse experiments, we did not make comparable measurements in one-pulse experiments. Ideally, experiments in which we could activate or overexpress Gβγ in DRG neurons would clarify this scenario.

3.3.7 DRG calcium imaging experiments do not implicate NALCN in setting the gain on TRPA1 neurons.

Given that NALCN in some species can act to functionally silence TRPA1 neurons[150], we wanted to explore whether this channel might play a similar role, particularly in the neurons that had very high response thresholds. In other words, higher expression and/or activity of this channel within this population of neurons might change their electrophysiological properties, and make them less likely to fire action potentials than their high-sensitivity, low-threshold counterparts. If this were indeed the case, we would expect that inhibiting NALCN could relieve this "brake" on the low-sensitivity neurons, and shift their sensitivity in such a way that they would respond to lower-intensity stimuli. However, when NALCN was inhibited with 1 mM verapamil (VPL) in two-pulse inhibition experiments, no change in the percentage of "new responders" to the second pulse of 5 μM AITC was observed (control: 14.18 ± 3.70%; VPL: 12.65 ± 6.59, **Figure 9B**). Of the neurons that did respond to the second pulse, those that were treated with verapamil exhibited a small yet significant decrease in their response intensity to this stimulus (control: 0.73 ± 0.05, N=52 neurons; VPL: 0.50 ± 0.08, N=17 neurons, p= 0.0195, **Figure 9C**), which appeared to be primarily attributable to the subgroup that responded to all three pulses of AITC (p=0.0140). No other differences in neuronal recruitment or response intensity were observed within any of the functional TRPA1 subpopulations. This implies that NALCN is likely not acting differentially in TRPA1 neurons to help set the gain, though

exploring the role of this channel using other experimental formats (e.g., electrophysiology) may be helpful.

3.3.8 PLC activation sensitizes zebrafish behavioral responses to AITC.

Given our results from DRG calcium imaging experiments that identified PLC signaling as a likely pathway in setting the gain of TRPA1 neurons, we decided to further pursue the role of PLC activation in the sensitization of behavioral responses to TRPA1 agonists. While previous research has suggested an ability for PLC activation to sensitize behavioral responses to painful stimuli in the mouse[216], whether such findings could be recapitulated in other species was unknown. Similarly, PLC inhibition has been shown to reverse inflammation- and injury-induced hyperalgesia[217,219] in rodent models, but not in non-mammalian species. To determine whether any sort of bidirectional toggling of behavioral responses could be observed following PLC manipulation in the zebrafish, we performed a total locomotor assay with 3dpf and 5dpf larvae.

Incubation in 100 μM PLC did indeed sensitize behavioral responses to AITC for both 3dpf and 5dpf larval zebrafish—pre-treated fish locomoted significantly more than controls when immersed in low to intermediate concentrations of AITC (**Figure 10A, B**). Importantly, baseline locomotion in 0 μM AITC was not affected, indicating that PLC activation does not cause generalized heightened motor activity by itself.

While we did perform experiments inhibiting PLC with U-73122, we could not conclusively ascertain the effects of PLC inhibition upon behavior. Pre-incubation in 20 μM U-73122 (the concentration employed for DRG experiments) for 25 minutes drastically reduced baseline locomotion (**Figure 10C**). Even when we shortened the pre-incubation duration to 10 minutes and 5 minutes (**Figure 10D, E**), baseline locomotion was significantly affected. It was thus impossible to determine whether the subsequent reductions in locomotor responses

following PLC inhibition were due to shifting the response thresholds of TRPA1 neurons, or simply an artifact of global PLC inhibition that elicited reductions in activity/locomotion. In an attempt to resolve this issue, we employed this total locomotion assay to construct a behavioral dose-response curve for U-73122 in baseline conditions (**Figure 10F**). We identified 1 μM as a concentration that did not elicit significant declines in baseline motor activity. Unfortunately, incubation in this concentration of U-73122 yielded inconsistent effects upon zebrafish locomotor behavior, despite repetition of the assay several times and two experimental approaches: first, incubation in 1 μM U-73122 for 10 minutes prior to the assay (**Figure 10G, H**), and second, maintenance of 1 μM U-73122 in the AITC bath (**Figure 10I, J**). Baseline locomotion was frequently reduced, despite this 1 μM concentration having no deleterious effects in the experiments that established the dose-response curve. In many instances, locomotion to certain concentrations of AITC would be increased, while locomotion to other concentrations was decreased. These inconsistencies did not appear to be due simply to larval age, as they were present in assays using both 3dpf and 5dpf larvae. Therefore, we could not draw any conclusions about whether global PLC inhibition could significantly attenuate zebrafish behavioral responses to a TRPA1 agonist. Given the relevance of PLC signaling to systems beyond the regulation of peripheral somatosensory neurons, it is certainly possible that global PLC inhibition in our experiment had off-target effects upon central nervous system and motor functioning. Alternative approaches—determining if a "recovery period" following U-73122 exposure is necessary, devising a genetic strategy to specifically target PLC activity in TRPA1 neurons, etc.—may be necessary to fully ascertain the role of PLC inhibition on behavior in the zebrafish.

3.3.9 PLC activation affects neuronal recruitment *in vivo* in the zebrafish.

To determine whether PLC activation affects neuronal recruitment *in vivo*, we returned to CaMPARI calcium imaging, but this time using Tg(TrpA1b(ss)-CaMPARI) transgenics, which express this photoconvertible protein specifically in TPRA1 neurons. 3dpf larval zebrafish demonstrated a dose-dependent increase in neuronal recruitment in response to increasing AITC concentrations (**Figure 11A**). Pre-incubation in the PLC activator m-3M3FBS (100 μM) for 5 minutes prior to AITC exposure significantly increased the percentage of TRPA1 neurons responding to an intermediate concentration (20 μM) of AITC (control: 9.59 $\pm$ 4.30%, N=8 fish; m-3M3FBS: 48.98 + 11.26%, N=7 fish, $p < 0.001$). Recruitment of TRPA1 neurons to the 10 μM (control: 0%, N=6 fish; m-3M3FBS: 10.92 $\pm$ 6.42%, N=3 fish) and 30 μM AITC (control: 72.54 $\pm$ 5.88%, N=11 fish; m-3M3FBS: 92.33 $\pm$ 1.85%, N=3 fish) concentrations was also increased in the fish that had been treated with the PLC activator, but this difference was not significant (**Figure 11A**). We did not observe any significant change in the proportion of active neurons at baseline conditions (i.e., 0 μM AITC) between control and treated groups (both had an average of 0% converted neurons). In the event that the percentage of neurons we classified as "active" was not the best metric for comparing control and PLC activated conditions, we also compared red/green corrected total cell fluorescence (CTCF) ratios, which indicated the extent to which individual neurons were photoconverted. We observed that neurons from PLC activated fish had significantly higher red/green CTCF ratios than control fish at 20 μM AITC (control: 0.05 $\pm$ 0.01, N =168 neurons; m-3M3FBS: 0.24 $\pm$ 0.03, N= 134 neurons, $p < 0.001$, **Figure 11B**) and 30 μM AITC (control: 0.44 $\pm$ 0.03, N=178 neurons; m-3M3FBS: 0.91 $\pm$ 0.06, N= 58 neurons, $p < 0.001$, **Figure 11B**). As with neuronal recruitment, there was no significant difference in the red/green CTCF ratio at baseline between control and PLC inhibited groups

(control: -0.02 ± 0.004, N=220 neurons; m-3M3FBS: -0.016 ± 0.004, N=95 neurons). Together, these results indicate that PLC activation increased photoconversion levels—a proxy for neuronal activity—in TRPA1 neurons from fish that were exposed to medium concentrations of AITC. This could be reflective of a shift in the response threshold of these neurons; i.e., that less-sensitive, high-threshold neurons were rendered more sensitive to stimuli that might not ordinarily elicit their activation.

Unfortunately, as with the zebrafish behavioral experiments, we were unable to demonstrate a significant reduction in neuronal activity following PLC inhibition with U-73122. We observed no reduction in activity when 20 μM U-73122 was applied for 5, 10, 20, or 30 minute durations prior to AITC exposure and photoconversion (Tables 1, 2). Given the robust effect we observed in dissociated mouse DRG neurons, and the similarities we observed between these two species in several previous experiments, this inconsistency is puzzling. However, it may be possible that we did not find the ideal method of PLC inhibition for these experiments; it is also possible that the mechanisms for setting the gain in zebrafish TRPA1 neurons are similar, but not identical, to those of the mouse.

3.4 Discussion and Chapter Summary

The experiments outlined above provide further evidence that distinct subsets of TRPA1 neurons mediate different behavioral responses in response to stimuli of varying intensities. *In vitro* calcium imaging experiments of DiI-labeled neurons DRG neurons suggested that innervation destination was not a major factor in determining the sensitivity of TRPA1 agonists. DiI-labeled neurons from the highly-sensitive area of the hindpaw exhibited the same stratification into subpopulations of neurons with varying thresholds to TRPA1 agonists, as observed in our earliest experiments when all DRGs from an animal were pooled. We likewise

found no differences between labeled and unlabeled neurons from a subset of DRGs (lower thoracic and lumbar), further implying that a similar complement of multiple TRPA1-expressing subpopulations can be found in multiple areas throughout the body. However, it is certainly possible that more nuanced differences in sensitivity of TRPA1 neurons may exist and correlate with innervation target, and drawing comparisons across more restricted areas may be helpful. Additionally, it is possible that certain features that might establish a neuron's response threshold are obscured by this preparation—it has been postulated, for example, that differences in central arborization patterns in the dorsal horn is a major factor in the sensitivity differences between nonpeptidergic nociceptors that innervate distal vs. proximal targets[213]. As the central and peripheral processes of DRG neurons are clipped during harvesting, this method would not allow us to make comparable observations in our populations of TRPA1-expressing nociceptors. We would similarly be unable to determine whether more sensitive neurons projected to different regions of the epidermis, as has been documented with the broad categories of peptidergic and nonpeptidergic nociceptors[212].

Additionally, we found that the most sensitive neurons, those responding to low-intensity TRPA1 agonists (i.e., low concentrations of AITC), were significantly smaller than neurons responding to higher-intensity stimuli, suggesting that these most sensitive neurons are indeed part of a separate population. Previous work has demonstrated the link between neuronal size and function. The soma size of rat DRG neurons, for instance, correlates very well with conduction velocity[207]. A small size may even contribute to the heightened responsivity of these neurons. In general, cells with larger input resistances require less activating current to elicit a discharge[244]. Studies of motorneurons in both vertebrates and invertebrates have shown that neuronal size varies with input resistance, with smaller neurons having greater input resistance

than larger neurons[245,246]. Intriguingly, in a mollusk species, smaller neurons with greater input resistances are recruited before larger ones with lower input resistances[246], potentially indicating that they are more sensitive. Similar findings have been made in cat DRG neurons, where larger Aβ fibers had lower input resistances than smaller Aδ fibers[247]. While many other factors can contribute to the excitability of a neuron, and changes in conductance do not necessarily scale linearly with size[244], a larger input resistance due to a smaller size might be one factor underlying the greater sensitivity of these neurons.

When we probed a variety of intracellular pathways whose involvement in regulating TRP channels (particularly TRPA1) has previously been demonstrated, we identified PLC as one potential factor that may play a major role in establishing the response threshold of TRPA1 neurons. Calcium imaging experiments with dissociated DRG neurons showed that activating PLC significantly increased the proportion of neurons responding to a low-intensity stimulus, a potential indication that activating PLC reduced a neuron's response threshold. The reverse was also observed—a neuron's responsiveness to a medium-intensity AITC stimulus could be reduced following treatment with a PLC inhibitor.

There are numerous ways PLC activity might be involved in setting a baseline "gain" in TRPA1 neurons. Perhaps the most plausible of these is the ability of PLC to deplete PIP2 from the membrane, with the assumption that PIP2 is a negative regulator of TRPA1, as previously suggested by others in the field[220]. Depletion of a negative regulator would not necessarily directly activate TRPA1, thus avoiding issues pertaining to subsequent desensitization or inactivation. Instead, it would render the channel more susceptible to activation, which may be a preferable strategy in maintaining a tonic state of "readiness". However, we cannot rule out the possibility that other molecules resulting from PLC activation (such as DAG and AA) are

involved, as their role in activating TRPA1 has previously been documented[72]. IP3-mediated calcium release from intracellular stores may also play a role a role—intracellular calcium has previously been shown to activate TRPA1[248,249]. Intriguingly, one study also demonstrated that intracellular calcium was able to potentiate, but not inactivate, TRPA1 currents, whereas extracellular calcium influx could both potentiate and inactivate TRPA1[250]. The authors of this study proposed that this lack of inactivation could have resulted from relatively low levels of intracellular calcium released during their uncaging experiments; if this is indeed the case, it may support a mechanism in which increased basal PLC activity elevates intracellular calcium concentrations enough to potentiate, but not high enough to inhibit, TRPA1 responses to agonists. Another possibility is that heightened PLC activity in sensitive cells would lead to increased trafficking of TRPA1 to the membrane[216], and that this increased presence of TRPA1 would render a cell more responsive to TRPA1 agonists.

We were able to recapitulate these results in the zebrafish regarding PLC activation, which sensitized both behavioral responses to AITC as well as neuronal activation. However, we could not conclusively demonstrate the effects of PLC inhibition in the zebrafish *in vivo*, either through our behavioral assay or CaMPARI imaging experiments. Results from CaMPARI imaging suggest that inhibiting PLC may not affect the response properties of TRPA1 neurons, since incubations in U-73122 had no effect on neuronal photoconversion when fish were exposed to AITC stimuli. It is unlikely that this is due to factors such as penetrance, incubation duration, or U-73122 concentration, since we used a concentration that elicited strong behavioral effects on baseline locomotion when applied for shorter time periods. This may imply that while PLC signaling can potentiate TRPA1 responses, it may be unlikely to play a role in establishing baseline response properties in highly-sensitive TRPA1 neurons in the zebrafish, in contrast to

our *in vitro* studies in the mouse. However, some experimental caveats prevent us from drawing any definitive conclusions about the role of PLC inhibition in the zebrafish. Behavioral results from inhibition experiments were primarily inconclusive due to the effects of PLC inhibition upon baseline locomotion. Due to the lengthiness of CaMPARI imaging experiments, we did not exhaust every possible combination of U-73122 concentration and incubation time period, and it is possible (albeit somewhat unlikely) that we did not use ideal conditions to inhibit these neurons. It is also possible that similar phenomena we observed in DRG calcium imaging experiments during PLC inhibition also occur in the zebrafish, yet cannot be detected through CaMPARI imaging experiments, an approach which only provides a "snapshot" of neuronal activity. Unlike the DRG imaging experiments, we were unable to determine an individual neuron's responsiveness to test concentrations of AITC both before and after PLC activation or inhibition. It is possible that PLC inhibition induces in zebrafish a scenario analogous to that which we observed in dissociated mouse DRG neurons—i.e., a decrease in sensitivity within neurons that ordinarily responded to low-intensity AITC, accompanied by an increase in sensitivity within neurons that did not initially respond to low-intensity AITC. Our CaMPARI experiments would be unable to detect these nuances, instead only depicting the net levels of neuronal recruitment to AITC, which might not be different between PLC-inhibited and control conditions. An alternative approach would be to employ GCaMP imaging, which would allow us to observe neuronal activity in real time for a series of different stimuli.

Our results did not indicate a clear role of PKA, PKC, Gβγ, or NALCN in maintaining the gain on subpopulations of TRPA1 neurons. In the case of PKC, this is not particularly surprising, as it falls in line with previous research indicating that PKC does not appear to be involved in sensitizing TRPA1 following the activation of inflammatory pathways[215,220].

Experiments involving the pharmacological blockade of NALCN with verapamil implies that high expression of NALCN may not be a barrier to activation by TRPA1 agonists in low-sensitivity neurons; the fact that neurons were still able to respond to low-intensity AITC, however, also implies that NALCN may not be important for maintaining normal excitability in TRPA1 neurons in the mouse. Given the opposing roles that NALCN may play in regulating neuronal excitability—i.e., that its presence is necessary for maintaining proper excitability in CNS neurons, but high expression can dampen neuronal excitability—this was not particularly surprising[150,232]. Given previous reports that Gβγ can activate TRPA1 following stimulation of pruritic GPCRs such as SP1R3 and MrgprA3[84,85], we anticipated that blockade of this pathway would lead to a decrease in neurons responding to the second pulse of a medium-intensity AITC stimulus. Instead, we observed a significant increase in "new responders", implying that Gβγ might be negatively regulating this ion channel. Gβγ is important for the closure of some TRP channels, such as TRPM1 and TRPM3[242,243], but whether the same might be true for TRPA1 is unclear. Despite the findings of Wilson et al[85], Hill et al[84], and Lieu et al[83], other groups have reported a complete lack of interaction between Gβγ and TRPA1[243], further muddying the waters. It may be possible that an intermediate, as yet unidentified, molecule facilitates the interaction between Gβγ and TRPA1 neurons in some neurons. Perhaps most perplexing is the lack of involvement of PKA in sensitizing TRPA1 or affecting the baseline tone of DRG neurons in culture. Even if basal levels of PKA signaling were not involved in setting the gain at baseline, we expected to observe increases in the response intensity regardless of whether changes in neuronal recruitment also took place.

It is also possible that factors other than PLC signaling might be at work in regulating the gain of TRPA1 neurons in both zebrafish and mice. TRPA1 neurons might, for example, differ in

their electrophysiological properties, such as resting membrane potential and subthreshold electrical activity. For example, the increased responsivity of these high-sensitive neurons may be due to an increased resting membrane potential[251,252]. Another possible factor might be differences in subthreshold electrical activity. In rodents, it has been demonstrated that certain primary sensory neurons exhibit subthreshold oscillations in membrane potential—these oscillations are thought to be critical for proper neural activity, but when enhanced by nerve injury can contribute to hypersensitivity and hyperalgesia[253,254]. Whether this subthreshold activity is naturally variable between populations of neurons, or even exists in lower vertebrates such as the zebrafish, is unknown, and warrants further exploration. Subpopulations of TRPA1 neurons might also vary in TRPA1 expression level, the amount of TRPA1 present in the membrane, mechanics of TRPA1 trafficking, the complement of ion channels that help to establish resting membrane potential and facilitate action potential initiation, presence of peripheral opioid receptors, or any number of other factors.

All of the observations outlined above regarding the role of innervation destination, size, and PLC signaling provide valuable insight into the coding strategies for itch and pain sensations in both zebrafish and mice. They suggest that at some point in early evolutionarily history, vertebrates evolved a population coding strategies in order to convey information about stimuli of different intensities, which could have different contextual significances, in order to elicit appropriate behavioral responses (e.g. pruritic vs. nocifensive). In this strategy, a select population of TRPA1 neurons that can be activated by low-intensity agonists exhibit certain morphological features that distinguish them from less-sensitive neurons, such as cell size, that could potentially aid in increasing their excitability. Our findings that PLC manipulation could shift patterns in neuronal recruitment suggest that these neurons may also have heightened PLC

activity, though further experimentation is necessary to confirm this postulation. Understanding the mechanisms through which these important senses are coded not only provides valuable information about the underlying biology and evolutionary significance of itch and pain, but may also be clinically relevant. The hyperalgesia and allodynia experienced in neuropathic pain conditions often results from an increased sensitivity of neurons, an aberrant shifting of response thresholds[253,255]. It is possible that the same factors that establish differences in sensitivity and thresholds at baseline may also be involved in pathological conditions, and understanding the mechanistic underpinnings of sensitivity may yield insight into identifying novel treatment targets for pain and itch disorders.

3.5 Chapter Methods

Zebrafish husbandry: Adult zebrafish (*Danio rerio*) were raised with constant filtration, temperature control (28.5 ± 2°C), illumination (14 h:10 h light-dark cycle, lights on at 9:00 AM), and feeding. All animals were maintained in these standard conditions and the Institutional Animal Care and Use Committee approved all experiments. Adult zebrafish not used in behavioral experiments were bred in spawning traps (Thoren Caging Systems) from which embryos were collected. Embryonic and larval zebrafish were raised in petri dishes (Fisher Scientific) of E2 medium with no more than 50 embryos per dish at 28.5 ± 1°C in an incubator (Sanyo). Embryos were staged essentially as described[202] and kept until 5dpf.

Generation of CaMPARI transgenic zebrafish: Tg(TrpA1b(ss)-CaMPARI) was made using by amplifying a 5kb fragment of the BAC clone CHORI211-236I20 using with overlaps homologous to a modified version of the tol2 transgenesis vector pDestTol2pA-id2u-CBA-GFP (CBA- carb beta actin minimal promoter) using the following primers:

TrpA1b promoter:

Forward: gctttgtggtgaggatactagtgtag

Reverse: gatgcgttcattaagggccatgc

Vector (upper case indicates homology):

Forward: GTTTAATTACCCTACACTAGTATCCTCACCACAAAGCcccaacttttctatacaaagttg

Reverse: TCTCATGCTAAATTAGCATGGCCCTTAATGAACGCATCccaagtttgtacaaaaaagcag

The fragments were amplified by PCR and assembled using the SGI Gibson Assembly® HiFi 1 Step Kit (GA1100-10) following manufacturer's instructions.

The resulting construct was then digested NcoI and SalI to liberate the GFP fragment, while CaMPARI was amplified using the following primers:

Forward: TTGAGCTCCTCCACACGCTAGCGCTACCGGTCGCCACcatgctgcagaacgagcttgctc

Reverse: TCTAGATCCGGTGGATCCCGGGCCCGCGGTACCGTCGAgcatgcctgctattgtcttccc

The two fragments were ligated as previously described.

The resulting construct, called TrpA1b(ss) - CaMPARI, was injected at a concentration of 25ng /ul with 100ng/ul transposase RNA and found to robustly drive expression in Trigeminal and Rohon beard neurons by 3dpf. We therefore refer to this line as trpa1b somatosensory (ss) as it appears to only drive expression in those neurons. A stable line was established raising animals that showed broad transient expression and screening their progeny for fluorescence.

Mouse husbandry: All mice were housed under a 12 h light/dark cycle with food and water provided ad libitum. All experiments were performed in accordance with the guidelines of the National Institutes of Health and the International Association for the Study of Pain, and were approved by the Animal Studies Committee at Washington University School of Medicine.

DiI Injections: DiI (Invitrogen) was obtained from and reconstituted in anhydrous DMSO to make a stock solution of 34 mg/mL. Working concentrations of 17 mg/mL were prepared by making a 1:1 dilution of stock in sterile saline. Mice were briefly anesthetized with isoflurane and restrained in a 50 mL conical tube perforated with air holes for injections. One hindpaw was withdrawn from the tube and 10 μL of DiI was intradermally injected into the glabrous surface of the footpad with an insulin syringe equipped with a 33 gauge needle. If necessary, mice were administered ketoprofen via subcutaneous injection to combat inflammation following DiI treatment. Mice were euthanized 7-8 days following DiI labeling and DRGs were isolated and prepared as previously described[59], with the exception that only DRGs ipsilateral to the injected paw were pooled together to increase proportion of DiI-labeled neurons, and kept separate from control thoracic/lumbar DRGs from the contralateral side.

Ratiometric Calcium Imaging: DRGs were isolated from 6- to 12-week-old C57Bl/6J mice. All experiments were performed in compliance with institutional animal care and use committee standards and experiments were performed essentially as described[69]. Dissociation and culturing of mouse DRG neurons were performed as described with the following modifications[59]. Dissected DRGs were dissociated by incubation for 1 hour at 37°C in a solution of culture medium [Ham's F12/Dulbecco's modified Eagle's medium (DMEM) with 10% horse serum, 1%

penicillin-streptomycin (Life Technologies, Carlsbad, CA)] containing 0.125% collagenase (Worthington Biochemicals, Lakewood, NJ), followed by a 30-minute incubation in 10 ml of culture media plus 1.25 units of papain. Calcium imaging was performed essentially as described previously (Story et al, 2003). Growth media were supplemented with 100 ng/ml nerve growth factor. The buffer solution for all experiments was 10 mM HEPES in 1X Hanks' balanced salt solution (HBSS) (Invitrogen, Carlsbad, CA).

The threshold for activation was defined as 30% above baseline for both DRG and heterologous expression experiments. Student's t test was used for all statistical calculations unless otherwise indicated. All reported fluorescence values of each cell were normalized to the fluorescence of that cell during the initial baseline wash period. Maximum response values of each cell were calculated as the difference between the maximum and minimum fluorescence values of the cell during a stimulus application period. All averages represent mean $\pm$ S.E.M.

For DiI experiments, an additional image was taken of the field of view following each experiment to identify labeled neurons. For experiments correlating cell size and response threshold to AITC stimuli, a similar image was taken and processed using ImageJ software. Circular regions of interest were drawn around each cell, and the cross-sectional area was exported. A simple geometric calculation ($diameter = 2 * \sqrt{\frac{Area}{\pi}}$) was used to extrapolate the diameter of individual DRG neurons.

Examining neuronal activation with CaMPARI transgenic zebrafish: Tg(TrpA1b(ss)-CaMPARI) zebrafish in an AB background were simultaneously exposed to chemical stimuli and a 405 nm

light in order to permanently photoconvert active neurons[169]. Tg(TrpA1b(ss)-CaMPARI) zebrafish were outcrossed to wildtype fish to generate heterozygous offspring. Since it was difficult to distinguish heterozygous from homozygous CaMPARI expression during visual screening, all animals used in these experiments were heterozygous to avoid potential gene dosage confounds. Pigment formation was inhibited by exposing larvae to 1-phenyl 2-thiourea (PTU) at 24hpf, and larvae were screened for CaMPARI expression at 2dpf. On the day of imaging, 3dpf larval zebrafish were paralysed by injecting α-bungarotoxin protein (Sigma) into the chest cavity using microinjection needles pulled on a Flaming-Brown Micropipette Puller (model P-87, Sutter Instrument Co.) and a Picrosprizter II microinjection apparatus (General Valve Corporation). Paralysed fish were incubated in petri dishes filled with either EM, 100 μM m-3M3FBS (5 minutes), or 20 μM U-73122 (5-30 minutes, depending upon the experiment). Following this incubation period, zebrafish were lightly rinsed by placing them into a separate petri dish filled with EM, and were then transferred to small glass-bottomed dishes (Wilco Wells) filled with E2 media (EM) or AITC (5-50 μM) and allowed to incubate for 1 minute. Next, these glass-bottomed dishes were placed on the stage of an inverted fluorescent microscope (Olympus, model Ix81S1F-3) and the larvae were exposed to a 405 nm light for 7.5 seconds using MetaMorph software (Molecular Devices). Post-exposure fish were removed from the chemical and placed in a petri dish filled with embryo media and tricaine to prevent any future activation of sensory neurons. Immediately prior to imaging, larvae were mounted on coverslips in 1.5% agarose + tricaine in EM. TG and surrounding neural tissue were imaged using a 20x lens on an LSM 880 confocal microscope (Zeiss). Zen Black software was used to scan through the entire TG, acquiring a 1024 x 1024 pixel image slice at every ~2.5 μm that could then be stacked in the Z plane until the entire ganglion was imaged.

All images were processed using ImageJ software. Briefly, regions of interest were drawn around individual cells. For each frame with cell ROIs, four ROIs were placed in the background of these images; these were averaged in order to provide background fluorescence measurements for the image. Integrated density, area, and mean gray value were exported for all ROIs in both the green and the red channels. Corrected total cell fluorescence (CTCF) was calculated for each neuron as previous described[256] using the following formula: $CTCF = Integrated\ density - (Area * Mean\ background\ fluorescence)$. Red/green CTCF ratios were determined by dividing the red CTCF by the green CTCF for each cell. A cell was labeled as "active" (or responsive to a stimulus) if its red/green CTCF ratio was at least three standard deviations above the baseline (the average red/green CTCF of control fish photoconverted for 7.5 seconds). ANOVA (Graphpad Prism 6) was used to determine statistical significance unless otherwise noted. All reported values are expressed as means $\pm$ S.E.M.

Larval zebrafish behavior: At 3dpf or 5dpf, larval zebrafish (AB background) were placed into individual wells on a 96-well mesh bottom plate (Millipore) resting in a bath of E2 medium. The 96-well plate was then transferred to a hot plate that was maintained at a constant temperature of 28.5°C. Then the 96-well plate was moved from the E2 medium bath to a bath containing either control solution, 100 μM m-3M3FBS, or U-73122 (variable concentrations) to incubate (m-3M3FBS experiments: 5 minutes; U-73122: times were variable). Following this incubation period, the 96-well plate was quickly transferred to an experimental bath containing vehicle or one of the following AITC concentrations: 1 μM, 2 μM, 4 μM, 6 μM, and 10 μM. The behavioral response of the larval zebrafish was recorded with a HD camcorder (Canon) for four minutes. Experiments were performed blindly and each larva's total locomotive behavioral

response was tracked using Ethovision (Noldus). Statistical analysis was done using an analysis of variance (Graphpad Prism 6). All reported values are expressed as means + S.E.M. All experimental compounds were purchased from Sigma Aldrich unless otherwise noted and were made up in 1% dimethyl sulfoxide (DMSO, Sigma Aldrich) and E2 medium.

3.6 Chapter Figures and Tables

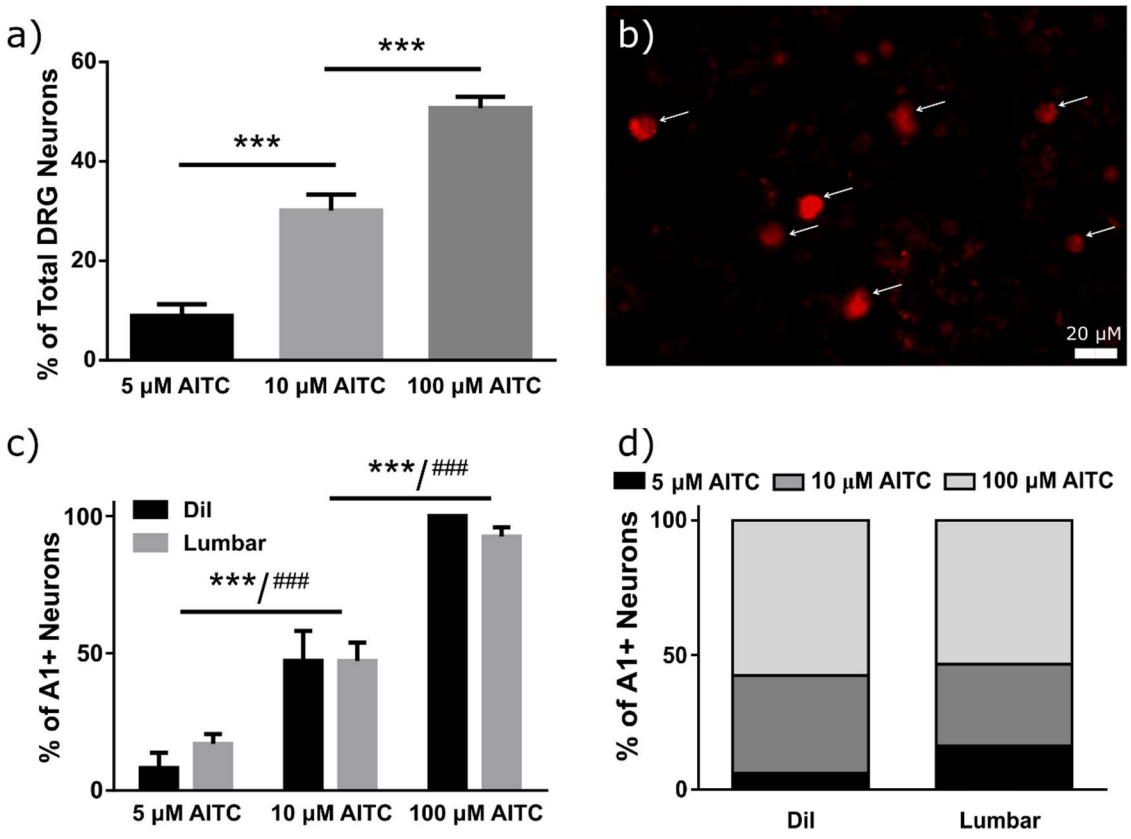

Figure 1: Dose-dependent neuronal recruitment to increasing concentrations of AITC occurs independently of innervation target. (A) The percent of total DRG neurons responding to an AITC stimulus significantly increases with increasing AITC concentration. N= total neurons. **(B)** Image of coverslip with neurons cultured from DiI-injected mouse. White arrows indicate labeled neurons. **(C)** Percentage of DiI-labeled versus unlabeled DRG neurons first responding to 5 µM, 10 µM, and 100 µM AITC. **(D)** Same as (**C**), but represented as a stacked bar chart. Values represent mean $\pm$ S.E.M. *** $P < 0.001$ for DiI injected neurons, ### $P < 0.001$ for unlabeled neurons, two-way ANOVA with Tukey's multiple comparison test. N for DiI-labeled neurons responding to 5 µM, 10 µM, and 100 µM respectively: 4, 24, 38. Unlabeled neurons: 40, 75, 132 responding respectively to 5 µM, 10 µM, and 100 µM AITC. Results are pooled from 3 mice.

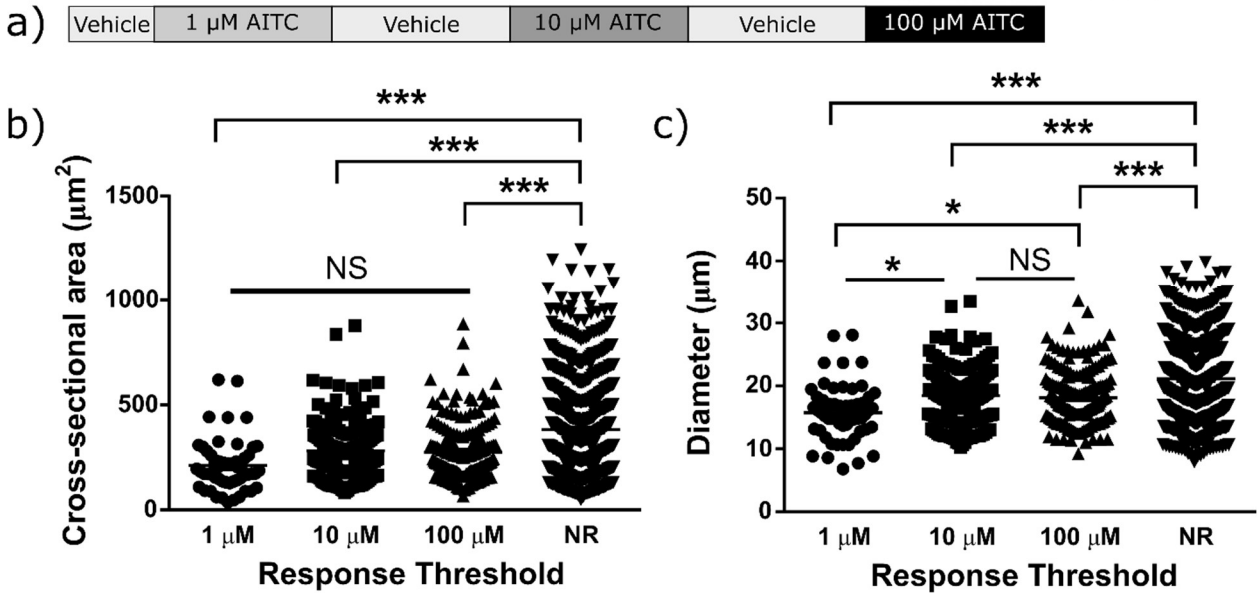

Figure 2: More sensitive neurons trend to smaller sizes. (A) Design of ratiometric calcium imaging experiments. Different concentrations of AITC were perfused over coverslips of dissociated DRG neurons (3 minutes per stimulus), separated by 2 minute vehicle washout periods. **(B)** Cross-sectional area of neurons that first responded to 1 μM (n=55 neurons), 10 μM (n=220 neurons), and 100 μM AITC (n=184 neurons), as well as non-responding neurons (n=764 neurons). **(C)** Diameter of neurons that first responded to 1 μM, 10 μM, and 100 μM AITC, as well as non-responding neurons. *P < 0.05, **P < 0.01, ***P < 0.001, one-way ANOVA with Tukey's multiple comparison test. Results are pooled data from 3 mice.

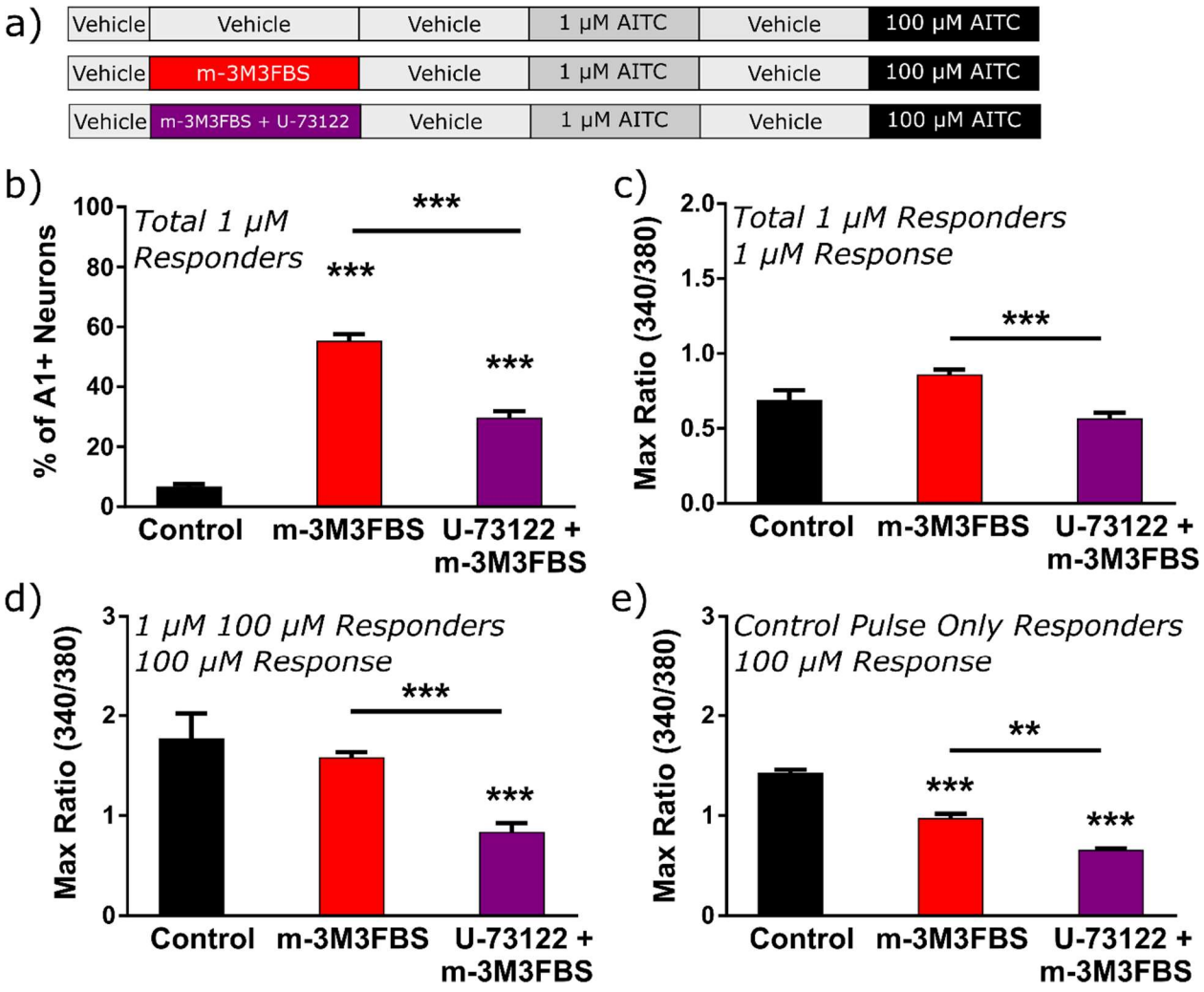

Figure 3: Manipulating the phospholipase C (PLC) pathway can shift neuronal recruitment in "one-pulse" experiments. (A) Design of ratiometric calcium imaging experiments with dissociated DRG neurons. After an initial baseline perfusion of vehicle across coverslips of dissociated DRG neurons, either a PLC activator (100 µM m-3M3FBS), PLC activator + inhibitor (100 µM m-3M3FBS + 20 µM U-73122), or continued vehicle was perfused over the coverslips for 3 minutes. After a brief washout period, 1 µM AITC was perfused across coverslips for 3 minutes. A 2-minute vehicle washout, and subsequently a 3-minute application of a positive control of 100 µM AITC to identify all TRPA1 neurons, followed. **(B)** Percentage of TRPA1+ neurons responding to 1 µM AITC during control, PLC activation, or a combination of PLC activation and inhibition conditions. **(C)** Response intensity to 1 µM AITC (of neurons that responded to this stimulus). **(D)** Response intensity to 100 µM AITC (of neurons that responded to both 1 µM and 100 µM). **(E)** Response intensity to 100 µM AITC (of neurons that only responded to 100 µM AITC). *P < 0.05, **P < 0.01, ***P < 0.001, one-way ANOVA with Tukey's test for multiple comparisons.

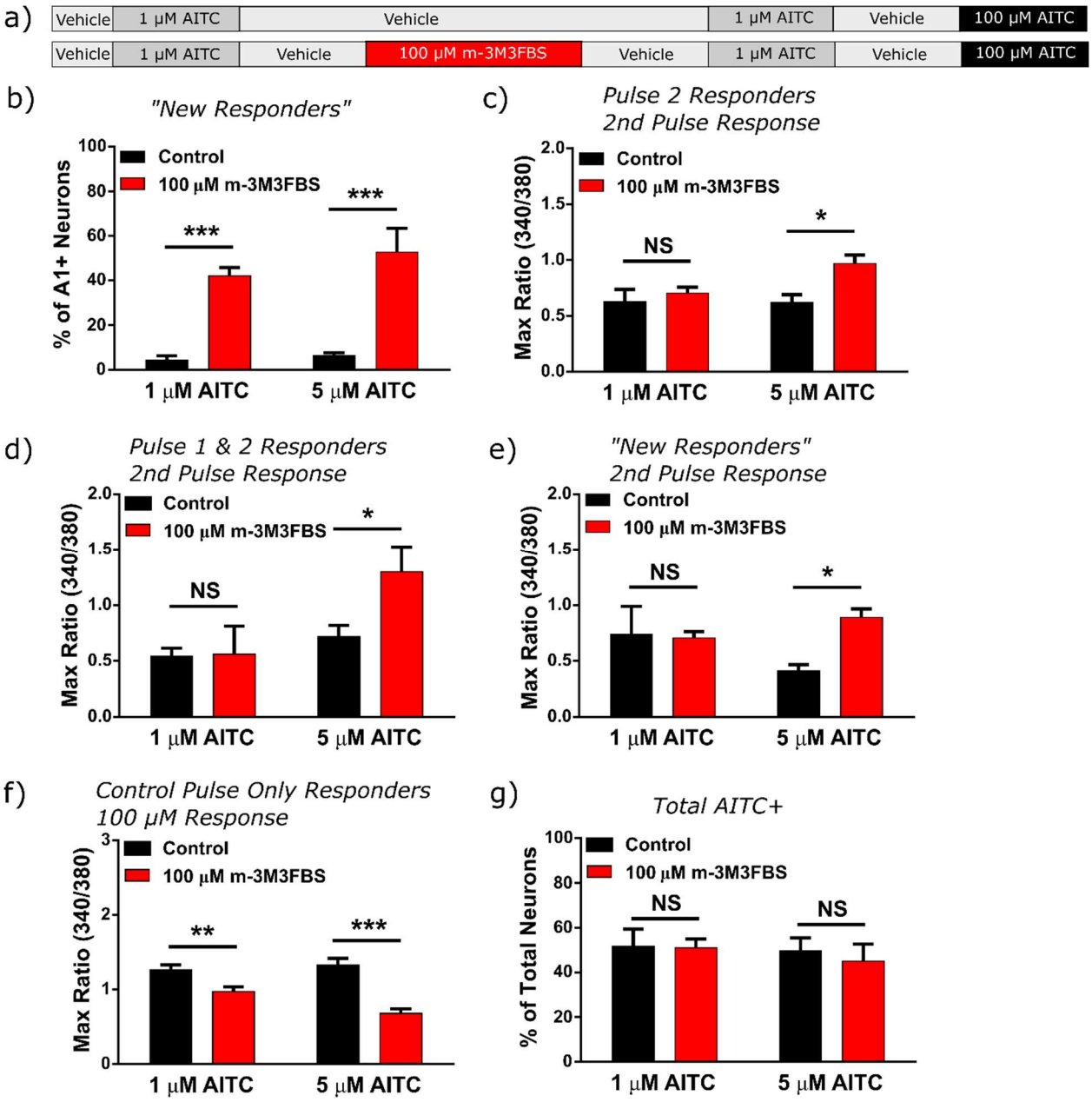

Figure 4: Activating PLC can increase neuronal recruitment to low-intensity stimuli in "two-pulse" experiments. (A) Design of ratiometric calcium imaging experiments with dissociated mouse DRG neurons. Following perfusion of either 1 or 5 µM AITC for 3 minutes, either vehicle or PLC activator (100 µM) was applied for 5 minutes. After a subsequent vehicle washout, a second 3-minute pulse of the 1 µM or 5 µM was applied. Like the "one-pulse" experiments, this AITC pulse was followed by a washout period and application of a positive control, 100 µM AITC pulse. **(B)** Percentage of TRPA1 neurons responding to the low-intensity AITC stimulus in control or PLC activated conditions. **(C)** Response intensity to the second pulse of 1 µM or 5 µM AITC in control or PLC activated conditions (of total neurons that responded to low-intensity stimuli). **(D)** Response intensity to the second pulse of 1 µM or 5 µM

AITC in control or PLC activated conditions (of neurons that responded to both pulses of low-intensity AITC). **(E)** Response intensity to the second pulse of 1 μM or 5 μM AITC in control or PLC activated conditions (of neurons that were "new responders", i.e. only responded to the second low-intensity AITC pulse and not the first. **(F)** Response intensity to 100 μM AITC (of neurons that only responded to 100 μM AITC and not any of the low-intensity stimuli). **(G)** Percentage of total TRPA1 (AITC-responsive) neurons. *P < 0.05, **P < 0.01, ***P < 0.001, two-way ANOVA with Sidak's multiple comparisons test.

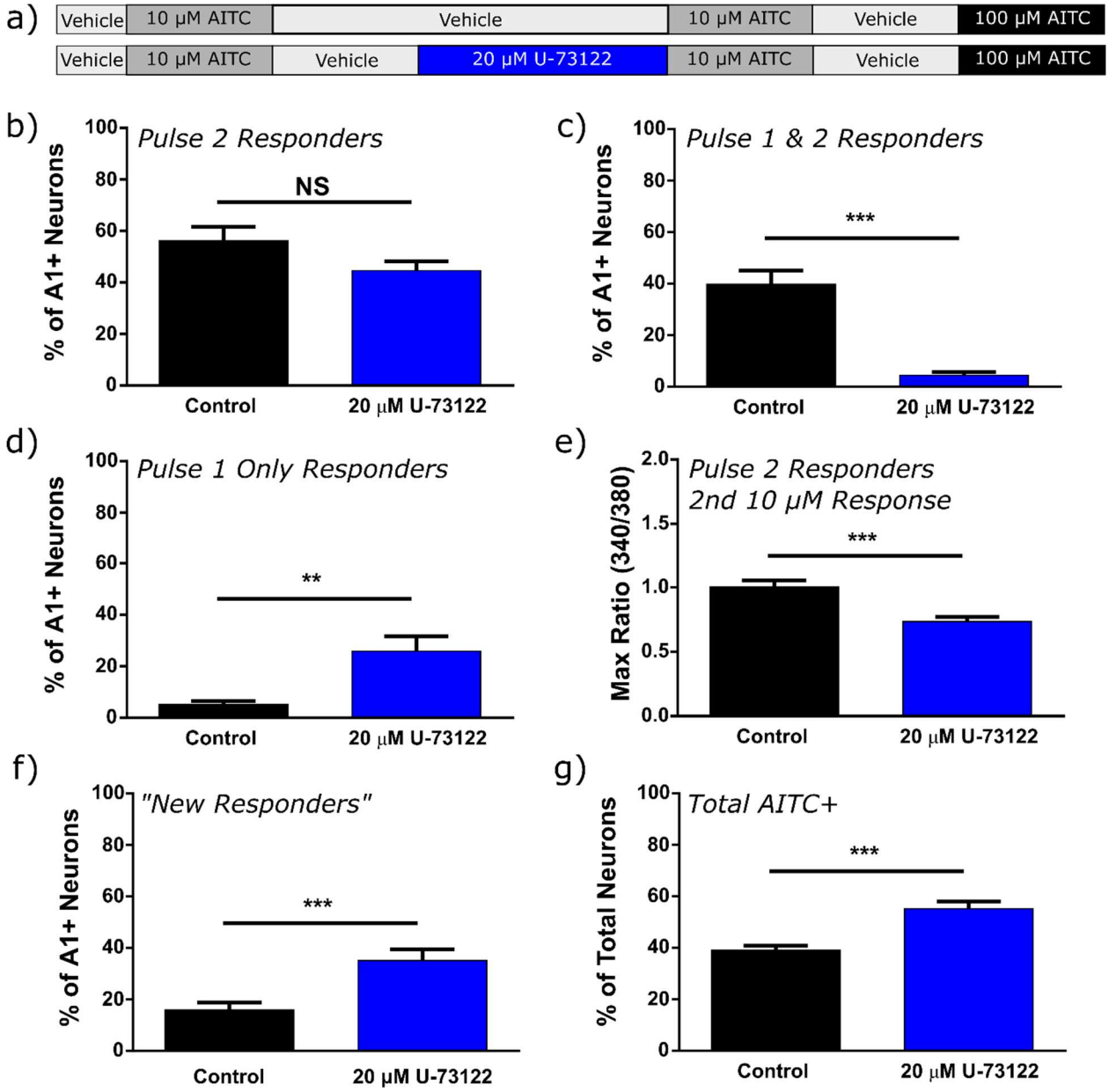

Figure 5: PLC inhibition affects neuronal recruitment to medium-intensity AITC stimuli. **(A)** Design of ratiometric calcium imaging experiments with dissociated mouse DRG neurons. After 10 μM AITC was applied to coverslips, either vehicle or PLC inhibitor (20 μM U-73122) was perfused across neurons. Neurons were allowed to incubate in this chemical for 20 minutes. A second pulse of 10 μM was then applied, followed by a washout and application of 100 μM AITC. **(B)** The percentage of TRPA1 neurons responding to the second 10 μM pulse of AITC. **(C)** Percentage of TRPA1 neurons responding to both pulses of 10 μM AITC. **(D)** Percentage of TRPA1 neurons that responded to the first, but not second, pulse of 10 μM AITC. **(E)** Response intensity to the second pulse of 10 μM AITC (of total neurons that responded to the second pulse). **(F)** Percentage of TRPA1 neurons that were "new responders", i.e., only responded to the second pulse of 10 μM AITC. **(G)** Percentage of TRPA1 (AITC-responsive) neurons out of total

N. **P < 0.01, ***P < 0.001, unpaired two-tailed Student's t-test.

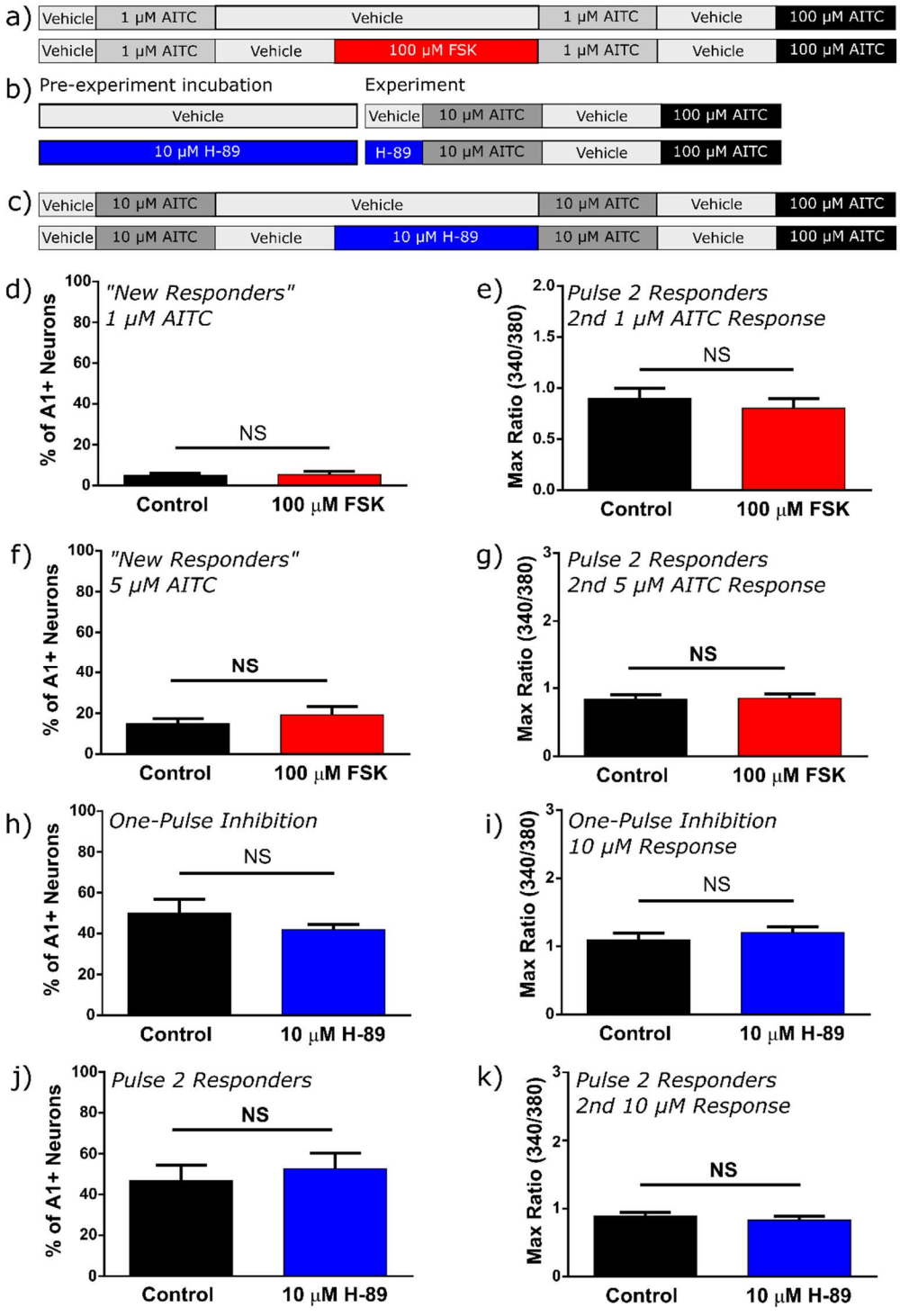

Figure 6: PKA manipulation does not affect neuronal recruitment or response intensity to intermediate AITC stimuli. (A) Design of ratiometric calcium imaging experiments with dissociated mouse DRG neurons in two-pulse activation experiments. 100 μM forskolin (FSK) was perfused across coverslips for 3 minutes between AITC pulses. Both 1 μM and 5 μM AITC were used as concentrations for test pulses. **(B)** Design of ratiometric calcium imaging

experiments with dissociated mouse DRG neurons in one-pulse inhibition experiments. Imaging experiments were preceded with a 30-minute incubation in either vehicle or PKA inhibitor (10 μM H-89). **(C)** Design of ratiometric calcium imaging experiments involving two-pulse inhibition of PKA. The PKA inhibitor H-89 (10 μM) was perfused across neurons for 3 minutes between AITC pulses. **(D)** Percentage of TRPA1 neurons that responded to 1 μM AITC stimulus in control or PKA-activated conditions. **(E)** Response intensity to 1 μM AITC (of neurons that responded to this stimulus). **(F)** Percentage of TRPA1 neurons that responded to 5 μM AITC stimulus in control vs. PKA activated conditions. **(G)** Response intensity to 5 μM AITC (of neurons that responded to this stimulus. **(H)** Percentage of TRPA1 neurons that responded to 10 μM AITC in one-pulse inhibition experiments. **(I)** Response intensity to 10 μM AITC (of neurons that responded to this stimulus). **(J)** Percentage of TRPA1 neurons that responded to the second pulse of 10 μM AITC. **(K)** Response intensity of TRPA1 neurons responding to the second 10 μM AITC pulse (total second pulse responding neurons). Unpaired two-tailed Student's t-test was used for all statistical comparisons.

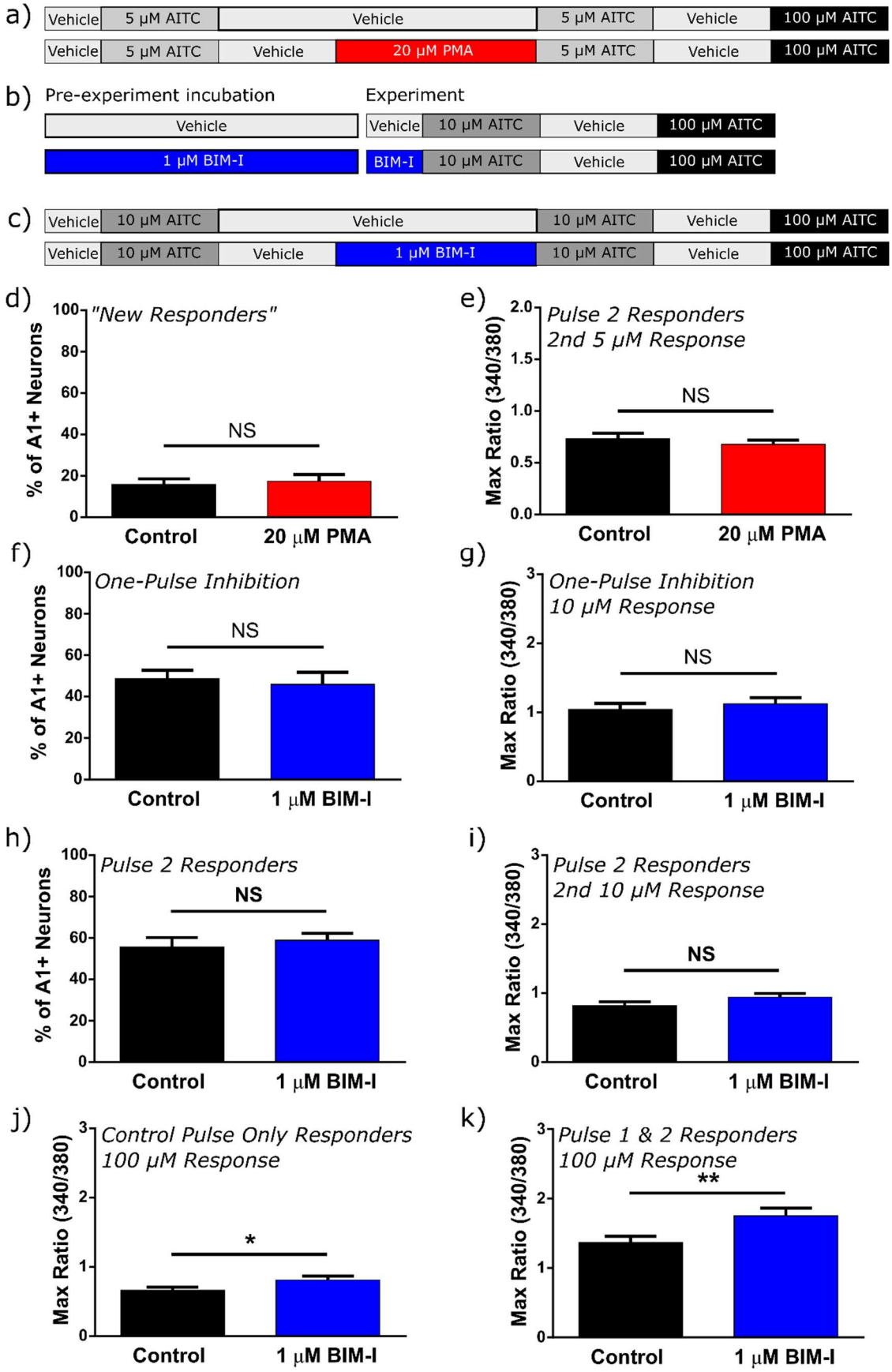
a)
Vehicle
5 μM AITC
Vehicle
5 μM AITC
Vehicle
100 μM AITC
Vehicle
5 μM AITC
Vehicle
20 μM PMA
5 μM AITC
Vehicle
100 μM AITC
b)
Pre-experiment incubation
Experiment
Vehicle
Vehicle
10 μM AITC
Vehicle
100 μM AITC
1 μM BIM-I
BIM-I
10 μM AITC
Vehicle
100 μM AITC
c)
Vehicle
10 μM AITC
Vehicle
10 μM AITC
Vehicle
100 μM AITC
Vehicle
10 μM AITC
Vehicle
1 μM BIM-I
10 μM AITC
Vehicle
100 μM AITC
d)
"New Responders"
% of A1+ Neurons
NS
Control
20 μM PMA
e)
Pulse 2 Responders
2nd 5 μM Response
Max Ratio (340/380)
NS
Control
20 μM PMA
f)
One-Pulse Inhibition
% of A1+ Neurons
NS
Control
1 μM BIM-I
g)
One-Pulse Inhibition
10 μM Response
Max Ratio (340/380)
NS
Control
1 μM BIM-I
h)
Pulse 2 Responders
% of A1+ Neurons
NS
Control
1 μM BIM-I
i)
Pulse 2 Responders
2nd 10 μM Response
Max Ratio (340/380)
NS
Control
1 μM BIM-I
j)
Control Pulse Only Responders
100 μM Response
Max Ratio (340/380)
*
Control
1 μM BIM-I
k)
Pulse 1 & 2 Responders
100 μM Response
Max Ratio (340/380)
**
Control
1 μM BIM-I

Figure 7: PKC manipulation does not affect neuronal recruitment or response intensity to intermediate AITC stimuli. (A) Design of two-pulse PKC activation ratiometric calcium imaging experiments of dissociated mouse DRG neurons. 20 μM PMA was perfused over DRG neurons for 3 minutes in between pulses of 5 μM AITC. **(B)** Design of one-pulse PKC inhibition calcium imaging experiments of dissociated mouse DRG neurons. Imaging experiments were preceded with a 30-minute incubation in either vehicle or PKC inhibitor (1 μM BIM-I). **(C)** Design of two-pulse PKC inhibition calcium imaging experiments of dissociated mouse DRG neurons. 1 μM BIM-I was applied for three minutes in between pulses of 10 μM AITC. **(D)** Percentage of TRPA1 neurons that responded to the low-intensity 5 μM AITC stimulus. **(E)** Response intensity to 5 μM AITC (of total neurons that responded to this stimulus). **(F)** Percentage of TRPA1 neurons responding to 10 μM AITC in one-pulse inhibition experiments. **(G)** Response intensity to 10 μM AITC of neurons responding to this stimulus. **(H)** Percentage of TRPA1 neurons responding to the second pulse of 10 μM AITC in two-pulse inhibition experiments. **(I)** Response intensity to the second pulse of 10 μM AITC (of total neurons responding to this stimulus). Unpaired two-tailed Student's t-test was used for all statistical comparisons. **(J)** Response intensity to 100 μM AITC (of neurons that only responded to 100 μM AITC). **(K)** Response intensity to 100 μM AITC (of neurons that responded to 100 μM AITC as well as both pulses of 10 μM AITC). *$P < 0.05$, **$P < 0.01$, unpaired two-tailed Student's t-test.

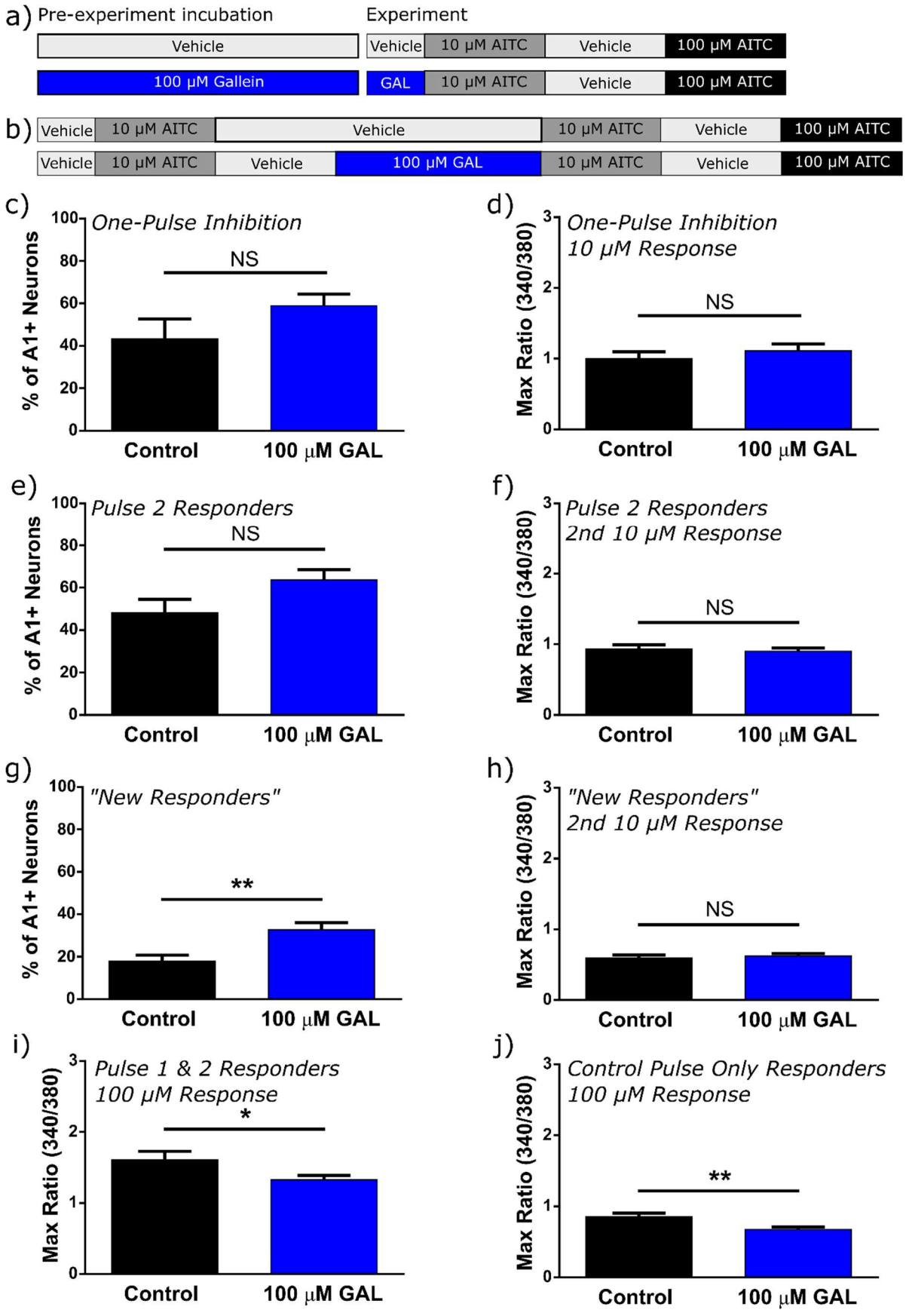
a)
Pre-experiment incubation
Experiment
Vehicle
Vehicle
10 μM AITC
Vehicle
100 μM AITC
100 μM Gallein
GAL
10 μM AITC
Vehicle
100 μM AITC
b)
Vehicle
10 μM AITC
Vehicle
10 μM AITC
Vehicle
100 μM AITC
Vehicle
10 μM AITC
Vehicle
100 μM GAL
10 μM AITC
Vehicle
100 μM AITC
c)
One-Pulse Inhibition
% of A1+ Neurons
NS
Control
100 μM GAL
d)
One-Pulse Inhibition
10 μM Response
Max Ratio (340/380)
NS
Control
100 μM GAL
e)
Pulse 2 Responders
% of A1+ Neurons
NS
Control
100 μM GAL
f)
Pulse 2 Responders
2nd 10 μM Response
Max Ratio (340/380)
NS
Control
100 μM GAL
g)
"New Responders"
% of A1+ Neurons
**
Control
100 μM GAL
h)
"New Responders"
2nd 10 μM Response
Max Ratio (340/380)
NS
Control
100 μM GAL
i)
Pulse 1 & 2 Responders
100 μM Response
Max Ratio (340/380)
*
Control
100 μM GAL
j)
Control Pulse Only Responders
100 μM Response
Max Ratio (340/380)
**
Control
100 μM GAL

Figure 8: Gβγ inhibition does not appear to set the gain on TRPA1 neurons. (A) Design of ratiometric calcium imaging experiments involving one-pulse inhibition of Gβγ. Imaging experiments were preceded with a 30-minute incubation in either vehicle or Gβγ inhibitor (100 μM gallein). **(B)** Design of two-pulse inhibition calcium imaging experiments of dissociated mouse DRG neurons. 100 μM gallein (GAL) was perfused across cells for 3 minutes between 10 μM AITC pulses. **(C)** Percentage of TRPA1 neurons responding to 10 μM AITC in one-pulse inhibition experiments. **(D)** Response intensity to 10 μM AITC (of neurons that responded to this stimulus) in one-pulse inhibition experiments. **(E)** Percentage of TRPA1 neurons responding to the second pulse of 10 μM AITC in two-pulse inhibition experiments. **(F)** Response intensity to the second 10 μM AITC pulse (of total neurons that responded to this pulse). **(G)** Percentage of TRPA1 neurons that were "new responders", i.e., responded to the second 10 μM AITC pulse but not the first. **(H)** Response intensity to the second 10 μM AITC pulse of neurons that were "new responders". **(I)** Response to 100 μM AITC (of neurons that responded to the second pulse 10 μM pulse as well as the 100 μM positive control pulse). **(J)** Response intensity to 100 μM AITC (of neurons that only responded to the 100 μM pulse). *$P < 0.05$, **$P < 0.01$, unpaired two-tailed Student's t-test.

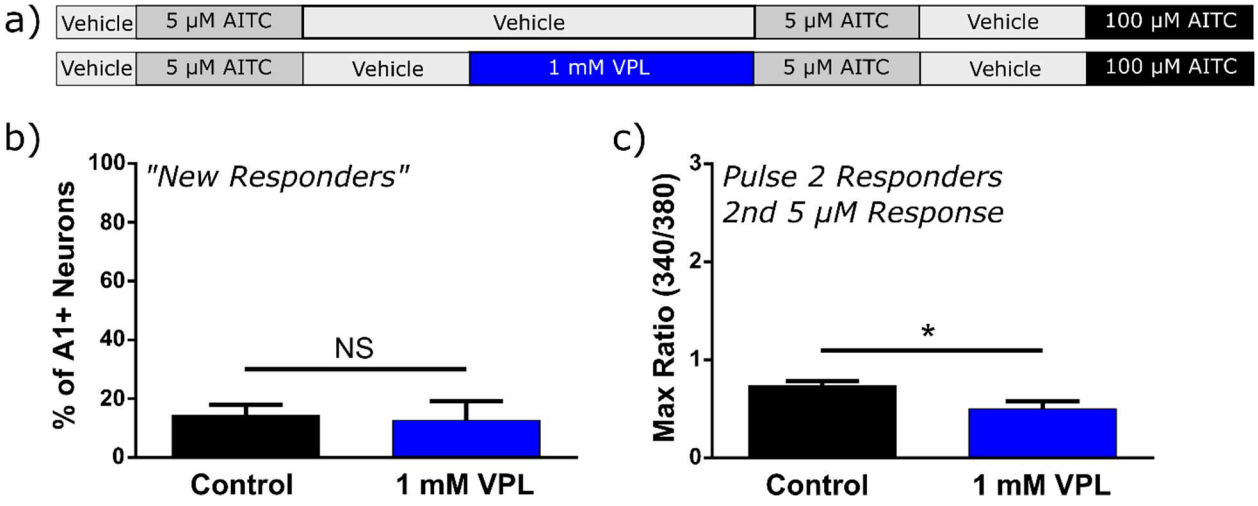

Figure 9: NALCN inhibition does not affect neuronal recruitment to AITC stimuli. (A) Design of two-pulse inhibition calcium imaging experiments of dissociated mouse DRG neurons. 1 mM verapamil (VPL) was perfused across cells for 5 minutes between 5 μM AITC pulses. **(B)** Percent of TRPA1 neurons that were "new responders" to the second 5 μM AITC pulse. **(C)** Response intensity to the second 5 μM AITC pulse (of neurons that responded to this stimulus. *P < 0.05, unpaired two-tailed Student's t test.

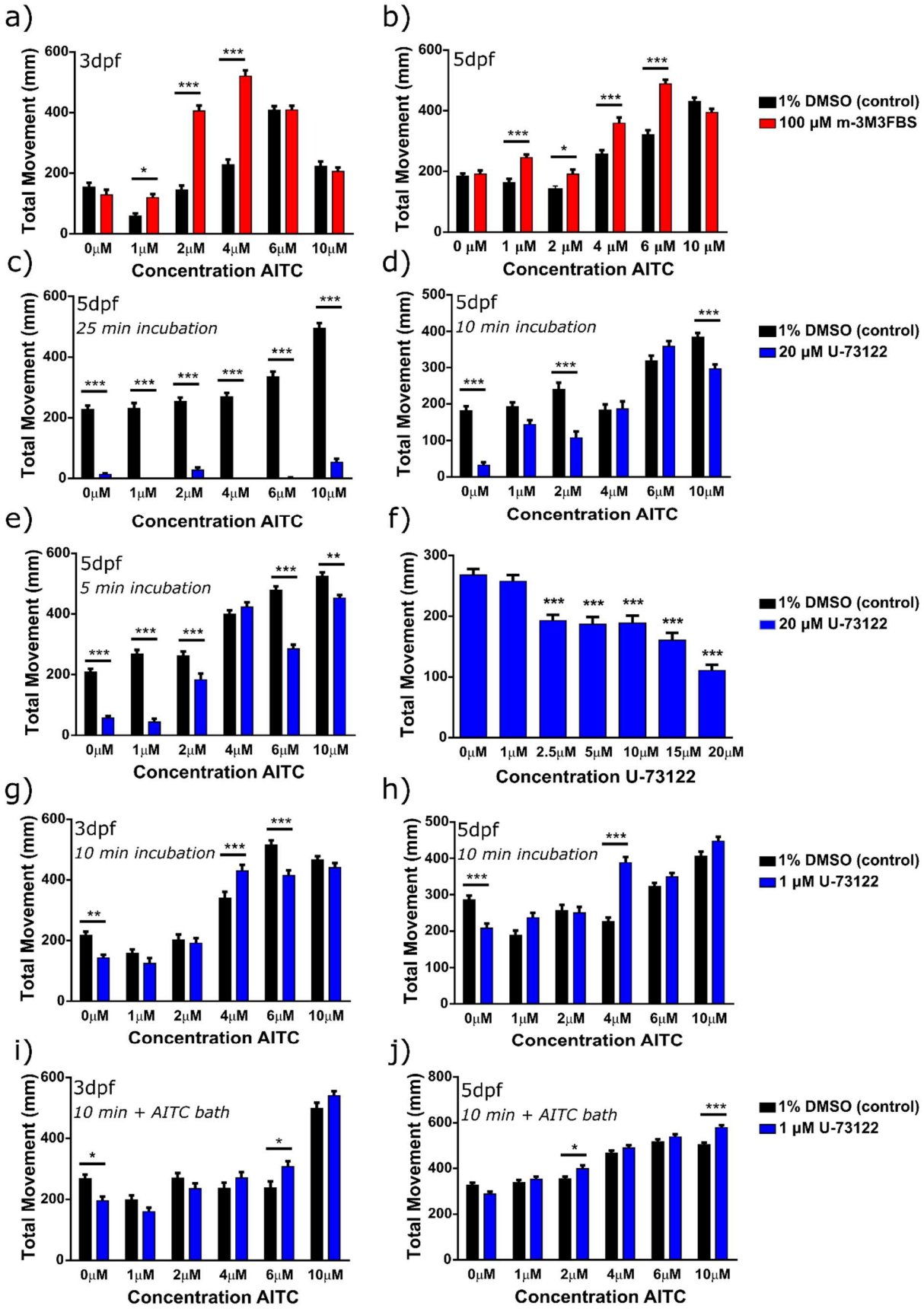
a)
3dpf
Total Movement (mm)
600
400
200
0
0μM 1μM 2μM 4μM 6μM 10μM
Concentration AITC
b)
5dpf
Total Movement (mm)
600
400
200
0
0 μM 1 μM 2 μM 4 μM 6 μM 10 μM
Concentration AITC
1% DMSO (control)
100 μM m-3M3FBS
c)
5dpf
25 min incubation
Total Movement (mm)
600
400
200
0
0μM 1μM 2μM 4μM 6μM 10μM
Concentration AITC
d)
5dpf
10 min incubation
Total Movement (mm)
500
400
300
200
100
0
0μM 1μM 2μM 4μM 6μM 10μM
Concentration AITC
1% DMSO (control)
20 μM U-73122
e)
5dpf
5 min incubation
Total Movement (mm)
600
400
200
0
0μM 1μM 2μM 4μM 6μM 10μM
Concentration AITC
f)
Total Movement (mm)
300
200
100
0
0μM 1μM 2.5μM 5μM 10μM 15μM 20μM
Concentration U-73122
1% DMSO (control)
20 μM U-73122
g)
3dpf
10 min incubation
Total Movement (mm)
600
400
200
0
0μM 1μM 2μM 4μM 6μM 10μM
Concentration AITC
h)
5dpf
10 min incubation
Total Movement (mm)
500
400
300
200
100
0
0μM 1μM 2μM 4μM 6μM 10μM
Concentration AITC
1% DMSO (control)
1 μM U-73122
i)
3dpf
10 min + AITC bath
Total Movement (mm)
600
400
200
0
0μM 1μM 2μM 4μM 6μM 10μM
Concentration AITC
j)
5dpf
10 min + AITC bath
Total Movement (mm)
800
600
400
200
0
0μM 1μM 2μM 4μM 6μM 10μM
Concentration AITC
1% DMSO (control)
1 μM U-73122

Figure 10: PLC manipulation affects behavioral responses of larval zebrafish to AITC stimuli. (A) Behavioral AITC dose-response curve for 3dpf zebrafish in control or PLC activated conditions. **(B)** Behavioral AITC dose-response curve for 5dpf zebrafish in control or PLC activated conditions. **(C)** Behavioral dose-response curve for 5dpf zebrafish in control or PLC inhibited conditions (20 μM U-73122, 25 minute pre-incubation). **(D)** Same as (c), but with a 10 minute pre-incubation. **(E)** Same as (**C**) and (**D**), but with a 5 minute pre-incubation. **(F)** Behavioral dose-response curve for U-73122, in control conditions. 5dpf larvae were pre-incubated in U-73122 for 10 minutes. **(G)** Behavioral AITC dose-response curve for 3dpf larvae in control or PLC-inhibited conditions (1 μM AITC, 10 minute pre-incubation). **(H)** Same as (**G**), but with 5dpf larvae. **(I)** Same as (**G**), but with sustained 1 μM U-73122 in the AITC bath. **(J)** Same as (**H**), but with sustained 1 μM U-73122 in the AITC bath. *$P < 0.05$, **$P < 0.01$, ***$P < 0.001$. A two-way ANOVA with Sidak's multiple comparisons test was used for all analyses except for the data in (**F**), in which a one-way ANOVA with Dunnett's multiple comparisons test was used.

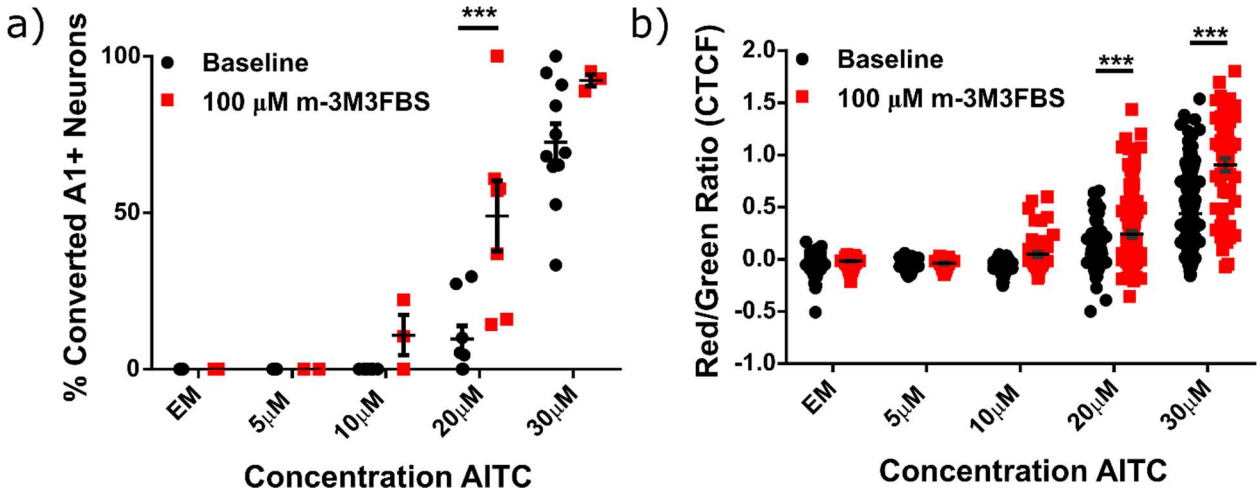

Figure 11: PLC activation shifts neuronal recruitment to intermediate doses of AITC in larval zebrafish. **(A)** Percent of active TRPA1 neurons following application of different intensity AITC stimuli in control baseline or PLC-activated conditions. Each data point represents values from an individual fish. **(B)** Red/green corrected total cell fluorescence (CTCF) ratio for all neurons exposed to different concentrations of AITC in either control baseline or PLC-activated conditions. ***P < 0.001, two-way ANOVA with Sidak's test for multiple comparisons.

Table 1: Percentage of active TRPA1 neurons in CaMPARI imaging experiments

Bath	Control			100 µM m-3M3FBS			20 µM U-7122 (5 min)			20 µM U-7122 (10 min)			20 µM U-7122 (20 min)			20 µM U-7122 (30 min)		
Condition	Mean	SEM	N	Mean	SEM	N	Mean	SEM	N	Mean	SEM	N	Mean	SEM	N	Mean	SEM	N
EM	0	0	11	0	0	5							21.0526	0	2	6.25	6.25	2
5 µM	0	0	5	0	0	2												
10 µM	0	0	6	10.91617	6.417958	3												
20 µM	9.588875	4.298056	8	48.97609	11.2606	7							29.1667	0	1	47.0588	0	1
30 µM	72.54322	5.882556	11	92.32804	1.851848	3	100	0	1	97.3684	2.631599	2	80.3268	9.972618	3	54.54547	29.22319	3
50 µM	70.81462	7.360198	11				100	0	2	88.5621	0.3268	2						

Table 2: Red/Green CTCF ratios of TRPA1 neurons in CaMPARI imaging experiments

Bath	Control			100 µM m-3M3FBS			20 µM U-7122 (5 min)			20 µM U-7122 (10 min)			20 µM U-7122 (20 min)			20 µM U-7122 (30 min)		
Condition	Mean	SEM	N	Mean	SEM	N	Mean	SEM	N	Mean	SEM	N	Mean	SEM	N	Mean	SEM	N
EM	-0.0205	0.004451	220	-0.0157	0.004478	95							0.143817	0.017319	38	0.033962	0.01664	22
5 µM	-0.04298	0.006515	76	-0.03567	0.007755	37												
10 µM	-0.04392	0.00584	103	0.048205	0.021562	58												
20 µM	0.048769	0.011321	168	0.241558	0.030308	134							0.14075	0.015354	24	0.257313	0.07059	17
30 µM	0.439312	0.027368	178	0.90565	0.061568	58	1.110156	0.353863	5	0.398675	0.038364	21	0.462687	0.043288	58	0.594978	0.074492	36
50 µM	0.387921	0.020575	189				0.476615	0.049293	24	0.396319	0.034516	26						

Chapter 4: Future Directions

In this thesis, I have demonstrated that a lower vertebrate, the zebrafish, is indeed capable of behaviorally responding to pruritic stimuli in a manner distinct from nocifensive behaviors. The mechanism of this form of itch transduction is distinct from the established way itch stimuli are processed in mammals, where pruritic receptors on itch neurons respond to pruritogens and activate TRP ion channels. In this alternate mechanism, itch instead results from the direct activation of a TRPA1 on a highly-sensitive subpopulation of TRPA1 neurons that are primed to respond to weaker, pruritic stimuli. This mechanism is conserved in the mouse, suggesting that it persisted throughout evolutionary history and may be relevant for multiple species. Certain factors, such as size, distinguish these highly-sensitive neurons from other, less-sensitive TRPA1 neurons. Other morphological factors such as region of innervation do not appear to be a factor in establishing the sensitivity of neurons. Furthermore, the phospholipase C (PLC) intracellular signaling pathway may be involved in setting the gain and establishing the baseline responsivity of these TRPA1 neurons in both species, and is likely involved in sensitizing zebrafish behavioral responses to AITC stimuli. While these findings provide new insight into the underlying mechanisms through which itch and pain are coded in two species, they also raise many questions that could be explored in much greater depth.

Our findings that soma size correlates with response threshold in mouse DRG neurons imply that more sensitive neurons are part of a distinct subpopulation, and hint at a possible physiological mechanism for heightened sensitivity (e.g., through increased input resistance). Results from DiI experiments indicate that different populations of neurons innervate the same general area, which potentially implying that they have overlapping receptive fields. However, these are only two metrics of measuring morphology, and the vast array of other possibility

morphological distinctions is a fruitful ground for future research. We had initially wanted to explore more morphological characteristics using Tg(TrpA1b(ss)-CaMPARI) zebrafish, which express the photoconvertible calcium indicator CaMPARI solely in TRPA1 neurons. In such experiments, fish would be exposed to low-intensity pruritic stimuli in tandem with a blue light to photoconvert active neurons. The morphology of photoconverted and unconverted neurons would be compared with respect to soma size, dendritic branching patterns, and both peripheral and central projection patterns. Differences revealed by such analysis could provide valuable information regarding the selective coding of itch versus pain—for example, it may reveal that more sensitive (itch-responsive) neurons project to more superficial locations on the skin, as opposed to more deeply-localized less sensitive (pain-responsive) neurons, which has been suggested to occur in mammals and is the proposed mechanism underlying the spatial-contrast theory of itch coding[13,92]. Determining whether neurons that photoconverted in response to low-intensity stimuli tile with each other would likewise be informative. Previous work in both the zebrafish and fruit fly demonstrate that dendritic projections of neurons within the same populations tile, whereas those from neurons in different populations overlap[257–259]; findings in mammals, however, have been mixed. In mice, neurons within the same broad population of nonpeptidergic nociceptors overlap extensively with each other as well as with peptidergic nociceptors[213], but whether multiple subpopulations that do exhibit tiling exist within these overarching groups is unknown.

Technical limitations, however, prevented us from being able to explore this in full, as it was difficult to discern both peripheral processes and central processes of lightly-photoconverted neurons consistently. In the future, similar experiments could be performed using alternate methods. In the zebrafish, tracer dyes could be injected into the soma of peripheral neurons using

iontophoretic methods to examine their morphology, as has been demonstrated previously[260]. Such experiments could provide information on connectivity and circuit wiring in addition to morphological data on peripheral and central processes. Another approach would be to use nuclear-localized CaMPARI in transgenics expressing zebrabow (the zebrafish equivalent of Brainbow) in somatosensory neurons[261] which would allow us to simultaneously assess neuronal activity and the tracing of processes, which would be brightly labeled in diversity of colors. In the mouse, employing techniques such as targeted recombination in active populations (TRAP, TRAP2) could label neurons that were active following exposure to differing intensity stimuli[262,263]. Such experiments would allow us to make similar quantifications of central and peripheral morphology (axonal branching, receptive field size, overlap with other neurons, etc.) that could yield valuable insight into circuit connectivity and thus itch and pain coding mechanisms. These techniques would also provide an alternate method to confirm our observations that increasing stimulus intensity recruits more active neurons. Additionally, TRAP and TRAP2 can be used to not only label, but express certain effectors in transiently active neurons, allowing for manipulation of these neurons[262,263].

Unlike our imaging studies in the zebrafish, all of our calcium imaging in the mouse was performed *in vitro*, with cultured, dissociated neurons that have literally been ripped away from their peripheral and central processes. While these studies have yielded valuable information, we would ideally like to perform similar experiments in animals with intact circuity, to confirm that these observations are relevant *in vivo*. This could be accomplished using *in vivo* calcium imaging of the trigeminal or dorsal root ganglia in animals expressing GCaMP in certain neuronal populations, which has previously done in the investigation of high-threshold mechanoreceptors[211] as well as injury-induced tactile allodynia[264]. Through such experiments,

we could confirm the existence of dose-dependent increases in neuronal recruitment, and whether this changes in conditions of PLC activation or inhibition, in a living mammal.

Exploring the specific ways in which PLC signaling may function to potentiate responses in TRPA1 neurons would likewise be helpful. As outlined in Chapter 3, PLC activation leads to hydrolysis of PIP2 as well as the generation of multiple downstream signaling molecules, a number of which have been shown to modulate TRPA1. Which of these factors—PIP2 itself or downstream effectors such as DAG, AA, or IP3—participate in the PLC-induced potentiation of neuronal responses in TRPA1 neurons remains to be determined. PIP2 dynamics could be examined with fluorescent reporter constructs, which have previously been employed in zebrafish models to quantify PIP2 breakdown and localization[265–267]. Such techniques would be especially powerful if coupled with calcium imaging (using either CaMPARI or GCaMP transgenics), allowing us to establish whether there are differences in the quantity, localization, and rate of depletion of PIP2 in neurons that have different response thresholds to AITC. While it has been shown that DAG, AA, and intracellular calcium are capable of directly activating TRPA1 in heterologous expression systems[64,72,248–250], whether any of these factors are relevant in tonic sensitization or inhibition of TRPA1-expressing somatosensory neurons is unknown. To resolve this, individual downstream effectors could be pharmacologically inhibited during and/or after PLC activation, and the responses of DRG neurons to TRPA1 agonists could be measured using ratiometric calcium imaging, electrophysiology, or some combination thereof. If inhibition of any of these individual effectors reversed the PLC-induced increases in neuronal recruitment, it would be indicative that such a molecule may be involved in establishing the sensitivity of neuronal subpopulations. Pharmacological methods of blocking these individual components have previously been documented in the literature. Xestospongins, for example, have been used

to block the IP3 receptor and thus prevent the release of calcium from intracellular stores[268,269]. The conversion of DAG to AA can similarly be blocked by inhibiting the DAG and MAG lipases[270].

Supplementing our results with additional behavioral experiments would help establish the ethological relevance of the changes we observed in neuronal recruitment to intermediate doses of AITC following PLC activation or inhibition. While we did observe potentiation of behavior in the zebrafish following PLC activation—consistent with the hypothesis that increasing neuronal recruitment intensifies behavioral responses—whether the reverse is true in zebrafish is currently unknown. The technical limitations that undermined our attempts to do this with larval zebrafish behavior could potentially be surmounted with a tissue-specific knockout of PLC (both generally and targeted towards specific isoforms of the enzyme). Such CRISPR/Cas9-based techniques have previously been employed in the zebrafish[271,272], so it should be feasible to knockout PLC specifically in TRPA1 neurons in the zebrafish. This approach would theoretically allow us to inhibit PLC without reducing baseline locomotion would be ideal for use in our zebrafish total locomotion assay.

Additionally, it would greatly behoove us to perform behavioral assays that can allow us to distinguish between itch and pain responses, helping to further test the hypothesis that changes in neuronal recruitment have behavioral relevance. In the zebrafish this could be achieved with the lip injection and "open tank" assay outlined in Chapter 2; in the mouse, this could be accomplished through the cheek assay[153,154]. Were we to sensitize neurons with PLC activation, less-sensitive neurons would be recruited by stimuli that would only normally only elicit itch behaviors such as scratching or rubbing, so would expect to see pain behaviors (or a mixture of pain and itch behaviors) following the application of low-intensity TRPA1 agonists in these

conditions. Given the complexity of our DRG imaging results, however, one could imagine multiple scenarios unfolding following PLC inhibition. We observed that U-73122 application significantly reduced responses to medium-intensity AITC in neurons that had previously been responsive to this stimulus. If these neurons are the predominant determinants of behavioral response, we would expect that under conditions of PLC inhibition, high-threshold pain neurons would no longer be recruited by stimuli that would normally elicit nocifensive responses, leaving only the most highly-sensitive itch neurons to respond. Thus, we would expect to observe itch behaviors following application of ordinarily painful stimuli. However, we also observed an increase in the percentage of TRPA1 neurons that were "new responders" to medium-intensity stimuli, raising questions about the identity of these neurons and the circuits into which they feed. Are these neurons high-threshold TRPA1 responders somehow sensitized by PLC inhibition, in which case we might observe equivalent pain responses or even an increase in pain behaviors resulting from their recruitment, as opposed to itch replacing pain? Are these neurons perhaps not even TRPA1 neurons, as suggested by the increase in the total percentage of AITC-responsive neurons following PLC inhibition? If, for example, AITC is ectopically activating TRPV1, which population of TRPV1 neurons is responding? One could speculate that an analogous itch coding strategy may be in place for TRPV1 neurons, in which a subset of highly-sensitive neurons are primed to respond to low-intensity TRPV1 agonists to relay itch. If only these highly-sensitive neurons were recruited by medium-intensity AITC during conditions of PLC inactivation, would we observe only itch behaviors, and no or little pain? Employing nuanced essays that would allow us to distinguish these two sensations to complement standard nociception tests would help to resolve this quandary. Coupling these behavioral assays with *in vitro* studies of TRPA1 or TRPV1-transfectd HEK cells would also help untangle the potential

role of TRPV1-expressing neurons in conditions of PLC inhibition. The role of TRPV1 could also be probed through *in vitro* calcium imaging experiments of dissociated mouse DRG neurons in which TRPV1 was antagonized with capsazepine[273], or using tissue obtained from TRPV1$^{-/-}$ mice.

Ideally, we would like to correlate our observations from calcium imaging experiments to possible differences in electrical activity and gene expression. This could be accomplished through a combination of calcium imaging and patch-seq techniques. For example, DRG neurons from GCaMP-expressing mice could be dissociated and cultured, and stimulated with agonists of different intensities. Neurons that responded to certain stimuli could then be targeted for whole-cell patch clamp experiments, which would allow us to determine characteristics such as resting membrane potential, input resistance, and rheobase, among other factors, providing us with valuable insight about the electrical properties of these TRPA1 neurons and which factors might be contributing to differences in excitability between neurons with different AITC response thresholds. Furthermore, the contents of patched cells could be isolated and used for single-cell RNAseq studies, as has previously been performed on cortical neurons[274,275]. These transciptomic profiling studies demonstrated that gene expression patterns could be used to infer morphology and physiological properties (axonal arborization patterns, action potential amplitude, etc.), so it is certainly plausible that a similar approach could be taken with somatosensory neurons to yield critical information about the differences between populations that could contribute to variations in their sensitivity to TRPA1 agonists. This data could confirm, for instance, whether there was differential expression of certain genes—PLC isoforms, ion channels that establish the resting membrane potential, even TRPA1 itself—within these various functional subpopulations of TRPA1 neurons.

A similar approach could be taken with the zebrafish. It is possible to make electrophysiological recordings from larval trigeminal[276] and Rohon-Beard[277] neurons. It should be feasible to similarly aspirate cell contents for sequencing purposes. An alternate approach available in the zebrafish, which could bypass the need for calcium imaging and allow us to examine the electrical properties of many neurons in tandem, would be to employ a genetically encoded voltage indicator, such as ArcLight[278–280] expressed either pan-neuronally or restricted to TRPA1 neurons. Neurons that responded to low-, medium-, or high-intensity stimuli could then be targeted for extraction of cell contents for use in similar RNAseq studies.

While we established that zebrafish were capable of experiencing itch and identified a potential coding mechanism underlying this sensation, so much remains to be learned about itch and pain circuitry in lower vertebrates. Exploring more sources of itch, including those that may be of greater ethological relevance to fish, such as skin pathogens that are enriched in aquatic environments compared terrestrial ones[281], may be illuminating. Both eurkaryotic parasites and bacterial pathogens can evoke robust immune responses in fish[282]. Though we did target known mammalian endogenous pruritogens released during immune and inflammatory responses (such as histamine, serotonin, and the protease SLIGRL) in our initial screening experiments, it is unlikely that we exhausted all of the possible pruritic contenders. Histamine and serotonin may not, for instance, play as important a role in zebrafish immune responses as they do in mammals. As mentioned in Chapter 2, unlike mammalian mast cells, zebrafish mast cells release a complex assortment of proteolytic enzymes and antimicrobial peptides instead of histamine following insult[199]. In zebrafish and other species, the skin itself contains a similar complement of bacteriolytic enzymes, acid and alkaline phosphatases, proteases, and pro-inflammatory cytokines[281,282]. Zebrafish also possess a diverse array of interleukins[283], which in mammals have

been implicated in both allergic contact dermatitis (a skin condition that results from exposure to pruritogens and irritants like urushiol, a molecule found in poison ivy) as well as atopic dermatitis (an inflammatory skin condition associated with intense pruritus)[284,285]. To the best of our knowledge, the potential roles of these immune molecules as endogenous pruritogens has yet to be explored. A more thorough survey of potential pruritogens could potentially identify novel pruritic stimuli in the zebrafish, as well as illuminate whether our model of itch transduction in the zebrafish extrapolates to such pruritogens. In zebrafish, as in mammals, it may be possible that both the direct activation of TRP ion channels as well as activation of upstream immune-related pruritic receptors can elicit sensations of itch. Further exploration of these possibilities would help to clarify the mechanisms lower vertebrates employ to transduce itch.

The sensation of itch extends beyond the peripheral somatosensory neurons, the first detectors of pruritic stimuli, and probing the spinal circuity involved in itch transduction would likewise be enlightening. Population coding theories of itch, particularly those like the selectivity theory in which pain transmission overrides itch signaling, implies a degree of downstream processing beyond peripheral somatosensory neurons. In mammals, local inhibitory interneurons in the dorsal horn of the spinal cord help to refine the sensations of itch and pain. Painful stimuli inhibit the effects of itch by activating these inhibitory neurons, which synapse onto second-order itch neurons. Organisms lacking these neurons, which can be identified through the expression of markers such as Bhlhb5 and dynorphin, often exhibit uncontrolled itch phenotypes[41]. Likewise, blocking the kappa opioid receptors on second-order itch projection neurons, through which these neurons mediate their effects, has also been shown to promote itch in mammals; conversely, activating them suppresses itch[286,287]. Whether similar circuitry exists in the zebrafish is unknown. Zebrafish are known to express orthologs for genes considered to be

markers for some of these interneuron subpopulations, such as Bhlhb5 and dynorphin[133,288], as well as those coding for kappa opioid receptors[134] that mediate the inhibitory action of these neurons. Behavioral experiments involving pharmacological manipulation of these targets could elucidate whether they are actively involved in the transduction of itch stimuli. Both larval and adult zebrafish could be screened for behavioral responses to both pruritic and nociceptive stimuli following the application of kappa-opioid receptor agonists and antagonists such as nor-binaltorphimine, bremazocine, and U-69593[289–292]. If inhibition mediated by kappa opioid receptors is responsible for suppressing itch in zebrafish, then pharmacological stimulation of these receptors should eliminate itch behavioral responses, while pain-induced behavioral changes should be unaffected. Blocking these receptors, by contrast, should potentiate the behavioral response to itch stimuli, perhaps even eliciting spontaneous itch behaviors following the application of control stimuli, as has been observed in the mouse[293]. If such behavioral experiments do yield promising data, systematic manipulation of individual targets via genetic strategies could help to further dissect their roles in itch circuitry. For example, Bhlbh5 neurons could be ablated or optogenetically stimulated, or the Bhlbh5 gene could be knocked out; other candidates such as kappa opioid receptors could similarly be deleted. Spinal processing is not merely limited to inhibition, however, and exploring other aspects of itch transduction in the spinal cord would also be of great interest. Nppb and GRP are key itch-related neuropeptides in the mammalian spinal cord[91], and while both of these are present in the genomes of zebrafish and other teleost fish, they have primarily been explored in the contexts of cardiac function[294,295], sleep/wake cycles[296], and regulating food intake[297–300]. Probing the potential role of these neuropeptides in fish itch, and comparing them to the roles they play in mammals, could yield

valuable information about the evolutionary history of spinal processing mechanisms of pruritic stimuli.

Lastly, examining the brain regions involved in itch sensation in the zebrafish would provide additional insight into how itch and pain are coded in this species. Initial experiments could take the form of whole-brain imaging to identify certain regions differentially activated by pruritic vs. painful stimuli. Lightsheet microscopy could be a useful tool in such experiments, as it has been employed extensively in the zebrafish for whole-brain imaging purposes in the zebrafish[301–303]. Transgenic zebrafish expressing CaMPARI pan-neuronally could be used in such experiments; alternatively, immunohistochemical techniques using antibodies targeted towards markers of neuronal activity, such as c-Fos or phosphor ERK, could similarly be employed[304–306]. While we did not have great success using c-Fos antibodies to label active trigeminal neurons in the zebrafish, perhaps due to low baseline expression levels of c-Fos observed by others[306], labeling active neurons in larval zebrafish using phospho-ERK staining[305] has been satisfactorily performed in the lab, and would be a promising tool for future experiments.

Together, these proposed experiments would allow us to identify other morphological characteristics of highly-sensitive itch neurons, illuminate the exact ways in which PLC signaling exerts its effects on neuronal recruitment, and establish the behavioral relevance of phenomena we observed in imaging experiments. Additionally, we would be able to identify electrophysiological properties and differences in gene expression that may contribute the heightened sensitivity of TRPA1-expressing itch neurons. Lastly, these experiments would allow us to expand upon our knowledge base of itch in fish, providing valuable insight as to how itch signals are processed beyond the periphery. As such, they will further our understanding of itch

transduction mechanisms in different species and allow us for formulate hypotheses about how itch evolved, and at what times certain aspects of itch coding strategies emerged in evolutionary history. Understanding the molecular basis and neural circuitry of itch and pain may also improve understanding of various pathological conditions, perhaps even aiding in the identification of novel therapeutic targets for the treatment of itch and pain disorders.

References

1. Merskey, H. The definition of pain. *Eur. psychiatry* (1991).
2. Basbaum, A. I., Bautista, D. M., Scherrer, G. & Julius, D. Cellular and Molecular Mechanisms of Pain. *Cell* **139**, 267–284 (2009).
3. Basbaum, A. I. & Jessell, T. M. The Perception of Pain. in *Principles of Neural Science* (eds. Kandel, E. R., Schwartz, J. & Jessell, T. M.) 472–491 (Appleton and Lange, 2000).
4. Dubin, A. E. & Patapoutian, A. Nociceptors : the sensors of the pain pathway. *J. Clin. Invest.* **120**, 3760–3772 (2010).
5. Ikoma, A., Steinhoff, M., Ständer, S., Yosipovitch, G. & Schmelz, M. The neurobiology of itch. *Nat. Rev. Neurosci.* **7**, 535–547 (2006).
6. Price, T. J. & Dussor, G. Evolution: The advantage of 'maladaptive' pain plasticity. *Curr. Biol.* **24**, R384–R386 (2014).
7. Crook, R. J., Dickson, K., Hanlon, R. T. & Walters, E. T. Nociceptive sensitization reduces predation risk. *Curr. Biol.* **24**, 1121–1125 (2014).
8. Browne, L. E. *et al.* Time-Resolved Fast Mammalian Behavior Reveals the Complexity of Protective Pain Responses. *Cell Rep.* **20**, 89–98 (2017).
9. Deuis, J. R., Dvorakova, L. S. & Vetter, I. Methods used to evaluate pain behaviors in rodents. *Front. Mol. Neurosci.* **10**, 1–17 (2017).
10. Ehrensing, R. H., Michell, G. F. & Kastin, A. J. Similar antagonism of morphine analgesia by MIF-1 and naloxone in Carassius auratus. *Pharmacol. Biochem. Behav.* **17**, 757–761 (1982).
11. Fernö, A. & Huse, I. The effect of experience on the behaviour of cod (Gadus morhua L.) Towards a baited hook. *Fish. Res.* **2**, 19–28 (1983).
12. Bitterman, M. E. Classical conditioning in the goldfish as a function of the CS-UCS interval. *J. Comp. Physiol. Psychol.* **58**, 359–366 (1964).
13. Ross, S. E. Pain and itch: Insights into the neural circuits of aversive somatosensation in health and disease. *Curr. Opin. Neurobiol.* **21**, 880–887 (2011).
14. Cox, J. J. *et al.* An SCN9A channelopathy causes congenital inability to experience pain. *Nature* **444**, 894–898 (2006).
15. Cox, J. J. *et al.* Congenital insensitivity to pain: Novel SCN9A missense and in-frame deletion mutations. *Hum. Mutat.* **31**, 1670–1686 (2010).
16. Zhang, S. *et al.* Clinical features for diagnosis and management of patients with PRDM12 congenital insensitivity to pain. *J. Med. Genet.* **53**, 533–535 (2016).
17. Nagasako, E. M., Oaklander, A. L. & Dworkin, R. H. Congenital insensitivity to pain: an update. *Pain 101* 213–219 (2003). doi:10.1016/S0304-3959(02)00482-7
18. Dahlhamer, J. *et al.* Prevalence of Chronic Pain and High-Impact Chronic Pain Among Adults — United States, 2016. *Morb. Mortal. Wkly. Rep.* **67**, (2018).
19. Scholl, L., Seth, P., Kariisa, M., Wilson, N. & Baldwin, G. Drug and Opioid-Involved Overdose Deaths — United States, 2013–2017. *MMWR. Morb. Mortal. Wkly. Rep.* **67**, 2013–2017 (2018).
20. Rajka, G. *Essential Aspects of Atopic Dermatitis*. (Springer, 1989).
21. Weisshaar, E. & Dalgard, F. Epidemiology of itch: Adding to the burden of skin morbidity. *Acta Derm. Venereol.* **89**, 339–350 (2009).
22. Weisshaar, E. & Matterne, U. Chapter 2: Epidemiology of Itch. in *Itch: Mechanisms and Treatment* (eds. Carstens, E. & Akiyama, T.) (CRC Press/Taylor & Francis, 2014).
23. Yosipovitch, G., Goon, A., Wee, J., Chan, Y. H. & Goh, C. L. The prevalence and clinical

characteristics of pruritus among patients with extensive psoriasis. *Br. J. Dermatol.* **143**, 969–973 (2000).
24. St. Sauver, J. L. *et al.* Why do patients visit their doctors? Assessing the most prevalent conditions in a defined US population. *Mayo Clin Proc.* **88**, 56–67 (2013).
25. Ständer, S. *et al.* Prevalence of Chronic Pruritus in Germany: Results of a Cross-Sectional Study in a Sample Working Population of 11,730. *Dermatology* **221**, 229–235 (2010).
26. Gardner, E. P. & Johnson, K. O. The Somatosensory System: Receptors and Central Pathways. in *Principles of Neural Science* (eds. Kandel, E. R., Schwartz, J. H., Jessell, T. M., Siegelbaum, S. A. & Hudspeth, A. J.) 475–497 (McGraw-Hill, 2013).
27. Le Pichon, C. E. & Chesler, A. T. The functional and anatomical dissection of somatosensory subpopulations using mouse genetics. *Front. Neuroanat.* **8**, 21 (2014).
28. Erlanger, J. & Gasser, H. S. *Electrical Signs and Nervous Activity*. (University of Philadelphia Press, 1938).
29. Johnson, E. O., Babis, G. C., Soultanis, K. C. & Soucacos, P. N. Functional Neuroanatomy of Proprioception. *J. Surg. Orthop. Adv.* **17**, 159–164 (2008).
30. Vallbo, A. B., Hagbarth, K. E., Torebjork, H. E. & Wallin, B. G. Somatosensory, proprioceptive, and sympathetic activity in human peripheral nerves. *Physiol. Rev.* **59**, 919–957 (1979).
31. Johansson, R. S. & Vallbo, Å. B. Tactile sensibility in the human hand: relative and absolute densities of four mechanoreceptive units in glabrous skin. *J. Physiol.* **286**, 283–300 (1979).
32. Woolf, C. J. & Ma, Q. Nociceptors-Noxious Stimulus Detectors. *Neuron* **55**, 353–364 (2007).
33. Björnsdotter, M., Morrison, I. & Olausson, H. Feeling good: On the role of C fiber mediated touch in interoception. *Exp. Brain Res.* **207**, 149–155 (2010).
34. Caterina, M. J. *et al.* Impaired Nociception and Pain Sensation in Mice Lacking the Capsaicin Receptor. *Science (80-.).* **288**, 306 LP – 313 (2000).
35. Dhaka, A., Viswanath, V. & Patapoutian, A. Trp Ion Channels and Temperature Sensation. *Annu. Rev. Neurosci.* **29**, 135–161 (2006).
36. Hensel, H. & Boman, K. Afferent impulses in cutaneous sensory nerves in human subjects. *J. Physiol.* 564–578 (1960).
37. Usoskin, D. *et al.* Unbiased classification of sensory neuron types by large-scale single-cell RNA sequencing. *Nat. Neurosci.* **18**, 145–153 (2014).
38. Gatto, G., Smith, K. M., Ross, S. E. & Goulding, M. Neuronal diversity in the somatosensory system: bridging the gap between cell type and function. *Curr. Opin. Neurobiol.* **56**, 167–174 (2019).
39. Case, L. K. *et al.* Encoding of touch intensity but not pleasantness in human primary somatosensory cortex. *J. Neurosci.* **36**, 5850–5860 (2016).
40. Melzack, R. & Wall, P. D. Pain Mechanisms: A New Theory. *Science (80-.).* **150**, 971–979 (1965).
41. Ross, S. E. *et al.* Loss of Inhibitory Interneurons in the Dorsal Spinal Cord and Elevated Itch in Bhlhb5 Mutant Mice. *Neuron* **65**, 886–898 (2010).
42. Bourane, S. *et al.* Gate control of mechanical itch by a subpopulation of spinal cord interneurons. *Science (80-.).* **350**, 550–554 (2015).
43. Braz, J., Solorzano, C., Wang, X. & Basbaum, A. I. Transmitting Pain and Itch Messages: A Contemporary View of the Spinal Cord Circuits that Generate Gate Control. *Neuron* **82**,

522–536 (2014).
44. Duan, B. *et al.* Identification of spinal circuits transmitting and gating mechanical pain. *Cell* **159**, 1417–1432 (2014).
45. Corder, G., Castro, D. C., Bruchas, M. R. & Scherrer, G. Endogenous and Exogenous Opioids in Pain. *Annu. Rev. Neurosci.* **41**, 453–473 (2018).
46. Behbehani, M. M. Functional characteristics of the midbrain periaqueductal gray. *Prog. Neurobiol.* **46**, 575–605 (1995).
47. Corder, G. *et al. An amygdalar neural ensemble that encodes the unpleasantness of pain*. *Science* **363**, (2019).
48. Gauriau, C. & Bernard, J. Physiological Society Symposium Nociceptors as Homeostatic Afferents : Central Processing Pain pathways and parabrachial circuits in the rat. *Exp. Physiol.* **87**, 251–258 (2010).
49. Benarroch, E. E. Pain-autonomic interactions. *Neurol. Sci.* **27**, 130–133 (2006).
50. Chen, Y. B. *et al.* Serotoninergic projection from dorsal raphe nucleus to insular cortex is involved in acute itch sensation processing in mice. *Brain Res.* **1715**, 224–234 (2019).
51. Ramsey, I. S., Delling, M. & Clapham, D. E. AN INTRODUCTION TO TRP CHANNELS doi:10.1146/annurev.physiol.68.040204.100431. *Annu. Rev. Physiol.* **68**, 619–647 (2006).
52. Montell, C. The TRP superfamily of cation channels. *Sci. STKE* **2005**, re3 (2005).
53. Clapham, D. E. TRP channels as cellular sensors. *Nature* **426**, 517–524 (2003).
54. Hoenderop, J. G. J. *et al.* Homo- and heterotetrameric architecture of the epithelial Ca2+ channels TRPV5 and TRPV6. *EMBO J.* **22**, 776–785 (2003).
55. Pedersen, S. F., Owsianik, G. & Nilius, B. TRP channels: An overview. *Cell Calcium* **38**, 233–252 (2005).
56. Ryazanova, L. V, Dorovkov, M. V, Ansari, A. & Ryazanov, A. G. Characterization of the Protein Kinase Activity of TRPM7/ChaK1, a Protein Kinase Fused to the Transient Receptor Potential Ion Channel. *J. Biol. Chem.* **279**, 3708–3716 (2003).
57. Yamaguchi, H., Matsushita, M., Nairn, A. C. & Kuriyan, J. Crystal Structure of the Atypical Protein Kinase Domain of a TRP Channel with Phosphotransferase Activity. *Mol. Cell* **7**, 1047–1057 (2001).
58. Caterina, M. J. *et al.* The capsaicin receptor: A heat-activated ion channel in the pain pathway. *Nature* **389**, 816–824 (1997).
59. Story, G. M. *et al.* ANKTM1, a TRP-like channel expressed in nociceptive neurons, is activated by cold temperatures. *Cell* **112**, 819–829 (2003).
60. Namer, B., Seifert, F., Handwerker, H. O. & Maihöfner, C. TRPA1 and TRPM8 activation in humans: effects of cinnamaldehyde and menthol. *Neuroreport* **16**, 955–959 (2005).
61. Macpherson, L. J. *et al.* Noxious compounds activate TRPA1 ion channels through covalent modification of cysteines. *Nature* **445**, 541–545 (2007).
62. Bautista, D. M. *et al.* TRPA1 Mediates the Inflammatory Actions of Environmental Irritants and Proalgesic Agents. *Cell* **124**, 1269–1282 (2006).
63. Trevisani, M. *et al.* 4-Hydroxynonenal, an endogenous aldehyde, causes pain and neurogenic inflammation through activation of the irritant receptor TRPA1. *Proc. Natl. Acad. Sci. U. S. A.* **104**, 13519–24 (2007).
64. Jordt, S.-E. *et al.* Mustard oils and cannabinoids excite sensory nerve fibres through the TRP channel ANKTM1. *Nature* **427**, 260–265 (2004).
65. Prober, D. a *et al.* Zebrafish TRPA1 channels are required for chemosensation but not for

thermosensation or mechanosensory hair cell function. *J. Neurosci.* **28**, 10102–10110 (2008).
66. Kwan, K. Y. *et al.* TRPA1 Contributes to Cold, Mechanical, and Chemical Nociception but Is Not Essential for Hair-Cell Transduction. *Neuron* **50**, 277–289 (2006).
67. Vriens, J. *et al.* TRPM3 Is a Nociceptor Channel Involved in the Detection of Noxious Heat. *Neuron* **70**, 482–494 (2011).
68. Yang, F. & Zheng, J. Understand spiciness: mechanism of TRPV1 channel activation by capsaicin. *Protein Cell* **8**, 169–177 (2017).
69. Kimball, C., Luo, J., Yin, S., Hu, H. & Dhaka, A. The Pore Loop Domain of TRPV1 Is Required for Its Activation by the Volatile Anesthetics Chloroform and Isoflurane. *Mol. Pharmacol.* **88**, 131–138 (2015).
70. Gau, P. *et al.* The zebrafish ortholog of TRPV1 is required for heat-induced locomotion. *Ann. Intern. Med.* **158**, 5249–5260 (2013).
71. Jordt, S. E. & Julius, D. Molecular basis for species-specific sensitivity to 'hot' chili peppers. *Cell* **108**, 421–430 (2002).
72. Bandell, M. *et al.* Noxious cold ion channel TRPA1 is activated by pungent compounds and bradykinin. *Neuron* **41**, 849–857 (2004).
73. Dhaka, A. *et al.* TRPM8 Is Required for Cold Sensation in Mice. *Neuron* **54**, 371–378 (2007).
74. Dhaka, A., Earley, T. J., Watson, J. & Patapoutian, A. Visualizing cold spots: TRPM8-expressing sensory neurons and their projections. *J. Neurosci.* **28**, 566–575 (2008).
75. McKemy, D. D., Neuhausser, W. M. & Julius, D. Identification of a cold receptor reveals a general role for TRP channels in thermosensation. *Nature* **416**, 52–58 (2002).
76. Peier, A. M. *et al.* A TRP channel that senses cold stimuli and menthol. *Cell* **108**, 705–715 (2002).
77. Laing, R. J. & Dhaka, A. ThermoTRPs and Pain. *Neurosci.* **22**, 171–187 (2016).
78. Huang, Y., Fliegert, R., Guse, A. H., Lü, W. & Du, J. A structural overview of the ion channels of the TRPM family. *Cell Calcium* **85**, (2020).
79. Huang, Y., Roth, B., Lü, W. & Du, J. Ligand recognition and gating mechanism through three Ligand-binding sites of human TRPM2 channel. *Elife* **8**, 1–18 (2019).
80. Greka, A., Navarro, B., Oancea, E., Duggan, A. & Clapham, D. E. TRPC5 is a regulator of hippocampal neurite length and growth cone morphology. *Nat. Neurosci.* **6**, 837–845 (2003).
81. Woo, S. H. *et al.* Piezo2 is the principal mechanotransduction channel for proprioception. *Nat. Neurosci.* **18**, 1756–1762 (2015).
82. Ranade, S. S. *et al.* Piezo2 is the major transducer of mechanical forces for touch sensation in mice. *Nature* **516**, 121–125 (2014).
83. Lieu, T. *et al.* The Bile Acid Receptor TGR5 Activates the TRPA1 Channel to Induce Itch in Mice. *Gastroenterology* (2014). doi:10.1053/j.gastro.2014.08.042
84. Hill, R. Z., Morita, T., Brem, R. B. & Bautista, D. M. S1PR3 mediates itch and pain via distinct TRP channel-dependent pathways. *J. Neurosci.* **38**, 7833–7843 (2018).
85. Wilson, S. R. *et al.* TRPA1 is required for histamine-independent, Mas-related G protein-coupled receptor-mediated itch. *Nat. Neurosci.* **14**, 595–602 (2011).
86. Liu, Q. *et al.* Sensory Neuron-Specific GPCR Mrgprs Are Itch Receptors Mediating Chloroquine-Induced Pruritus. *Cell* **139**, 1353–1365 (2009).
87. Alemi, F. *et al.* The TGR5 receptor mediates bile acid – induced itch and analgesia Find

the latest version : The TGR5 receptor mediates bile acid – induced itch and analgesia. **123**, 1513–1530 (2013).
88. Shim, W.-S. *et al.* TRPV1 mediates histamine-induced itching via the activation of phospholipase A2 and 12-lipoxygenase. *J Neurosci* **27**, 2331–2337 (2007).
89. Zhang, X. Targeting TRP ion channels for itch relief. *Naunyn. Schmiedebergs. Arch. Pharmacol.* **388**, 389–399 (2014).
90. Liang, J., Bi, H. & Ji, W. Involvement of TRPA1 in ET-1-induced pain-like behavior in mice. *Neuroreport* **21**, 201–205 (2010).
91. Hoon, M. A. Molecular dissection of itch. *Curr. Opin. Neurobiol.* **34**, 61–66 (2015).
92. Bautista, D. M., Wilson, S. R. & Hoon, M. a. Why we scratch an itch: the molecules, cells and circuits of itch. *Nat. Neurosci.* **17**, 175–182 (2014).
93. Imamachi, N. *et al.* TRPV1-expressing primary afferents generate behavioral responses to pruritogens via multiple mechanisms. *Proc. Natl. Acad. Sci. U. S. A.* **106**, 11330–11335 (2009).
94. Akiyama, T. *et al.* Involvement of TRPV4 in serotonin-evoked scratching. *J. Invest. Dermatol.* **136**, 154–160 (2016).
95. Ma, Q. Labeled lines meet and talk: Population coding of somatic sensations. *J. Clin. Invest.* **120**, 3773–3778 (2010).
96. Roberson, D. P. *et al.* Activity-dependent silencing reveals functionally distinct itch-generating sensory neurons. *Nat Neurosci* **16**, 910–918 (2013).
97. Davidson, S. & Giesler, G. J. The multiple pathways for itch and their interactions with pain. *Trends Neurosci.* **33**, 550–558 (2010).
98. Graham, D. T., Goodell, H. & Wolff, H. G. Neural mechanisms involved in itch, 'itchy skin', and tickle sensations. *J. Clin. Invest.* **30**, 37–49 (1951).
99. McMahon, S. B. & Koltzenburg, M. Itching for an explanation. *Trends Neurosci.* **15**, 497–501 (1992).
100. Sikand, P., Shimada, S. G., Green, B. G. & LaMotte, R. H. Similar itch and nociceptive sensations evoked by punctate cutaneous application of capsaicin, histamine and cowhage. *PAIN*® **144**, 66–75 (2009).
101. Green, B. G. & Shaffer, G. S. The sensory response to capsaicin during repeated topical exposures: differential effects on sensations of itching and pungency. *Pain* **53**, 323–334 (1993).
102. Green, B. G. Spatial summation of chemical irritation and itch produced by topical application of capsaicin. *Percept. Psychophys.* **48**, 12–18 (1990).
103. Koppert, W., Reeh, P. W. & Handwerker, H. O. Conditioning of histamine by bradykinin alters responses of rat nociceptor and human itch sensation. *Neurosci. Lett.* **152**, 117–120 (1993).
104. Yosipovitch, G., Fast, K. & Bernhard, J. D. Noxious heat and scratching decrease histamine-induced itch and skin blood flow. *J. Invest. Dermatol.* **125**, 1268–1272 (2005).
105. Stevens, C. W. Opioid research in amphibians: An alternative pain model yielding insights on the evolution of opioid receptors. *Brain Res. Rev.* **46**, 204–215 (2004).
106. Rose, J. D. The Neurobehavioral Nature of Fishes and the Question of Awareness and Pain. *Rev. Fish. Sci.* **10**, 1–38 (2002).
107. Broom, D. M. The evolution of pain. *Vlaams Diergeneeskundig Tijdschrift* **70**, 17–21 (2001).
108. Bateson, P. Assesment of pain in animals. *Anim. Behav.* **42**, 827–839 (1991).

109. Nikolajsen, L. Phantom limb pain. *Br. J. Anaesth.* **87**, 107–116 (2001).
110. Leijon, G., Boivie, J. & Johansson, I. Central post-stroke pain - neurological symptoms and pain characteristics. *Pain* **36**, 13–25 (1989).
111. Corder, G. *et al.* An amygdalar neural ensemble that encodes the unpleasantness of pain. *Science (80-.).* **363**, 276–281 (2019).
112. Pastor, J., Soria, B. & Belmonte, C. Properties of the nociceptive neurons of the leech segmental ganglion. *J. Neurophysiol.* **75**, 2268–2279 (1996).
113. Walters, E. T., Byrne, J. H., Carew, T. J. & Kandel, E. R. Mechanoafferent neurons innervating tail of Aplysia.I.Response properties and synaptic connections. *J. Neurophysiol.* **50**, 1522–1542 (1983).
114. Tracey, W. D., Wilson, R. I., Laurent, G. & Benzer, S. painless, a Drosophila gene essential for nociception. *Cell* **113**, 261–273 (2003).
115. Smith, E. S. J. & Lewin, G. R. Nociceptors: a phylogenetic view. *J. Comp. Physiol. A. Neuroethol. Sens. Neural. Behav. Physiol.* **195**, 1089–1106 (2009).
116. Lawson, S. N. Phenotype and function of somatic primary afferent nociceptive neurones with C- , A d - or A a / b -fibres. *Exp. Physiol.* **87**, 239–244 (2002).
117. Sneddon, L. U. Evolution of nociception in vertebrates: Comparative analysis of lower vertebrates. *Brain Res. Rev.* **46**, 123–130 (2004).
118. Snow, P. J., Plenderleith, M. B., Wright, L. L. & Libraries, W. Quantitative study of primary sensory neurone populations of three species of elasmobranch fish. *J. Comp. Neurol.* **2900**, 97–103 (2016).
119. Dunlop, R. & Laming, P. Mechanoreceptive and nociceptive responses in the central nervous system of goldfish (Carassius auratus) and trout (Oncorhynchus mykiss). *J. Pain* **6**, 561–568 (2005).
120. Ashley, P. J., Sneddon, L. U. & McCrohan, C. R. Nociception in fish: stimulus-response properties of receptors on the head of trout Oncorhynchus mykiss. *Brain Res.* **1166**, 47–54 (2007).
121. Sneddon, L. U. Anatomical and electrophysiological analysis of the trigeminal nerve in a teleost fish, Oncorhynchus mykiss. *Neurosci. Lett.* **319**, 167–171 (2002).
122. Reilly, S. C., Quinn, J. P., Cossins, A. R. & Sneddon, L. U. Behavioural analysis of a nociceptive event in fish: Comparisons between three species demonstrate specific responses. *Appl. Anim. Behav. Sci.* **114**, 248–259 (2008).
123. Sneddon, L. U., Braithwaite, V. a & Gentle, M. J. Do fishes have nociceptors? Evidence for the evolution of a vertebrate sensory system. *Proc. Biol. Sci.* **270**, 1115–21 (2003).
124. Sneddon, L. U. Pain perception in fish: indicators and endpoints. *ILAR J.* **50**, 338–342 (2009).
125. Oyadeyi, A. S., Ajao, F. O., Afolabi, A. O., Udoh, U. S. & Azeez, O. M. The Formalin Test in African Toad (Bufo regularis) - a Novel Pain Model in Amphibians. **2**, 24–28 (2007).
126. Kanui, T. I., Hole, K. & Miaron, J. O. Nociception in Crocodiles: Capsaicin Instillation, Formalin and Hot Plate Tests. *Zoolog. Sci.* **7**, 537–540 (1990).
127. Northcutt, R. G. EVOLUTION OF THE TELENCEPHALON IN NONMAMMALS. *Annu. Rev. Neurosci.* **4**, 301–350 (1981).
128. Cameron, A. A., Plenderleith, M. B. & Snow, P. J. Organization of the Spinal Cord in Four Species of Elasmobranch Fish: Cytoarchitecture and Distribution of Serotonin and Selected Neuropeptides. *J. Comp. Neurol.* **2900**, 201–18 (2016).

129. Zhai, X. Y. & Atsumi, S. Large dorsal horn neurons which receive inputs from numerous substance P-like immunoreactive axon terminals in the laminae I and II of the chicken spinal cord. *Neurosci. Res.* **28**, 147–154 (1997).
130. Lierz, M. & Korbel, R. Anesthesia and Analgesia in Birds. *J. Exot. Pet Med.* **21**, 44–58 (2012).
131. Paul-Murphy, J., McCutcheon, R. A., Standing, B., Steebeba, E. & Converse, A. Using emission tomography imaging of the parrot brain to study response to clinical pain. in *Proc 9th Conf Euro Assoc Avian Vet, Zurich* 293–297 (2007).
132. Snow, P. J., Renshaw, G. M. C. & Hamlin, K. E. Enkephalin Immunoreactivity. **273**, 264–273 (1996).
133. Gonzalez-Nuñez, V., Marrón Fernández de Velasco, E., Arsequell, G., Valencia, G. & Rodríguez, R. E. Identification of dynorphin a from zebrafish: A comparative study with mammalian dynorphin A. *Neuroscience* **144**, 675–684 (2007).
134. Alvarez, F. A. *et al. New kappa opioid receptor from zebrafish Danio rerio*. *Neuroscience Letters* **405**, (2006).
135. Davis, M. R., Mylniczenko, N., Storms, T., Raymond, F. & Dunn, J. L. Evaluation of intramuscular ketoprofen and butorphanol as analgesics in chain dogfish (Scyliorhinus retifer). *Zoo Biol.* **25**, 491–500 (2006).
136. Reiner, A., Davis, B. M., Brecha, N. C. & Karten, H. J. The distribution of enkephalinlike immunoreactivity in the telencephalon of the adult and developing domestic chicken. *J. Comp. Neurol.* **228**, 245–262 (1984).
137. Hawkins, M. G. The Use of Analgesics in Birds, Reptiles, and Small Exotic Mammals. *J. Exot. Pet Med.* **15**, 177–192 (2006).
138. Sneddon, L. U. The evidence for pain in fish: The use of morphine as an analgesic. *Appl. Anim. Behav. Sci.* **83**, 153–162 (2003).
139. Correia, A. D., Cunha, S. R., Scholze, M. & Stevens, E. D. A novel behavioral fish model of nociception for Testing Analgesics. *Pharmaceuticals* **4**, 665–680 (2011).
140. Steenbergen, P. J. & Bardine, N. Antinociceptive effects of buprenorphine in zebrafish larvae: An alternative for rodent models to study pain and nociception? *Appl. Anim. Behav. Sci.* **152**, 92–99 (2014).
141. Brenner, G. M., Klopp, A. J., Deason, L. L. & Stevens, C. W. Analgesic potency of alpha adrenergic agents after systemic administration in amphibians. *J. Pharmacol. Exp. Ther.* **270**, 540–545 (1994).
142. Willenbring, S. & Stevens, C. W. Thermal, mechanical and chemical peripheral sensation in amphibians: opioid and adrenergic effects. *Life Sci.* **58**, 125–133 (1996).
143. Kanui, T. I. & Hole, K. Morphine and pethidine antinociception in the crocodile. *J. Vet. Pharmacol. Ther.* **15**, 101–103 (1992).
144. Gallon, R. Effects of Shock Intensity on Shuttlebox Avoidance Conditioning in Goldfish. *Psychol. Rep.* **31**, 855–858 (1972).
145. Beukemaj, J. J. Acquired hook-avoidance in the pike Esox lucius L. fished with artificial and natural baits. *J. Fish Biol.* **2**, 155–160 (1970).
146. Overmier, J. B. & Papini, M. R. Factors modulating the effects of teleost telencephalon ablation on retention, relearning, and extinction of instrumental avoidance behavior. *Behav. Neurosci.* **100**, 190–199, 289 (1986).
147. Sneddon, L. U., Braithwaite, V. A. & Gentle, M. J. Novel object test: examining nociception and fear in the rainbow trout. *J. Pain* **4**, 431–440 (2003).

148. James, L. E., Williams, C. J. A., Bertelsen, M. F. & Wang, T. Evaluation of Feeding Behavior As an Indicator of Pain in Snakes. *J. Zoo Wildl. Med.* **48**, 196–199 (2017).
149. Rowe, A. H., Xiao, Y., Rowe, M. P., Cummins, T. R. & Zakon, H. H. Voltage-Gated Sodium Channel in Grasshopper Mice Defends Against Bark Scorpion Toxin. *Science (80-.).* **342**, 441–446 (2013).
150. Eigenbrod, O. *et al.* Rapid molecular evolution of pain insensitivity in multiple African rodents. *Science (80-.).* **364**, 852–859 (2019).
151. Smith, E. S. J. *et al.* Selective Inflammatory Pain Insensitivity in the African Naked Mole-Rat (Heterocephalus glaber). **6**, (2008).
152. Curtright, A. *et al.* Modeling nociception in zebrafish: A way forward for unbiased analgesic discovery. *PLoS One* **10**, 1–18 (2015).
153. Akiyama, T., Carstens, M. I. & Carstens, E. Differential itch- and pain-related behavioral responses and μ-opioid modulation in mice. *Acta Derm. Venereol.* **90**, 575–581 (2010).
154. Shimada, S. G. & LaMotte, R. H. Behavioral differentiation between itch and pain in mouse. *Pain* **139**, 681–687 (2008).
155. Chevalier-Skolnikoff, S. & Liska, J. Tool use by wild and captive elephants. *Animal Behaviour* **46**, 209–219 (1993).
156. Huber, R. *et al.* Grazing, social and comfort behaviour of Ankole and crossbred (Ankole × Holstein) heifers on pasture in south western Uganda. *Appl. Anim. Behav. Sci.* **112**, 223–234 (2008).
157. Deecke, V. B. Tool-use in the brown bear (Ursus arctos). *Anim. Cogn.* **15**, 725–730 (2012).
158. Green, G. I. & Mattson, D. J. Tree rubbing by yellowstone grizzly bears Ursus arctos. *Wildlife Biol.* **9**, 1–9 (2003).
159. DELIUS, J. D. Preening and Associated Comfort Behavior in Birds. *Ann. N. Y. Acad. Sci.* **525**, 40–55 (1988).
160. Fayet, A. L., Snær, E. & Biro, D. Evidence of tool use in a seabird. 18–20 (2019). doi:10.1073/pnas.1918060117
161. Shumaker, R. W., Walkup, K. R. & Beck, B. B. *Animal tool behavior: the use and manufacture of tools by animals*. (JHU Press, 2011).
162. Kaslin, J. & Panula, P. Comparative anatomy of the histaminergic and other aminergic systems in zebrafish (Danio rerio). *J. Comp. Neurol.* **440**, 342–377 (2001).
163. Pei, S. *et al.* Risk of prenatal depression and stress treatment: alteration on serotonin system of offspring through exposure to Fluoxetine. *Sci. Rep.* **6**, 33822 (2016).
164. Xu, H., Echemendia, N., Chen, S. & Lin, F. Identification and expression patterns of members of the protease-activated receptor (par) gene family during zebrafish development. *Dev. Dyn.* **240**, 278–287 (2011).
165. Schön, M. P. & Schön, M. Imiquimod: Mode of action. *Br. J. Dermatol.* **157**, 8–13 (2007).
166. Bell, J. K., McQueen, D. S. & Rees, J. L. Involvement of histamine H_4 and H_1 receptors in scratching induced by histamine receptor agonists in BalbC mice. *Br. J. Pharmacol.* **142**, 374–380 (2004).
167. Yamaguchi, T., Nagasawa, T., Satoh, M. & Kuraishi, Y. Itch-associated response induced by intradermal serotonin through 5-HT2 receptors in mice. *Neurosci. Res.* **35**, 77–83 (1999).
168. Tsujii, K., Andoh, T., Ui, H., Lee, J. & Kuraishi, Y. Involvement of Tryptase and

Proteinase-Activated Receptor-2 in Spontaneous Itch-Associated Response in Mice With Atopy-like Dermatitis. **395**, 388–395 (2009).
169. Fosque, B. F. *et al.* Labeling of active neural circuits in vivo with designed calcium integrators. **347**, (2015).
170. Maximino, C. Modulation of nociceptive-like behavior in zebrafish (Danio rerio) by environmental stressors. *Psychol. Neurosci.* **4**, 149–155 (2011).
171. Colwill, R. M. & Creton, R. Locomotor behaviors in zebrafish (Danio rerio) larvae. *Behav. Processes* **86**, 222–229 (2011).
172. Egan, R. J. *et al.* Understanding behavioral and physiological phenotypes of stress and anxiety in zebrafish. *Behav. Brain Res.* **205**, 38–44 (2009).
173. Levin, E. D., Bencan, Z. & Cerutti, D. T. Anxiolytic effects of nicotine in zebrafish. *Physiol. Behav.* **90**, 54–58 (2007).
174. Chang, Y. C., Madkan, V., Cook-Norris, R., Sra, K. & Tyring, S. Current and Potential Uses of Imiquimod. *South. Med. J.* **98**, 913–919 (2005).
175. Lebwohl, M. *et al.* Imiquimod 5% cream for the treatment of actinic keratosis: Results from two phase III, randomized, double-blind, parallel group, vehicle-controlled trials. *J. Am. Acad. Dermatol.* **50**, 714–721 (2004).
176. Liu, T., Xu, Z.-Z., Park, C.-K., Berta, T. & Ji, R.-R. Toll-like receptor 7 mediates pruritus. *Nat. Neurosci.* **13**, 1460–1462 (2010).
177. Kim, S.-J. *et al.* Analysis of cellular and behavioral responses to imiquimod reveals a unique itch pathway in transient receptor potential vanilloid 1 (TRPV1)-expressing neurons. *Proc. Natl. Acad. Sci. U. S. A.* **108**, 3371–3376 (2011).
178. Park, C. K. *et al.* Extracellular microRNAs Activate nociceptor neurons to elicit pain via TLR7 and TRPA1. *Neuron* **82**, 47–54 (2014).
179. Li, C.-L. *et al.* Somatosensory neuron types identified by high-coverage single-cell RNA-sequencing and functional heterogeneity. *Cell Res.* **26**, 83–102 (2016).
180. Bresciani, E. *et al.* CBFb and RUNX1 are required at 2 different steps during the development of hematopoietic stem cells in zebrafish. *Blood* **124**, 70–78 (2014).
181. Du, L. *et al.* Rumba and Haus3 are essential factors for the maintenance of hematopoietic stem/progenitor cells during zebrafish hematopoiesis. *Development* **138**, 619–629 (2011).
182. Kimura, Y., Hisano, Y., Kawahara, A. & Higashijima, S.-I. Efficient generation of knock-in transgenic zebrafish carrying reporter/driver genes by CRISPR/Cas9-mediated genome engineering. *Sci. Rep.* **4**, 6545 (2014).
183. Akerboom, J. *et al.* Optimization of a GCaMP Calcium Indicator for Neural Activity Imaging. *J. Neurosci.* **32**, 13819–13840 (2012).
184. Hornung, V. *et al.* Sequence-specific potent induction of IFN-α by short interfering RNA in plasmacytoid dendritic cells through TLR7. *Nat. Med.* **11**, 263–270 (2005).
185. Mitchell, T. & Sugden, B. Stimulation of NF-kappa B-mediated transcription by mutant derivatives of the latent membrane protein of Epstein-Barr virus. *J. Virol.* **69**, 2968–2976 (1995).
186. Chen, T.-W. *et al.* Ultrasensitive fluorescent proteins for imaging neuronal activity. *Nature* **499**, 295–300 (2013).
187. Liu, X. Y. *et al.* Unidirectional cross-activation of GRPR by MOR1D uncouples itch and analgesia induced by opioids. *Cell* **147**, 447–458 (2011).
188. Colwill, R. M. & Creton, R. Imaging escape and avoidance behavior in zebrafish larvae. *Rev. Neurosci.* **22**, 63–73 (2011).

189. Højland, C. R., Andersen, H. H., Poulsen, J. N., Arendt-Nielsen, L. & Gazerani, P. A human surrogate model of itch utilizing the TRPA1 agonist trans-cinnamaldehyde. *Acta Derm. Venereol.* **95**, 798–803 (2015).
190. Goswami, S. C. *et al.* Itch-associated peptides: RNA-Seq and bioinformatic analysis of natriuretic precursor peptide B and gastrin releasing peptide in dorsal root and trigeminal ganglia, and the spinal cord. *Mol. Pain* **10**, 4–11 (2014).
191. Schmelz, M. Itch and pain. *Neurosci. Biobehav. Rev.* 171–176 (2010).
192. Meijer, A. H. *et al.* Expression analysis of the Toll-like receptor and TIR domain adaptor families of zebrafish. *Mol. Immunol.* **40**, 773–783 (2004).
193. Kanwal, Z., Wiegertjes, G. F., Veneman, W. J., Meijer, A. H. & Spaink, H. P. Comparative studies of Toll-like receptor signalling using zebrafish. *Dev. Comp. Immunol.* **46**, 35–52 (2014).
194. Zhou, Z. xia & Sun, L. Immune effects of R848: Evidences that suggest an essential role of TLR7/8-induced, Myd88- and NF-??B-dependent signaling in the antiviral immunity of Japanese flounder (Paralichthys olivaceus). *Dev. Comp. Immunol.* **49**, 113–120 (2015).
195. Tanekhy, M., Kono, T. & Sakai, M. Cloning, characterization, and expression analysis of Toll-like receptor-7 cDNA from common carp, Cyprinus carpio L. *Comp. Biochem. Physiol. Part D. Genomics Proteomics* **5**, 245–55 (2010).
196. Kileng, Ø., Albuquerque, A. & Robertsen, B. Induction of interferon system genes in Atlantic salmon by the imidazoquinoline S-27609, a ligand for Toll-like receptor 7. *Fish Shellfish Immunol.* **24**, 514–522 (2008).
197. Yang, C., Su, J., Zhang, R., Peng, L. & Li, Q. Identification and expression profiles of grass carp Ctenopharyngodon idella tlr7 in responses to double-stranded RNA and virus infection. *J. Fish Biol.* **80**, 2605–2622 (2012).
198. Peitsaro, N., Sundvik, M., Anichtchik, O. V., Kaslin, J. & Panula, P. Identification of zebrafish histamine H1, H2 and H3 receptors and effects of histaminergic ligands on behavior. *Biochem. Pharmacol.* **73**, 1205–1214 (2007).
199. Prykhozhij, S. V. & Berman, J. N. The progress and promise of zebrafish as a model to study mast cells. *Dev. Comp. Immunol.* **46**, 74–83 (2014).
200. Mulero, I., Sepulcre, M. P., Meseguer, J., Garcia-Ayala, A. & Mulero, V. Histamine is stored in mast cells of most evolutionarily advanced fish and regulates the fish inflammatory response. *Proc. Natl. Acad. Sci.* **104**, 19434–19439 (2007).
201. Sackerman, J. *et al.* Zebrafish Behavior in Novel Environments: Effects of Acute Exposure to Anxiolytic Compounds and Choice of Danio rerio Line. *Int. J. Comp. Psychol.* **23**, 43–61 (2010).
202. Kimmel, C. B., Ballard, W. W., Kimmel, S. R., Ullmann, B. & Schilling, T. F. Stages of embryonic development of the zebrafish. *Dev. Dyn. an Off. public* **203**, 253–310 (1995).
203. Cruz-Orengo, L. *et al.* Cutaneous Nociception Evoked by 15-delta PGJ2 via Activation of Ion Channel TRPA1. *Mol. Pain* **4**, 1744-8069-4–30 (2008).
204. Meeker, N. D., Hutchinson, S. A., Ho, L. & Trede, N. S. Method for isolation of PCR-ready genomic DNA from zebrafish tissues. *Biotechniques* **43**, 610–614 (2007).
205. Shah, A. N., Davey, C. F., Whitebirch, A. C., Miller, A. C. & Moens, C. B. Rapid Reverse Genetic Screening Using CRISPR in Zebrafish. *Zebrafish* **13**, 152–153 (2016).
206. Feng, J. *et al.* The antimicrobial peptide hBD2 promotes itch through Toll-like receptor 4 signaling in mice. *J. Allergy Clin. Immunol.* (2017). doi:10.1016/j.jaci.2017.03.035
207. Harper, A. A. & Lawson, S. N. Conduction velocity is related to morphological cell type

in rat dorsal root ganglion neurones. *J. Physiol.* **359**, 31–46 (1985).
208. Li, L. *et al.* The functional organization of cutaneous low-threshold mechanosensory neurons. *Cell* **147**, 1615–1627 (2011).
209. Bai, L. *et al.* Genetic Identification of an Expansive Mechanoreceptor Sensitive to Skin Stroking. *Cell* **163**, 1783–1795 (2015).
210. Bardoni, R. *et al.* Delta opioid receptors presynaptically regulate cutaneous mechanosensory neuron input to the spinal cord dorsal horn. *Neuron* **81**, 1312–1327 (2014).
211. Ghitani, N. *et al.* Specialized Mechanosensory Nociceptors Mediating Rapid Responses to Hair Pull. *Neuron* **95**, 944-954.e4 (2017).
212. Zylka, M. J., Rice, F. L. & Anderson, D. J. Topographically distinct epidermal nociceptive circuits revealed by axonal tracers targeted to Mrgprd. *Neuron* **45**, 17–25 (2005).
213. Olson, W. *et al.* Sparse genetic tracing reveals regionally specific functional organization of mammalian nociceptors. 1–26 (2017).
214. Pan, Y. a., Choy, M., Prober, D. a. & Schier, a. F. Robo2 determines subtype-specific axonal projections of trigeminal sensory neurons. *Development* **139**, 591–600 (2012).
215. Wang, S. *et al.* Phospholipase C and protein kinase A mediate bradykinin sensitization of TRPA1: A molecular mechanism of inflammatory pain. *Brain* **131**, 1241–1251 (2008).
216. Schmidt, M., Dubin, A. E., Petrus, M. J., Earley, T. J. & Patapoutian, A. Nociceptive Signals Induce Trafficking of TRPA1 to the Plasma Membrane. *Neuron* **64**, 498–509 (2009).
217. Shi, T. J. S. *et al.* Phospholipase Cβ3 in mouse and human dorsal root ganglia and spinal cord is a possible target for treatment of neuropathic pain. *Proc. Natl. Acad. Sci. U. S. A.* **105**, 20004–20008 (2008).
218. Galeotti, N., Stefano, G. B., Guarna, M., Bianchi, E. & Ghelardini, C. Signaling pathway of morphine induced acute thermal hyperalgesia in mice. *Pain* **123**, 294–305 (2006).
219. Joseph, E. K., Bogen, O., Alessandri-Haber, N. & Levine, J. D. PLC-β3 signals upstream of PKCε in acute and chronic inflammatory hyperalgesia. *Pain* **132**, 67–73 (2007).
220. Dai, Y. *et al.* Sensitization of TRPA1 by PAR2 contributes to the sensation of inflammatory pain. *J. Clin. Invest.* **117**, 1979–1987 (2007).
221. Senning, E. N., Collins, M. D., Stratiievska, A., Ufret-Vincenty, C. A. & Gordon, S. E. Regulation of TRPV1 ion channel by phosphoinositide (4,5)-bisphosphate: The role of membrane asymmetry. *J. Biol. Chem.* **289**, 10999–11006 (2014).
222. Chuang, H. H. *et al.* Bradykinin and nerve growth factor release the capsaicin receptor from PtdIns(4,5)P2-mediated inhibition. *Nature* **411**, 957–962 (2001).
223. Cao, E., Cordero-morales, J. F., Liu, B., Qin, F. & Julius, D. Article TRPV1 Channels Are Intrinsically Heat Sensitive and Negatively Regulated by Phosphoinositide Lipids. *Neuron* **77**, 667–679 (2013).
224. Jalili, T., Takeishi, Y. & Walsh, R. A. Signal transduction during cardiac hypertrophy: The role of Gα(q), PLC βI, and PKC. *Cardiovasc. Res.* **44**, 5–9 (1999).
225. Dai, Y. *et al.* Proteinase-Activated Receptor 2-Mediated Potentiation of Transient Receptor Potential Vanilloid Subfamily 1 Activity Reveals a Mechanism for Proteinase-Induced Inflammatory Pain. *J. Neurosci.* **24**, 4293–4299 (2004).
226. Kádková, A., Synytsya, V., Krusek, J., Zímová, L. & Vlachová, V. Molecular Basis of TRPA1 Regulation in Nociceptive Neurons. A Review. *Physiol. Res* **66**, 425–439 (2017).
227. Liebmann, C. & Bohmer, F. Signal Transduction Pathways of G Protein-coupled

Receptors and Their Cross-Talk with Receptor Tyrosine Kinases Lessons from Bradykinin Signaling. *Curr. Med. Chem.* **7**, 911–943 (2000).
228. Dascal, N. Ion-channel regulation by G proteins. *Trends Endocrinol. Metab.* **12**, 391–398 (2001).
229. Cochet-Bissuel, M., Lory, P. & Monteil, A. The sodium leak channel, NALCN, in health and disease. *Front. Cell. Neurosci.* **8**, 1–17 (2014).
230. Swayne, L. A. *et al.* The NALCN ion channel is activated by M3 muscarinic receptors in a pancreatic β-cell line. *EMBO Rep.* **10**, 873–880 (2009).
231. Lu, B. *et al.* The Neuronal Channel NALCN Contributes Resting Sodium Permeability and Is Required for Normal Respiratory Rhythm. *Cell* **129**, 371–383 (2007).
232. Ford, N. C., Ren, D. & Baccei, M. L. NALCN channels enhance the intrinsic excitability of spinal projection neurons. *Pain* **159**, 1719–1730 (2018).
233. Ohta, T., Imagawa, T. & Ito, S. Novel agonistic action of mustard oil on recombinant and endogenous porcine transient receptor potential V1 (pTRPV1) channels. *Biochem. Pharmacol.* **73**, 1646–1656 (2007).
234. Everaerts, W. *et al.* The capsaicin receptor TRPV1 is a crucial mediator of the noxious effects of mustard oil. *Curr. Biol.* **21**, 316–321 (2011).
235. Alpizar, Y. A. *et al.* Allyl isothiocyanate sensitizes TRPV1 to heat stimulation. *Pflugers Arch. Eur. J. Physiol.* **466**, 507–515 (2014).
236. Brauchi, S. *et al.* Dissection of the components for PIP2 activation and thermosensation in TRP channels. *Proc. Natl. Acad. Sci. U. S. A.* **104**, 10246–10251 (2007).
237. Stein, A. T., Ufret-Vincenty, C. A., Hua, L., Santana, L. F. & Gordon, S. E. Phosphoinositide 3-kinase binds to TRPV1 and mediates NGF-stimulated TRPV1 trafficking to the plasma membrane. *J. Gen. Physiol.* **128**, 509–522 (2006).
238. Sigel, E. & Baur, R. Activation of protein kinase C differentially modulates neuronal Na+, Ca2+, and γ-aminobutyrate type A channels. *Proc. Natl. Acad. Sci. U. S. A.* **85**, 6192–6196 (1988).
239. Smart, T. G. Regulation of excitatory and inhibitory neurotransmitter-gated ion channels by protein phosphorylation. *Curr. Opin. Neurobiol.* **7**, 358–367 (1997).
240. Bourinet, E., Soong, T. W., Stea, A. & Snutch, T. P. Determinants of the G protein-dependent opioid modulation of neuronal calcium channels. *Proc Natl Acad Sci USA* **93**, 1486–1491 (1996).
241. Law, P.-Y., Wong, Y. H. & Loh, H. H. Molecular mechanisms and regulation of opioid receptor signaling. *Annu. Rev. Pharmacol. Toxicol.* **40**, 389–430 (2000).
242. Shen, Y., Rampino, M. A. F., Carroll, R. C. & Nawy, S. G-protein-mediated inhibition of the Trp channel TRPM1 requires the Gβγ dimer. *Proc. Natl. Acad. Sci. U. S. A.* **109**, 8752–8757 (2012).
243. Dembla, S. *et al.* Anti-nociceptive action of peripheral mu- opioid receptors by G-beta-gamma protein-mediated inhibition of TRPM3 channels. *Elife* **6**, 1–32 (2017).
244. Kernell, D. & Zwaagstra, B. Input conductance, axonal conduction velocity and cell size among hindlimb motoneurones of the cat. *Brain Res.* **204**, 311–326 (1981).
245. Lux, H. D., Schubert, P. & Kreutzberg, G. W. Direct matching of morphological and electrophysiological data in cat spinal motoneurons. in *Excitatory synaptic mechanisms* 189–198 (1970).
246. Kovac, M. P., Davis, W. J., Matera, E. & Gillette, R. Functional and structural correlates of cell size in paracerebral neurons of Pleurobranchaea californica. *J. Neurophysiol.* **47**,

909–927 (1982).
247. Koerber, H. R., Druzinsky, R. E. & Mendell, L. M. Properties of somata of spinal dorsal root ganglion cells differ according to peripheral receptor innervated. *J. Neurophysiol.* **60**, 1584–1596 (1988).
248. Zurborg, S., Yurgionas, B., Jira, J. A., Caspani, O. & Heppenstall, P. A. Direct activation of the ion channel TRPA1 by Ca2+. *Nat. Neurosci.* **10**, 277–279 (2007).
249. Cavanaugh, E. J., Simkin, D. & Kim, D. Activation of transient receptor potential A1 channels by mustard oil, tetrahydrocannabinol and Ca2+ reveals different functional channel states. *Neuroscience* **154**, 1467–1476 (2008).
250. Wang, Y. Y., Chang, R. B., Waters, H. N., McKemy, D. D. & Liman, E. R. The nociceptor ion channel TRPA1 is potentiated and inactivated by permeating calcium ions. *J. Biol. Chem.* **283**, 32691–32703 (2008).
251. Glenn, L. L. & Dement, W. C. Membrane Potential, Synaptic Activity, and Excitability of Hindlimb Motoneurons During Wakefulness and Sleep. *J. Neurophysiol.* **46**, (1981).
252. Kiernan, M. C., Bostock, H. & Bostock, C. H. Effects of membrane polarization and ischaemia on the excitability properties of human motor axons. 2542–2551 (2000).
253. Liu, C. N., Michaelis, M., Amir, R. & Devor, M. Spinal nerve injury enhances subthreshold membrane potential oscillations in DRG neurons: relation to neuropathic pain. *J. Neurophysiol.* **84**, 205–215 (2000).
254. Amir, R., Michaelis, M. & Devor, M. Membrane potential oscillations in dorsal root ganglion neurons: role in normal electrogenesis and neuropathic pain. *J Neurosci* **19**, 8589–8596 (1999).
255. Zhang, J. M., Song, X. J. & Lamotte, R. H. Enchanced excitability of sensory neurons in rats with cutaneous hyperalgesia produced by chronic compression of the dorsal root ganglion. *J. Neurophysiol.* **82**, 3359–3366 (1999).
256. Ansari, N., Müller, S., Stelzer, E. H. K. & Pampaloni, F. *Quantitative 3D Cell-Based Assay Performed with Cellular Spheroids and Fluorescence Microscopy*. *Methods in Cell Biology* **113**, (Elsevier, 2013).
257. Grueber, W. B., Jan, L. Y. & Jan, Y. N. Tiling of the Drosophila epidermis by multidendritic sensory neurons. *Development* **129**, 2867–2878 (2002).
258. Sagasti, A., Guido, M. R., Raible, D. W. & Schier, A. F. Repulsive interactions shape the morphologies and functional arrangement of zebrafish peripheral sensory arbors. *Curr. Biol.* **15**, 804–814 (2005).
259. Grueber, W. B. & Sagasti, A. Self-avoidance and Tiling: Mechanisms of Dendrite and Axon Spacing. 1–17 (2010).
260. Kittelberger, J. M., Land, B. R. & Bass, A. H. Midbrain periaqueductal gray and vocal patterning in a teleost fish. *J. Neurophysiol.* **96**, 71–85 (2006).
261. Albert Pan, Y. *et al.* Zebrabow: Multispectral cell labeling for cell tracing and lineage analysis in zebrafish. *Dev.* **140**, 2835–2846 (2013).
262. DeNardo, L. A. *et al.* Temporal evolution of cortical ensembles promoting remote memory retrieval. *Nat. Neurosci.* **22**, 460–469 (2019).
263. Guenthner, C. J., Miyamichi, K., Yang, H. H., Heller, H. C. & Luo, L. Permanent genetic access to transiently active neurons via TRAP: Targeted recombination in active populations. *Neuron* **78**, 773–784 (2013).
264. Szczot, M. *et al.* PIEZO2 mediates injury-induced tactile pain in mice and humans. *Sci. Transl. Med.* **10**, 1–10 (2018).

265. Chisari, M., Saini, D. K., Cho, J. H., Kalyanaraman, V. & Gautam, N. G protein subunit dissociation and translocation regulate cellular response to receptor stimulation. *PLoS One* **4**, (2009).
266. Gong, B. *et al.* The sec14-like phosphatidylinositol transfer proteins sec14l3/SEC14l2 act as GTPase proteins to mediate Wnt/Ca2+ signaling. *Elife* **6**, 1–24 (2017).
267. Xu, W. *et al.* The joubert syndrome protein Inpp5e controls ciliogenesis by regulating phosphoinositides at the apical membrane. *J. Am. Soc. Nephrol.* **28**, 118–129 (2017).
268. Gafni, J. *et al.* Xestospongins: Potent membrane permeable blockers of the inositol 1,4,5-trisphosphate receptor. *Neuron* **19**, 723–733 (1997).
269. Oka, T., Sato, K., Hori, M., Ozaki, H. & Karaki, H. Xestospongin C, a novel blocker of IP3 receptor, attenuates the increase in cytosolic calcium level and degranulation that is induced by antigen in RBL-2H3 mast cells. *Br. J. Pharmacol.* **135**, 1959–1966 (2002).
270. Tang, X., Edwards, E. M., Holmes, B. B., Falck, J. R. & Campbell, W. B. Role of phospholipase C and diacylglyceride lipase pathway in arachidonic acid release and acetylcholine-induced vascular relaxation in rabbit aorta. *Am. J. Physiol. - Hear. Circ. Physiol.* **290**, 37–45 (2006).
271. Ablain, J., Durand, E. M., Yang, S., Zhou, Y. & Zon, L. I. A CRISPR/Cas9 vector system for tissue-specific gene disruption in zebrafish. *Dev. Cell* **32**, 756–764 (2015).
272. De Santis, F., Di Donato, V. & Del Bene, F. Clonal analysis of gene loss of function and tissue-specific gene deletion in zebrafish via CRISPR/Cas9 technology. *Methods Cell Biol.* **135**, 171–188 (2016).
273. Bevan, S. *et al.* Capsazepine: a competitive antagonist of the sensory neurone excitant capsaicin. *Br. J. Pharmacol.* **107**, 544–552 (1992).
274. Cadwell, C. R. *et al.* Electrophysiological, transcriptomic and morphologic profiling of single neurons using Patch-seq. *Nat. Biotechnol.* **34**, 199–203 (2016).
275. Cadwell, C. R. *et al.* Multimodal profiling of single-cell morphology, electrophysiology, and gene expression using Patch-seq. *Nat. Protoc.* **12**, 2531–2553 (2017).
276. Douglass, A. D., Kraves, S., Deisseroth, K., Schier, A. F. & Engert, F. Escape Behavior Elicited by Single, Channelrhodopsin-2-Evoked Spikes in Zebrafish Somatosensory Neurons. *Curr. Biol.* **18**, 1133–1137 (2008).
277. Knafo, S. *et al.* Mechanosensory neurons control the timing of spinal microcircuit selection during locomotion. *Elife* **6**, 1–21 (2017).
278. Cao, G. *et al.* Genetically targeted optical electrophysiology in intact neural circuits. *Cell* **154**, 904–913 (2013).
279. Han, Z. *et al.* Fluorescent protein voltage probes derived from ArcLight that respond to membrane voltage changes with fast kinetics. *PLoS One* **8**, 1–9 (2013).
280. Jin, L. *et al.* Single Action Potentials and Subthreshold Electrical Events Imaged in Neurons with a Fluorescent Protein Voltage Probe. *Neuron* **75**, 779–785 (2012).
281. Rakers, S. *et al.* 'Fish matters': The relevance of fish skin biology to investigative dermatology. *Exp. Dermatol.* **19**, 313–324 (2010).
282. Ángeles Esteban, M. An Overview of the Immunological Defenses in Fish Skin. *ISRN Immunol.* **2012**, 1–29 (2012).
283. Secombes, C. J., Wang, T. & Bird, S. The interleukins of fish. *Dev. Comp. Immunol.* **35**, 1336–1345 (2011).
284. Liu, B. *et al.* IL-33/ST2 signaling excites sensory neurons and mediates itch response in a mouse model of Poison ivy contact allergy. *Proc. Natl. Acad. Sci. U. S. A.* **113**, E7572–

E7579 (2016).
285. Furue, M., Yamamura, K., Kido-Nakahara, M., Nakahara, T. & Fukui, Y. Emerging role of interleukin-31 and interleukin-31 receptor in pruritus in atopic dermatitis. *Allergy* 1–8 (2017). doi:10.1111/all.13239
286. Phan, N. Q., Lotts, T., Antal, A., Bernhard, J. D. & Ständer, S. Systemic kappa Opioid receptor agonists in the treatment of chronic pruritus: A literature review. *Acta Derm. Venereol.* **92**, 555–560 (2012).
287. Inan, S. & Cowan, A. Kappa opioid agonists suppress chloroquine-induced scratching in mice. *Eur. J. Pharmacol.* **502**, 233–237 (2004).
288. Skaggs, K., Martin, D. M. & Novitch, B. G. Regulation of spinal interneuron development by the Olig-related protein Bhlhb5 and Notch signaling. *Development* **138**, 3199–3211 (2011).
289. Leander, J. *Buprenorphine has potent kappa opioid receptor antagonist activity*. *Neuropharmacology* **26**, (1987).
290. Takemori, A. E., Ho, B. Y., Naeseth, J. S. & Portoghese, P. S. Nor-binaltorphimine, a highly selective kappa-opioid antagonist in analgesic and receptor binding assays. *J. Pharmacol. Exp. Ther.* **246**, 255 LP – 258 (1988).
291. Heidbreder, C. A., Goldberg, S. R. & Shippenberg, T. S. *The kappa-opioid receptor agonist U-69593 attenuates cocaine-induced behavioral sensitization in the rat*. *Brain Research* **616**, (1993).
292. Römer, D. *et al.* Bremazocine: A potent, long-acting opiate kappa-agonist. *Life Sci.* **27**, 971–978 (1980).
293. Kamei, J. *et al.* Antipruritic activity of the kappa-opioid receptor agonist, TRK-820. *Eur. J. Pharmacol.* **435**, 259–264 (2002).
294. Becker, J. R. *et al.* Differential activation of natriuretic peptide receptors modulates cardiomyocyte proliferation during development. *Dev.* **141**, 335–345 (2014).
295. Sun, Y. *et al.* Activation of the Nkx2.5-Calr-p53 signaling pathway by hyperglycemia induces cardiac remodeling and dysfunction in adult zebrafish. *DMM Dis. Model. Mech.* **10**, 1217–1227 (2017).
296. Chen, S. *et al.* Light-Dependent Regulation of Sleep and Wake States by Prokineticin 2 in Zebrafish. *Neuron* **95**, 153-168.e6 (2017).
297. Koven, W. & Schulte, P. The effect of fasting and refeeding on mRNA expression of PepT1 and gastrointestinal hormones regulating digestion and food intake in zebrafish (Danio rerio). *Fish Physiol. Biochem.* **38**, 1565–1575 (2012).
298. Thorndyke, M. C., Reeve, J. R. & Vigna, S. R. Biological activity of a bombesin-like peptide extracted from the intestine of the ratfish, Hydrolagus colliei. *Comp. Biochem. Physiol. Part C, Comp.* **96**, 135–140 (1990).
299. Xu, M. & Volkoff, H. Molecular characterization of ghrelin and gastrin-releasing peptide in Atlantic cod (Gadus morhua): Cloning, localization, developmental profile and role in food intake regulation. *Gen. Comp. Endocrinol.* **160**, 250–258 (2009).
300. Canosa, L. F., Unniappan, S. & Peter, R. E. Periprandial changes in growth hormone release in goldfish: Role of somatostatin, ghrelin, and gastrin-releasing peptide. *Am. J. Physiol. - Regul. Integr. Comp. Physiol.* **289**, 125–133 (2005).
301. Vladimirov, N. *et al.* Light-sheet functional imaging in fictively behaving zebrafish. *Nat. Methods* **11**, 883–884 (2014).
302. Yang, Z. *et al.* Dual-slit confocal light sheet microscopy for in vivo whole-brain imaging

of zebrafish. *Biomed. Opt. Express* **6**, 1797 (2015).
303. Logan, S. L. *et al.* Automated high-throughput light-sheet fluorescence microscopy of larval zebrafish. *PLoS One* **13**, 1–14 (2018).
304. Ellis, L. D., Seibert, J. & Soanes, K. H. Distinct models of induced hyperactivity in zebrafish larvae. *Brain Res.* **1449**, 46–59 (2012).
305. Randlett, O. *et al.* Whole-brain activity mapping onto a zebrafish brain atlas. *Nat. Methods* **12**, 1039–1046 (2015).
306. Baraban, S. C., Taylor, M. R., Castro, P. A. & Baier, H. Pentylenetetrazole induced changes in zebrafish behavior, neural activity and c-fos expression. *Neuroscience* **131**, 759–768 (2005).